

Cover Page



Universiteit Leiden



The handle <http://hdl.handle.net/1887/66118> holds various files of this Leiden University dissertation.

Author: Duijn, S. van

Title: MRI and histologic studies on early markers of Alzheimer's disease

Issue Date: 2018-10-10

MRI and histologic studies on early markers of Alzheimer's disease



S. van Duijn

Colophon
MRI and histologic studies on early markers of Alzheimer's
disease

© Sara van Duijn 2018

Thesis Leiden University Medical Centre

Cover Illustration: Fried Westland

MRI and histologic studies on early markers of Alzheimer's disease

Proefschrift

ter verkrijging van de graad van Doctor aan de Universiteit Leiden op gezag van Rector Magnificus prof. mr. C.J.J.M. Stolker, volgens besluit van het College voor Promoties te verdedigen op woensdag 10 oktober 2018 klokke 10.00 uur

door

Sara van Duijn

geboren te Amsterdam in 1979

Promotor: Prof. Dr. M.A. van Buchem

Co-promotor: Dr. R. Natté
Dr. S.G. van Duinen

Leden promotiecommissie: Dr. L. van der Weerd
Prof. Dr. G.J. Blauw
Prof. Dr. S.A.R.B. Rombouts
Prof. Dr. A. Alia (Universitat Leipzig)
Prof. Dr. A. Rozemuller (VUMC)

The work presented in this thesis was carried out at the department of Pathology at the Leiden University Medical Centre.

Content

| | | |
|-----------|---|-----|
| Chapter 1 | General Introduction | 9 |
| Chapter 2 | MRI artifacts in human brain tissue after prolonged formalin storage | 27 |
| Chapter 3 | Comparison of histological techniques to visualize iron in paraffin embedded brain tissue of patients with Alzheimer's disease | 49 |
| Chapter 4 | Cortical iron reflects severity of Alzheimer's disease | 69 |
| Chapter 5 | Detection of cortical changes in Alzheimer's disease patients at ultra-high field MRI | 95 |
| Chapter 6 | Longitudinal monitoring of sex related in vivo metabolic changes in the brain of Alzheimer's disease transgenic mouse using magnetic resonance spectroscopy | 119 |
| Chapter 7 | Summary and General discussion | 139 |

Appendices

| | |
|--------------------------|-----|
| Nederlandse samenvatting | 155 |
| Dankwoord | 159 |
| Curriculum vitae | 163 |
| Publication list | 167 |

Chapter 1

General Introduction

This thesis addresses a variety of aspects of the early diagnosis of Alzheimer's disease (AD). AD is a complex clinical syndrome characterized by a cluster of symptoms and signs comprising difficulties in memory, changes in behaviour, disturbance in language and other cognitive functions causing impairments in activities of daily living. (Ferri et al., 2005; Qiu et al., 2009; Villemagne et al., 2013). In 2010, 5,4% of the European population at the age of 60+ had dementia, which was (at that time) 6.3 million people (Wittchen et al., 2011). AD accounts for 75% of all dementia cases, implying 4.7 million people in Europe had AD in 2010 and this number is further increasing. Brookmeyer et al., predicted an AD incidence of 1 in 85 persons worldwide in 2050 (Brookmeyer et al., 2007). As a result, AD represents an important socio-economic and public health concern. Results from human studies suggest that females are at higher risk for developing AD than men (Andersen et al., 1999; Corder et al., 2004; Grimm et al., 2012; Janicki and Schupf, 2010; Musicco, 2009)

Due to an incomplete understanding of the pathophysiology of the disease, an effective therapy is currently not available. Limitations in studying the early stages of the disease during life, have been partly responsible for lack of knowledge about the pathophysiology of AD. However, there are promising strategies, some of which are already effective in animal models and some are tested in clinical trials including immunotherapy (Lambracht-Washington and Rosenberg, 2015; Landlinger et al., 2015), inhibition of A β production (Howell et al., 2015; Wang et al., 2012) or tau aggregation (Harrington et al., 2015; Richter et al., 2014; Wischik et al., 2014; Wischik et al., 2015). The ability to detect the disease in an early stage would help increasing the knowledge on the pathophysiology of AD, would improve the chances for developing effective treatments, and would widen the therapeutic window for effective treatment.

However, at the moment AD is difficult to diagnose at an early stage and even at advanced stages of the disease a definitive diagnosis of AD still requires an autopsy. Therefore, diagnostic methods are needed allowing early in vivo detection of AD pathology (Jack, Jr. et al., 2010).

Pathology

The main pathological hallmarks of AD are atrophy, neurofibrillary degeneration and extracellular amyloid plaques (figure 1 and 2) (Doens and Fernandez, 2014; Dore et al., 2013; Ma et al., 2014; Price et al., 1991; Takahashi et al., 2010; Villemagne et al., 2013). All these can also be demonstrated in non-demented elderly subjects and therefore, are not

specific for AD but their quantity and distribution in relation to the clinical symptoms is specific (Thal et al., 2014). It has been demonstrated that plaques and tangles lead to synaptic dysfunction, mitochondrial damage, inflammation and neuronal death (Doens and Fernandez, 2014; Takahashi et al., 2010). It still remains unknown how these pathological hallmarks are related to each other. Another frequent finding in AD is cerebral amyloid angiopathy (CAA) that can also contribute to the cognitive decline (Weller et al., 2009). More recently, changes in iron distribution have been noted (Bartzokis, 2011; Crichton et al., 2002; Haacke et al., 2005; Meadowcroft et al., 2015a; Meadowcroft et al., 2015b).

Atrophy

Shrinkage of the brain associated with AD is regarded as a valid marker of disease state and progression. Brain atrophy is correlated to neurofibrillary tangles (NFT) and neuropsychological deficits. It starts, in the majority of AD patients, in the hippocampus and the enthorinal cortex, extending to the temporal, parietal and frontal neocortices during the disease progression (Frisoni et al., 2010).

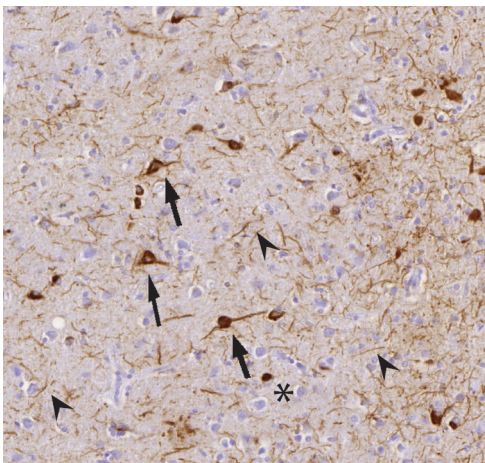


Figure 1: Examples of neurofibrillary tangles (arrows), neuropil threads (arrowheads) and dystrophic neurites (asterix).

Neurofibrillary degeneration

Neurofibrillary tangles (NFT) are one of the manifestations of neurofibrillary degeneration, the other being neuropil threads (NT) and dystrophic neurites (DN) (figure 1). In all these lesions there is intracellular accumulation of hyper-phosphorylated tau protein, forming soluble aggregates and paired helical filaments (PHF) (Kidd, 1963). NFT are neuronal cell bodies filled with PHF whereas in NT these PHF are present in the neuronal processes. DN are NT with irregular, dilated and distorted shapes. Normally tau proteins are involved in structural and reg-

ulatory function of the cytoskeleton where they promote the assembly of microtubule and their stability (Alonso et al., 2008; Grundke-Iqbal et al., 1986). However, when tau becomes hyper phosphorylated it exerts the exact opposite effect, leading to the dismantling of the same microtubule.

The resulting loss of neuronal structure impairs axonal transport, leading to disturbed proper synaptic, neuronal signalling and eventually leads to neuronal death (Ballatore et al., 2007). The degree of tau pathology correlates very well with dementia but neurofibrillary degeneration is not specific for AD: it is also seen in other neurodegenerative diseases, although with a different distribution in the brain.

Plaques

Plaques represent a wide array of lesions that contain extracellular deposits of amyloid β protein ($A\beta$) of which variable amounts are present as amyloid. Histologically, plaques are classified as diffuse, compact, classical and neuritic plaques. The type of plaque depends on the density and circumscription of $A\beta$ (diffuse vs. compact plaques), the presence of an $A\beta$ amyloid core (classical plaque) and the coexistence of dystrophic neurites (neuritic plaque) (figure 2) (Duyckaerts et al., 2009). $A\beta$ plaques in an extensive amount is typical for AD but there is poor correlation between the amount of plaques and the degree of dementia.

Cerebral $A\beta$ is generally cleaved by α -secretase and either degraded or cleared from the brain across the blood-brain barrier. $A\beta$ peptide is generated by β - and γ -secretase induced cleavage of the amyloid precursor protein (APP), a transmembrane protein, forming predominantly $A\beta_{1-40}$ or $A\beta_{1-42}$. According to the amyloid cascade hypothesis, AD is initiated by an imbalance in $A\beta$ production and clearance (Hardy, 2009; Hardy and Selkoe, 2002). This hypothesis is supported by the finding that APP gene mutations around the α , β - and γ -cleavage sites and gene mutations in proteins involved in cleavage at the APP γ -site lead to increased $A\beta$ production and often early onset AD with an autosomal dominant pattern of inheritance. However, these mutations account for only < 5% of all AD cases. The other 95% of sporadic AD probably has a more complex multifactorial etiology (Minati et al., 2009).

Due to its fibrillogenic nature, high local concentrations of $A\beta_{1-42}$ aggregate into soluble oligomers. These oligomers cluster into larger insoluble $A\beta$ fibrils that allow the formation of β -sheet structures, which are characteristic for amyloid. This clustering of oligomers triggers the misfolding

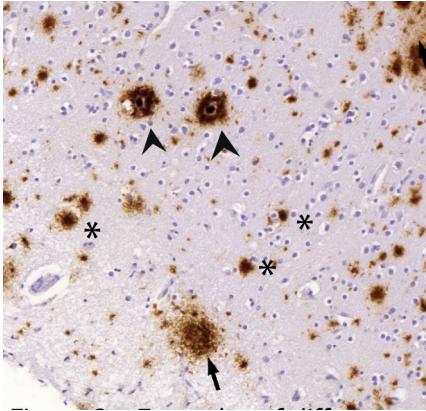


Figure 2: Examples of diffuse plaques (arrows), classical plaques (arrowheads) and compact plaques (asterix).

of other A β species, including the more soluble A β 1-40, forming plaques (Duyckaerts et al., 2009).

The study of Corder et al. suggested an acceleration of amyloid deposition in women of late middle age associated with APOE4 (Corder et al., 2004). In some AD mouse models, a similar sex-related difference was found, showing more A β accumulation in female mice (Callahan et al., 2001; Wang et al., 2003).

CAA

In the majority of AD cases different amounts of CAA are found in the brain (Natte et al., 2001; van Rooden et al., 2009; Weller et al., 2009). CAA is caused by the same A β deposits as in plaques, mainly A β 1-40 and always forms amyloid which leads to stiffness and a loss of structure of the vesselwall. CAA can occur as a sporadic disease with little or no parenchymal A β deposits and is considered a major cause of cerebral microbleeds, haemorrhages and cognitive loss.

Inflammation

In AD, microglia may play an important role in disease progression by activating different inflammatory cytokines, causing neuronal damage and cell death (Doens and Fernandez, 2014; Hardy and Selkoe, 2002; Kettenmann et al., 2011). Microglia cluster especially around plaques and CAA.

Iron

Iron was recently identified as one of the pathological changes in the AD brain (Bartzokis, 2011; Meadowcroft et al., 2009; van Duijn et al., 2013). There are two hypotheses on the role of iron in AD. The first hypothesis claims that iron would directly contribute to the development of AD, due to its neurotoxic characteristics when not properly regulated (Bartzokis, 2011). The second is the idea of iron deposits being secondary to the formation of plaques and tangles (Peters et al., 2015); not playing a leading role in the development of AD, but following the formation of plaques. Iron also has relevance in AD research because it can be detected with

high sensitivity by magnetic resonance imaging (MRI) and may serve as an in vivo marker for AD.

Magnetic resonance imaging (MRI) and spectroscopy (MRS) in AD

The in vivo diagnosis of AD is now based on clinical and neuropsychological criteria, with additional techniques such as neuroimaging and cerebrospinal fluid biomarkers playing a supportive role, resulting in “probable” AD at best. This diagnosis is not always accurate and needs post mortem histological confirmation (Fox et al., 1996; Hyman et al., 2012; Jack, Jr. et al., 2010). An MR-based hallmark for AD is hippocampal atrophy. This measurement, however, is neither conclusive nor specific for AD and consequently of limited use in clinical setting (Nasrallah and Wolk, 2014). Furthermore, cerebral atrophy in AD is found in a late stage of the disease (Jack, Jr. et al., 2010) and therefore intrinsically a poor candidate for early diagnosis. Iron is a potential interesting target for the detection of early changes in AD. MRI is particularly sensitive to iron deposition in tissues, due to the changes it induces in the magnetic field.

Earlier studies demonstrated that increased iron accumulation in amyloid plaques induces a magnetic susceptibility effect. This is visible as hypointens foci on T2*-weighted or susceptibility-weighted (SW) MRI in the cerebral cortex of transgenic AD mouse models and in human post-mortem brain slices (Chamberlain et al., 2011; Meadowcroft et al., 2009; van Rooden et al., 2009). The high magnetic field strengths needed to obtain these results only recently became available for in vivo human use. These high field human MRI systems (> 7 Tesla) may offer new possibilities to specifically detect the neuropathological hallmarks of AD, with iron as main field of focus. Perhaps changes in iron distribution can be detected even at an earlier stage than the traditional hippocampal atrophy.

MRS is a non-invasive tool which can be used to measure the concentration of various brain metabolites in vivo (Marjanska et al., 2005; Oberg et al., 2008; Rupsingh et al., 2011). MRS uses MR to study the quantity of metabolites by measuring the interaction of a radiofrequency electromagnetic field with molecular nuclei inside an external high magnetic field (Azevedo et al., 2008). Measuring these metabolic changes in vivo, could help identify AD at an early stage since metabolic levels are believed to precede structural changes (Jack, Jr. et al., 2010).

Numerous MRS studies have been performed in transgenic (tg) mouse models of AD. Several tg mouse models are available that develop sim-

ilar, but not identical, pathology as compared to human AD. The results of previous MRS studies have shown AD-related abnormalities for several metabolites (Braakman et al., 2008; Chen et al., 2009; Choi et al., 2010; Dedeoglu et al., 2004; Marjanska et al., 2005; Oberg et al., 2008; von Kienlin M. et al., 2005; Westman et al., 2009; Xu et al., 2010). N-acetylaspartate (NAA) in the brain is predominantly present in neuronal cell bodies. Decreased NAA levels, indicating neuronal damage, have been found in tg mice in comparison to wild type (wt) mice (Chen et al., 2009; Choi et al., 2010; Dedeoglu et al., 2004; Marjanska et al., 2005; Oberg et al., 2008; von Kienlin M. et al., 2005). Myo inositol (mIns) and taurine play a role in osmoregulation and are mainly found in astrocytes of brain tissue. These metabolites were found to be higher in tg mice than in wt mice (Chen et al., 2009; Choi et al., 2010; Dedeoglu et al., 2004; Marjanska et al., 2005; Westman et al., 2009). Glutamate (glu) is an excitatory neurotransmitter, involved in learning, memory formation, and cognition, which is found to be decreased in mice with AD (Braakman et al., 2008; Choi et al., 2010; Dedeoglu et al., 2004; Marjanska et al., 2005; Oberg et al., 2008; von Kienlin M. et al., 2005).

Tg mouse models allow monitoring of the pathological and metabolic changes from the onset of AD in a longitudinal study, which is an effective way to investigate the early changes in the AD brain. However, no longitudinal study has been performed on AD mouse models using the non-invasive technique of MRS. Following mice from birth and investigating metabolic changes using MRS, the early start of AD might be detected making treatment more effective and giving us more insight in the pathogenesis of this disease.

Scope of this thesis

The overall aim of this thesis was to investigate MRI-based early markers of AD. We focused on correlation of radiological findings in AD with histology and we used MRS to study metabolic changes in brains of transgenic mice with AD.

Chapter 2 describes the effects of prolonged formalin fixation on MRI signal of brain tissue. This is important because such long fixed material is more readily available than brain tissue which is fixed for less than a year. In chapter 3 we compare different histological techniques to visualize iron in human brain tissue. Selection of the best techniques is crucial for reliable histological-radiological studies to assess the value of brain iron as an

MRI-based biomarker for AD.

Chapter 4 illustrates the relation between AD pathology and iron distribution in brain tissue of AD patients compared with normal aging subjects in different age groups. The difference of iron distribution between AD patients and aging was investigated in the frontal cortex.

Chapter 5 demonstrates a disturbed iron accumulation and myelin architecture in AD using MRI with histological correlation on ex vivo brain tissue.

In Chapter 6 we describe the first systematic longitudinal MRS study to investigate the differences in metabolic changes during development of AD in a transgenic mouse model.

Results of this thesis and recommendations for future studies are discussed in chapter 7.

Reference List

Alonso, A.C., Li, B., Grundke-Iqbal, I., Iqbal, K., 2008. Mechanism of tau-induced neurodegeneration in Alzheimer disease and related tauopathies. *Curr. Alzheimer Res.* 5, 375-384.

Andersen, K., Launer, L.J., Dewey, M.E., Letenneur, L., Ott, A., Copeland, J.R., Dartigues, J.F., Kragh-Sorensen, P., Baldereschi, M., Brayne, C., Lobo, A., Martinez-Lage, J.M., Stijnen, T., Hofman, A., 1999. Gender differences in the incidence of AD and vascular dementia: The EURODEM Studies. EURODEM Incidence Research Group. *Neurology* 53, 1992-1997.

Azevedo, D., Tatsch, M., Hototian, S.R., Bazzarella, M.C., Castro, C.C., Bottino, C.M., 2008. Proton spectroscopy in Alzheimer's disease and cognitive impairment no dementia: a community-based study. *Dement. Geriatr. Cogn Disord.* 25, 491-500.

Ballatore, C., Lee, V.M., Trojanowski, J.Q., 2007. Tau-mediated neurodegeneration in Alzheimer's disease and related disorders. *Nat. Rev. Neurosci.* 8, 663-672.

Bartzokis, G., 2011. Alzheimer's disease as homeostatic responses to age-related myelin breakdown. *Neurobiol. Aging* 32, 1341-1371.

Braakman, N., Oerther, T., de Groot, H.J., Alia, A., 2008. High resolution localized two-dimensional MR spectroscopy in mouse brain in vivo. *Magn Reson. Med.* 60, 449-456.

Brookmeyer, R., Johnson, E., Ziegler-Graham, K., Arrighi, H.M., 2007. Forecasting the global burden of Alzheimer's disease. *Alzheimer's Dement.* 3, 186-191.

Callahan, M.J., Lipinski, W.J., Bian, F., Durham, R.A., Pack, A., Walker, L.C., 2001. Augmented senile plaque load in aged female beta-amyloid precursor protein-transgenic mice. *Am. J. Pathol.* 158, 1173-1177.

Chamberlain, R., Wengenack, T.M., Poduslo, J.F., Garwood, M., Jack, C.R., Jr., 2011. Magnetic resonance imaging of amyloid plaques in transgenic mouse models of Alzheimer's disease. *Curr. Med. Imaging Rev.* 7, 3-7.

Chen, S.Q., Wang, P.J., Ten, G.J., Zhan, W., Li, M.H., Zang, F.C., 2009. Role of myo-inositol by magnetic resonance spectroscopy in early diagnosis of Alzheimer's disease in APP/PS1 transgenic mice. *Dement. Geriatr. Cogn Disord.* 28, 558-566.

Choi, J.K., Jenkins, B.G., Carreras, I., Kaymakcalan, S., Cormier, K., Kowall, N.W., Dedeoglu, A., 2010. Anti-inflammatory treatment in AD mice protects against neuronal pathology. *Exp. Neurol.* 223, 377-384.

Corder, E.H., Ghebremedhin, E., Taylor, M.G., Thal, D.R., Ohm, T.G., Braak, H., 2004. The biphasic relationship between regional brain senile plaque and neurofibrillary tangle distributions: modification by age, sex, and APOE polymorphism. *Ann. N. Y. Acad. Sci.* 1019, 24-28.

Crichton, R.R., Wilmet, S., Legssyer, R., Ward, R.J., 2002. Molecular and cellular mechanisms of iron homeostasis and toxicity in mammalian cells. *J. Inorg. Biochem.* 91, 9-18.

Dedeoglu, A., Choi, J.K., Cormier, K., Kowall, N.W., Jenkins, B.G., 2004. Magnetic resonance spectroscopic analysis of Alzheimer's disease mouse brain that express mutant human APP shows altered neurochemical profile. *Brain Res.* 1012, 60-65.

Doens, D., Fernandez, P.L., 2014. Microglia receptors and their implications in the response to amyloid beta for Alzheimer's disease pathogenesis. *J. Neuroinflammation.* 11, 48.

Dore, V., Villemagne, V.L., Bourgeat, P., Fripp, J., Acosta, O., Chetelat, G., Zhou, L., Martins, R., Ellis, K.A., Masters, C.L., Ames, D., Salvado, O., Rowe, C.C., 2013. Cross-sectional and longitudinal analysis of the relationship between A β deposition, cortical thickness, and memory in cognitively unimpaired individuals and in Alzheimer disease. *JAMA Neurol.* 70, 903-911.

Duyckaerts, C., Delatour, B., Potier, M.C., 2009. Classification and basic pathology of Alzheimer disease. *Acta Neuropathol.* 118, 5-36.

Ferri, C.P., Prince, M., Brayne, C., Brodaty, H., Fratiglioni, L., Ganguli, M., Hall, K., Hasegawa, K., Hendrie, H., Huang, Y., Jorm, A., Mathers, C., Me-

nezes, P.R., Rimmer, E., Scazufca, M., 2005. Global prevalence of dementia: a Delphi consensus study. *Lancet* 366, 2112-2117.

Fox, N.C., Freeborough, P.A., Rossor, M.N., 1996. Visualisation and quantification of rates of atrophy in Alzheimer's disease. *Lancet* 348, 94-97.

Frisoni, G.B., Fox, N.C., Jack, C.R., Jr., Scheltens, P., Thompson, P.M., 2010. The clinical use of structural MRI in Alzheimer disease. *Nat. Rev. Neurol.* 6, 67-77.

Grimm, A., Lim, Y.A., Mensah-Nyagan, A.G., Gotz, J., Eckert, A., 2012. Alzheimer's disease, oestrogen and mitochondria: an ambiguous relationship. *Mol. Neurobiol.* 46, 151-160.

Grundke-Iqbal, I., Iqbal, K., Quinlan, M., Tung, Y.C., Zaidi, M.S., Wisniewski, H.M., 1986. Microtubule-associated protein tau. A component of Alzheimer paired helical filaments. *J. Biol. Chem.* 261, 6084-6089.

Haacke, E.M., Cheng, N.Y., House, M.J., Liu, Q., Neelavalli, J., Ogg, R.J., Khan, A., Ayaz, M., Kirsch, W., Obenaus, A., 2005. Imaging iron stores in the brain using magnetic resonance imaging. *Magn Reson. Imaging* 23, 1-25.

Hardy, J., 2009. The amyloid hypothesis for Alzheimer's disease: a critical reappraisal. *J. Neurochem.* 110, 1129-1134.

Hardy, J., Selkoe, D.J., 2002. The amyloid hypothesis of Alzheimer's disease: progress and problems on the road to therapeutics. *Science* 297, 353-356.

Harrington, C.R., Storey, J.M., Clunas, S., Harrington, K.A., Horsley, D., Ishaq, A., Kemp, S.J., Larch, C.P., Marshall, C., Nicoll, S.L., Rickard, J.E., Simpson, M., Sinclair, J.P., Storey, L.J., Wischik, C.M., 2015. Cellular Models of Aggregation-dependent Template-directed Proteolysis to Characterize Tau Aggregation Inhibitors for Treatment of Alzheimer Disease. *J. Biol. Chem.* 290, 10862-10875.

Howell, M.D., Bailey, L.A., Cozart, M.A., Gannon, B.M., Gottschall, P.E., 2015. Hippocampal administration of chondroitinase ABC increases

plaque-adjacent synaptic marker and diminishes amyloid burden in aged APP^{sw}/PS1^{dE9} mice. *Acta Neuropathol. Commun.* 3, 54.

Hyman, B.T., Phelps, C.H., Beach, T.G., Bigio, E.H., Cairns, N.J., Carrillo, M.C., Dickson, D.W., Duyckaerts, C., Frosch, M.P., Masliah, E., Mirra, S.S., Nelson, P.T., Schneider, J.A., Thal, D.R., Thies, B., Trojanowski, J.Q., Vinters, H.V., Montine, T.J., 2012. National Institute on Aging-Alzheimer's Association guidelines for the neuropathologic assessment of Alzheimer's disease. *Alzheimers Dement.* 8, 1-13.

Jack, C.R., Jr., Knopman, D.S., Jagust, W.J., Shaw, L.M., Aisen, P.S., Weiner, M.W., Petersen, R.C., Trojanowski, J.Q., 2010. Hypothetical model of dynamic biomarkers of the Alzheimer's pathological cascade. *Lancet Neurol.* 9, 119-128.

Janicki, S.C., Schupf, N., 2010. Hormonal influences on cognition and risk for Alzheimer's disease. *Curr. Neurol. Neurosci. Rep.* 10, 359-366.

Kettenmann, H., Hanisch, U.K., Noda, M., Verkhratsky, A., 2011. Physiology of microglia. *Physiol Rev.* 91, 461-553.

Kidd, M., 1963. Paired helical filaments in electron microscopy of Alzheimer's disease. *Nature* 197, 192-193.

Lambracht-Washington, D., Rosenberg, R.N., 2015. A noninflammatory immune response in aged DNA Aβ₄₂-immunized mice supports its safety for possible use as immunotherapy in AD patients. *Neurobiol. Aging* 36, 1274-1281.

Landlinger, C., Oberleitner, L., Gruber, P., Noiges, B., Yatsyk, K., Santic, R., Mandler, M., Staffler, G., 2015. Active immunization against complement factor C5a: a new therapeutic approach for Alzheimer's disease. *J. Neuroinflammation.* 12, 150.

Ma, Y., Zhang, S., Li, J., Zheng, D.M., Guo, Y., Feng, J., Ren, W.D., 2014. Predictive accuracy of amyloid imaging for progression from mild cognitive impairment to Alzheimer disease with different lengths of follow-up: a systematic review. *Medicine (Baltimore)* 93, e150.

Marjanska, M., Curran, G.L., Wengenack, T.M., Henry, P.G., Bliss, R.L., Poduslo, J.F., Jack, C.R., Jr., Ugurbil, K., Garwood, M., 2005. Monitoring disease progression in transgenic mouse models of Alzheimer's disease with proton magnetic resonance spectroscopy. *Proc. Natl. Acad. Sci. U.S.A* 102, 11906-11910.

Meadowcroft, M.D., Connor, J.R., Smith, M.B., Yang, Q.X., 2009. MRI and Histological Analysis of Beta-Amyloid Plaques in Both Human Alzheimer's Disease and APP/PS1 Transgenic Mice. *Journal of Magnetic Resonance Imaging* 29, 997-1007.

Meadowcroft, M.D., Connor, J.R., Yang, Q.X., 2015a. Cortical iron regulation and inflammatory response in Alzheimer's disease and APPSWE/PS1DeltaE9 mice: a histological perspective. *Front Neurosci.* 9, 255.

Meadowcroft, M.D., Peters, D.G., Dewal, R.P., Connor, J.R., Yang, Q.X., 2015b. The effect of iron in MRI and transverse relaxation of amyloid-beta plaques in Alzheimer's disease. *NMR Biomed.* 28, 297-305.

Minati, L., Edginton, T., Bruzzone, M.G., Giaccone, G., 2009. Current concepts in Alzheimer's disease: a multidisciplinary review. *Am. J. Alzheimers Dis. Other Demen.* 24, 95-121.

Musicco, M., 2009. Gender differences in the occurrence of Alzheimer's disease. *Funct. Neurol.* 24, 89-92.

Nasrallah, I.M., Wolk, D.A., 2014. Multimodality imaging of Alzheimer disease and other neurodegenerative dementias. *J. Nucl. Med.* 55, 2003-2011.

Natte, R., Maat-Schieman, M.L., Haan, J., Bornebroek, M., Roos, R.A., van Duinen, S.G., 2001. Dementia in hereditary cerebral haemorrhage with amyloidosis-Dutch type is associated with cerebral amyloid angiopathy but is independent of plaques and neurofibrillary tangles. *Ann. Neurol.* 50, 765-772.

Oberg, J., Spenger, C., Wang, F.H., Andersson, A., Westman, E., Skoglund, P., Sunnemark, D., Norinder, U., Klason, T., Wahlund, L.O., Lindberg, M., 2008. Age related changes in brain metabolites observed by 1H MRS in

APP/PS1 mice. *Neurobiol. Aging* 29, 1423-1433.

Peters, D.G., Connor, J.R., Meadowcroft, M.D., 2015. The relationship between iron dyshomeostasis and amyloidogenesis in Alzheimer's disease: Two sides of the same coin. *Neurobiol. Dis.* 81, 49-65.

Price, J.L., Davis, P.B., Morris, J.C., White, D.L., 1991. The distribution of tangles, plaques and related immunohistochemical markers in healthy aging and Alzheimer's disease. *Neurobiol. Aging* 12, 295-312.

Qiu, C., Kivipelto, M., von, S.E., 2009. Epidemiology of Alzheimer's disease: occurrence, determinants, and strategies toward intervention. *Dialogues. Clin. Neurosci.* 11, 111-128.

Richter, M., Mewes, A., Fritsch, M., Krugel, U., Hoffmann, R., Singer, D., 2014. Doubly Phosphorylated Peptide Vaccines to Protect Transgenic P301S Mice against Alzheimer's Disease Like Tau Aggregation. *Vaccines. (Basel)* 2, 601-623.

Rupsingh, R., Borrie, M., Smith, M., Wells, J.L., Bartha, R., 2011. Reduced hippocampal glutamate in Alzheimer disease. *Neurobiol. Aging* 32, 802-810.

Smith, M.A., Harris, P.L., Sayre, L.M., Perry, G., 1997. Iron accumulation in Alzheimer disease is a source of redox-generated free radicals. *Proc. Natl. Acad. Sci. U.S.A* 94, 9866-9868.

Takahashi, R.H., Capetillo-Zarate, E., Lin, M.T., Milner, T.A., Gouras, G.K., 2010. Co-occurrence of Alzheimer's disease amyloid and tau pathologies at synapses. *Neurobiol. Aging* 31, 1145-1152.

Thal, D.R., Attems, J., Ewers, M., 2014. Spreading of amyloid, tau, and microvascular pathology in Alzheimer's disease: findings from neuropathological and neuroimaging studies. *J. Alzheimers Dis.* 42 Suppl 4, S421-S429.

van Duijn, S., Nabuurs, R.J., van Duinen, S.G., Natta, R., 2013. Comparison of histological techniques to visualize iron in paraffin-embedded brain tissue of patients with Alzheimer's disease. *J. Histochem. Cytochem.* 61,

785-792.

van Rooden, S., Maat-Schieman, M.L., Nabuurs, R.J., van der Weerd, L., van Duijn, S., van Duinen, S.G., Natta, R., van Buchem, M.A., van der Grond, J., 2009. Cerebral amyloidosis: postmortem detection with human 7.0-T MR imaging system. *Radiology* 253, 788-796.

Villemagne, V.L., Burnham, S., Bourgeat, P., Brown, B., Ellis, K.A., Salvado, O., Szoëke, C., Macaulay, S.L., Martins, R., Maruff, P., Ames, D., Rowe, C.C., Masters, C.L., 2013. Amyloid beta deposition, neurodegeneration, and cognitive decline in sporadic Alzheimer's disease: a prospective cohort study. *Lancet Neurol.* 12, 357-367.

von Kienlin M., Kunnecke, B., Metzger, F., Steiner, G., Richards, J.G., Ozmen, L., Jacobsen, H., Loetscher, H., 2005. Altered metabolic profile in the frontal cortex of PS2APP transgenic mice, monitored throughout their life span. *Neurobiol. Dis.* 18, 32-39.

Wang, H., Megill, A., He, K., Kirkwood, A., Lee, H.K., 2012. Consequences of inhibiting amyloid precursor protein processing enzymes on synaptic function and plasticity. *Neural Plast.* 2012, 272374.

Wang, J., Tanila, H., Puolivali, J., Kadish, I., van, G.T., 2003. Gender differences in the amount and deposition of amyloidbeta in APP^{swe} and PS1 double transgenic mice. *Neurobiol. Dis.* 14, 318-327.

Weller, R.O., Preston, S.D., Subash, M., Carare, R.O., 2009. Cerebral amyloid angiopathy in the aetiology and immunotherapy of Alzheimer disease. *Alzheimers Res. Ther.* 1, 6.

Westman, E., Spenger, C., Oberg, J., Reyer, H., Pahnke, J., Wahlund, L.O., 2009. In vivo ¹H-magnetic resonance spectroscopy can detect metabolic changes in APP/PS1 mice after donepezil treatment. *BMC. Neurosci.* 10, 33.

Wischik, C.M., Harrington, C.R., Storey, J.M., 2014. Tau-aggregation inhibitor therapy for Alzheimer's disease. *Biochem. Pharmacol.* 88, 529-539.

Wischik, C.M., Staff, R.T., Wischik, D.J., Bentham, P., Murray, A.D., Storey, J.M., Kook, K.A., Harrington, C.R., 2015. Tau aggregation inhibitor therapy: an exploratory phase 2 study in mild or moderate Alzheimer's disease. *J. Alzheimers Dis.* 44, 705-720.

Wittchen, H.U., Jacobi, F., Rehm, J., Gustavsson, A., Svensson, M., Jons-son, B., Olesen, J., Allgulander, C., Alonso, J., Faravelli, C., Fratiglioni, L., Jennum, P., Lieb, R., Maercker, A., van, O.J., Preisig, M., Salvador-Carulla, L., Simon, R., Steinhausen, H.C., 2011. The size and burden of mental disorders and other disorders of the brain in Europe 2010. *Eur. Neuropsychopharmacol.* 21, 655-679.

Xu, W., Zhan, Y.Q., Huang, W., Wang, X.X., Zhang, S.M., Lei, H., 2010. Reduction of Hippocampal N-Acetyl Aspartate Level in Aged APP(Swe)/PS1(dE9) Transgenic Mice Is Associated With Degeneration of CA3 Pyramidal Neurons. *Journal of Neuroscience Research* 88, 3155-3160.

Chapter 2

MRI artifacts in human brain tissue after prolonged formalin storage

Sara van Duijn, MSc* 1, Rob J.A. Nabuurs MD, PhD* 2, Sanneke van Rooden PhD 2, Marion L.C. Maat-Schieman, MD, PhD 3, Sjoerd G. van Duinen MD, PhD 1, Mark A. van Buchem, MD, PhD 2, Louise van der Weerd, PhD 2,4, Remco Naté, MD, PhD 1

* Authors have contributed to this work equally

Departments of Pathology (1), Radiology (2), Neurology (3) and Anatomy & Embryology (4), Leiden University Medical Centre, Leiden, the Netherlands

Mag Reson Med. 2011 June; 65 (6): 1750-1758

Abstract

For the interpretation of magnetic resonance imaging (MRI) abnormalities in brain pathology, often *ex vivo* tissue is used. The purpose of this study was to determine the pathological substrate of several distinct forms of MR hypointensities that were found in formalin-fixed brain tissue with amyloid-beta deposits. Samples of brain cortex were scanned using effective transverse relaxation time-weighted protocols at several resolutions on a 9.4T MRI scanner. High resolution MRI showed large coarse hypointensities throughout the cortical gray and white matter, corresponding to macroscopic discolourations and microscopic circumscribed areas of granular basophilic neuropil changes, without any further specific tissue reactions or amyloid-beta related pathology. These coarse MRI hypointensities were identified as localized areas of absent neuropil replaced by membrane/myelin sheath remnants using electron microscopy. Interestingly, the presence/absence of these tissue alterations was not related to amyloid deposits, but strongly correlated to the fixation time of the samples in unrefreshed formalin. These findings show that prolonged storage of formalin fixed brain tissue results in subtle histology artifacts, which show on MRI as hypointensities that on first appearance are indistinguishable from genuine brain pathology. This indicates that postmortem MRI should be interpreted with caution, especially if the history of tissue preservation is not fully known.

Keywords: MRI, *ex vivo*, formalin

Introduction

Magnetic resonance imaging (MRI) of postmortem brain tissue offers a valuable research method to study disease related changes in image contrast, because the findings can be correlated to histology (1-12). High resolution ex vivo imaging has been a useful tool in interpreting the MRI features of many neurodegenerative disorders, including multiple sclerosis (MS), Alzheimer's disease (AD), and (sporadic) cerebral amyloid angiopathy (1-3, 6-9, 11, 12). However, the MR characteristics of the tissue rapidly change in the postmortem situation because of tissue decomposition and chemical fixation; therefore direct translation of the findings to the clinical setting has to be done with caution (13-19).

First, tissue decomposition occurs during the postmortem interval (PMI), the time period between the patient's somatic death and beginning of the immersion-fixation of the tissue, which varies among subjects. Several studies have shown that an increasing PMI leads to a reduction of T1 and T2 (13, 15, 20). However, a more recent study suggested that these findings might mainly be due to tissue dehydration or the fixative itself. When these effects were minimized, proton density, T1 and T2 values all increased with longer PMI (17). Also, mean diffusivity and fractional anisotropy decrease with prolonged PMI (17, 21).

After autopsy, brain tissue will be immersed into a solution containing a chemical fixative, most frequently being formalin also known as formaldehyde. These solutions preserve tissue by slowly diffusing into it, leading to the cross-linking of proteins and immobilization of water molecules, thereby preventing autolysis and tissue decomposition (21-23). By its nature it is to be expected that this would affect MR characteristics, which indeed was confirmed by several postmortem brain MRI studies. A reverse in gray matter (GM)/white matter (WM) T1 contrast occurs within several days of fixation, merely due to a rapid decline in the latter combined with a general decrease in both continuing at least up to 3 months (18). Similarly, T2 relaxation declines with prolonged fixation affecting both GM and WM, reaching a stable plateau as shown by consecutively imaging up to 6 months fixation (13-15, 18).

All of the above has led to important considerations on the correct method to obtain and interpret postmortem MR images (13, 15).

However, similar studies investigating the effect of long fixation periods (> 6 months) on the MR characteristics have not yet been published. Nevertheless, this question is important, especially when using rare ma-

Table 1

Subject characteristics and corresponding macroscopic, MRI and histology scores

| Subject nr. | Age / Sex (yr) | Post mortem pathologic evaluation | Fixation period (yr) | PMI (hrs) | Macroscopic discoloration | Coarse MR Hypo intensities | Granular neuropil changes |
|-------------|----------------|-----------------------------------|----------------------|-----------|---------------------------|----------------------------|---------------------------|
| 1 | 88/F | AD | 0.3 | | Absent | Absent | Absent |
| 2 | 29/M | Control | 0.3 | | Absent | Absent | Absent |
| 3 | 70/F | sCAA | 0.5 | | Absent | Absent | Absent |
| 4 | 53/M | Control | 0.5 | | Absent | Absent | Absent |
| 5 | 53/M | Control | 0.5 | | Absent | Absent | Absent |
| 6 | 71/M | sCAA | 0.5 | | Absent | Unknown | Absent |
| 7 | 49/M | DS | 1 | 13 | Absent | Absent | Absent |
| 8 | 64/M | AD | 6 | 48 | Present | Present | Present |
| 9 | 58/M | HCHWA-D | 6 | 6 | Present | Present | Present |
| 10 | 73/M | AD | 7 | 9 | Present | Present | Present |
| 11 | 65/F | AD | 7 | 2 | Present | Extensive | Present |
| 12 | 50/F | HCHWA-D | 9 | 21 | Present | Extensive | Extensive |
| 13 | 45/F | HCHWA-D | 15 | | Present | Extensive | Extensive |
| 14 | 90/F | AD | 16 | | Present | Extensive | Extensive |
| 15 | 52/M | HCHWA-D | 17 | 1 | Present | Extensive | Extensive |
| 16 | 62/F | DS | 19 | | Present | Extensive | Extensive |
| 17 | 62/M | Control | 26 | | Present | Extensive | Extensive |
| 18 | 58/F | AD | 42 | 14 | Present | Extensive | Extensive |

M = Male; F = Female; sCAA = sporadic cerebral amyloid angiopathy; DS = Down's syndrome; AD = Alzheimer's disease; HCHWA-D = hereditary cerebral hemorrhage with amyloid Dutch type; PMI = Postmortem interval; MRI coarse hypointensities: Absent = 0; Present = 1 -10 hypointensities in one image; Extensive \geq 10 hypointensities in at least one of the two examined images. Granular neuropil changes: Absent = 0; Present = 1-4 changes per section; Extensive \geq 5 changes in at least 1 of the 3 sections.

terial from tissue archives, which are stored using fixatives like formalin for periods ranging from several years to decades. In a recent study using archival tissue with prolonged fixation times, we noticed unusually large coarse hypointensities, especially apparent on high resolution effective transverse relaxation time (T2*) weighted images, in several brain samples regardless of their pathological diagnosis. We hypothesized that these coarse hypointensities were the result of the extended formalin fixation period.

Therefore, the purpose of this study was to investigate the occurrence of these T2* changes with respect to their formalin fixation time in brain samples with different pathologies. To this end, MR images were obtained of 18 samples with fixation times ranging from 3 months to several decades. Subsequently, the samples were evaluated both macroscopically and microscopically to identify the occurrence and the microscopic substrate of tissue changes due to prolonged fixation.

Table 2: Granular neuropil changes of long and short fixed tissue from the same subjects.

| Subject | Age / Sex (yr) | Port mortem diagnosis | Granular neuropil changes | |
|---------|-------------------|--------------------------|------------------------------|-----------|
| | | | Fixation period: < 0.5 yr | 9 - 42 yr |
| 13 | 45/F | HCHWA-D | - | + |
| 15 | 52/M | HCHWA-D | - | + |
| 17 | 62/M | Control | - | + |
| 18 | 58/F | AD | - | + |

HCHWA-D = Hereditary cerebral hemorrhage with amyloid Dutch type,

AD = Alzheimer's disease

Materials and Methods

Subjects

We used brain tissue of six patients with AD, four patients with Hereditary Cerebral Haemorrhage with Amyloidosis, Dutch type (HCHWA-D), two patients with Down's Syndrome (DS), two patients with sporadic Cerebral Amyloid Angiopathy (CAA) and four control brains (Table 1). The brain tissue had been routinely immersed in buffered 10% formalin for several weeks to 6 months after which the wet tissue was archived in sealed plastic bags with a small excess of 10% formalin. Total fixation times varied from 4 months to 42 years. From a subset of subjects, several samples of the exact same brain had also been paraffin embedded at the beginning of their fixation process, normally within 1 month postmortem. This allowed a direct comparison of structural changes with tissue from the same patients that was archived in formalin and embedded in paraffin several years later (Table 2).

Table 3: pH-measurements

| Subject | Post mortem diagnosis | Fixation period (yr) | pH |
|----------------|--------------------------|-------------------------|------|
| 5 | Control | 0.5 | 6.62 |
| 12 | HCHWA-D | 9 | 6.11 |
| 15 | HCHWA-D | 17 | 4.98 |
| 17 | Control | 26 | 5.43 |
| 18 | AD | 42 | 5.12 |
| Fresh formalin | | | 7 |

HCHWA-D = Hereditary cerebral hemorrhage with amyloid Dutch type, AD = Alzheimer's disease

Magnetic Resonance Imaging

A slice of 20x15 mm brain tissue was selected from each subject and cut into a 4-mm-thick slice using a vibratome (VT1000S, Leica Microsystems, Wetzlar,

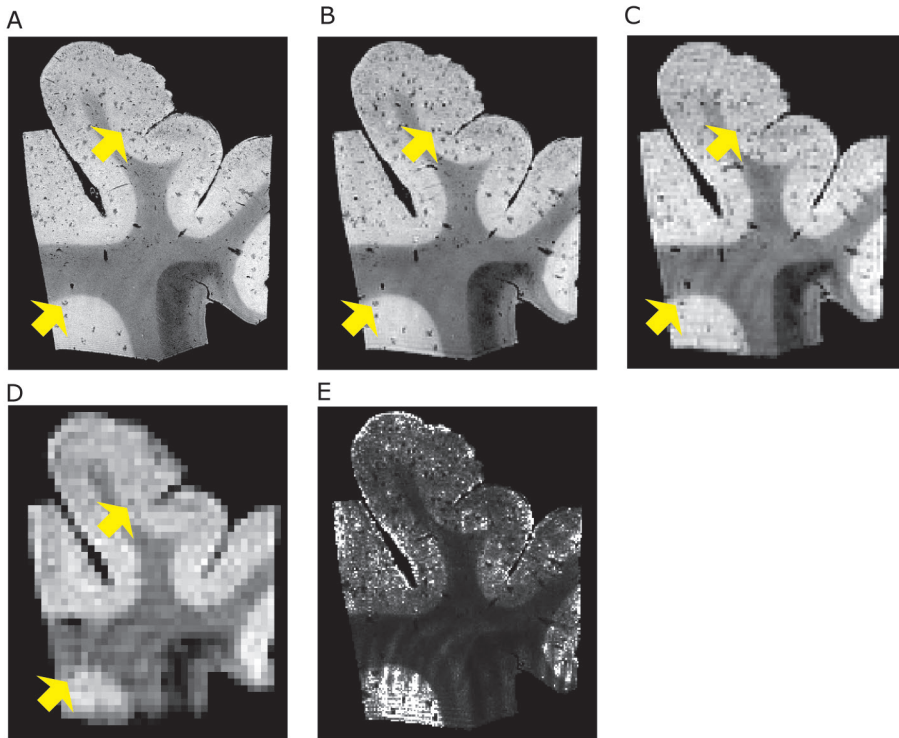


Figure 1: Similar T2* weighted MR images of subject 14 acquired with isotropic resolution of respectively A) 40 μm, B) 100 μm, C) 200 μm and D) 400 μm. Many coarse hypo intensities are detected in the higher resolution, but even in D) hypo intense voxels correlate back to them (white arrows). E) Shows the calculated T2* map of the section in B) with the previously seen hypo intensities having a lower T2* then the surrounding tissue.

Germany). The 4-mm slice was placed in a custom made tissue holder, immersed in a proton-free fluid (Fomblin, Solvay, Solexis, Milan, Italy) and positioned in a vertical small-bore 9.4T Bruker Avance 400WB MRI system, equipped with a 1T/m actively-shielded gradient insert and Paravision 4.0 imaging software (Bruker Biospin, Ettlingen, Germany). A 20-mm birdcage transmit/receive coil was used (Bruker BioSpin). Several three dimensional T2*-weighted gradient echo sequences were obtained with isotropic resolutions of 40 – 100 – 200 – 400 μm with the number of signal averages being 60 – 20 – 20 – 12 respectively, echotime/pulse repetition time = 12.26 / 75 ms, flip angle = 25°. With the matrix size depending on the shape of each sample, average scan time per resolution were 28 hrs, 2 hrs 40 min, 20 min. and 8 min respectively. For quantitative T2* measurements, 100 μm scans were also acquired using echo time = 8 – 10 – 12.26 – 15 ms.

Histology

Following MRI, brain slices were paraffin-embedded and serially cut in 8- μ m sections. Consecutive sections were stained for general microscopic morphology (hematoxylin and eosin (HE)), for myelin (Kluver-Barrera), for iron (Perls and a modified Perls DAB) (24), (FEIII-DAB, FEII-DAB) (25), copper (Romeis) and immunohistochemistry for A β (Dako, 6F/3D) (26), and glial fibrillary acidic protein (GFAP) (Dako, 6F2) (27). To allow correlation with MRI, sections were digitalized using a flatbed scanner (Agfa).

Electron microscopy

Electron microscopy was performed on a subset of subjects (Table 2) as previously described (28). Collection was done on copper grids instead of carbon grids. Sections were examined using a JEOL JEM-1011 electron microscope operating at 60 kV and digitalized using a MegaView III camera.

Analysis / Scoring

Two sequential MR slices from the three dimensional data sets at 40 μ m resolution were examined for "coarse" hypointensities defined by large size (120-1200 μ m), irregular contour and elongated to stellate shape. These coarse hypointensities were scored as follows: absent: 0 coarse hypo intensities, present: 1-9 coarse hypointensities, extensive: ≥ 10

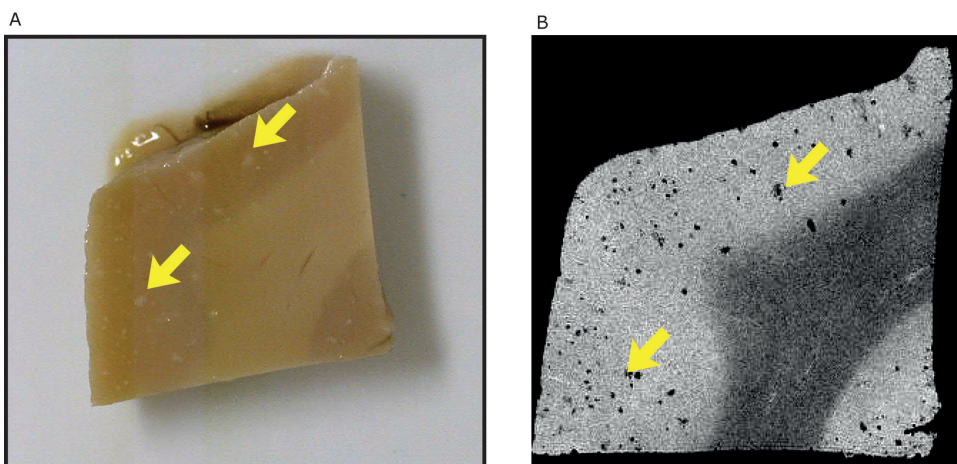


Figure 2: Images from subject 13 showing A) fixated brain tissue with white discolorations (white arrows) and B) high resolution (40 μ m) T2* weighted MR images of the same brain tissue with coarse hypointensities (white arrows).

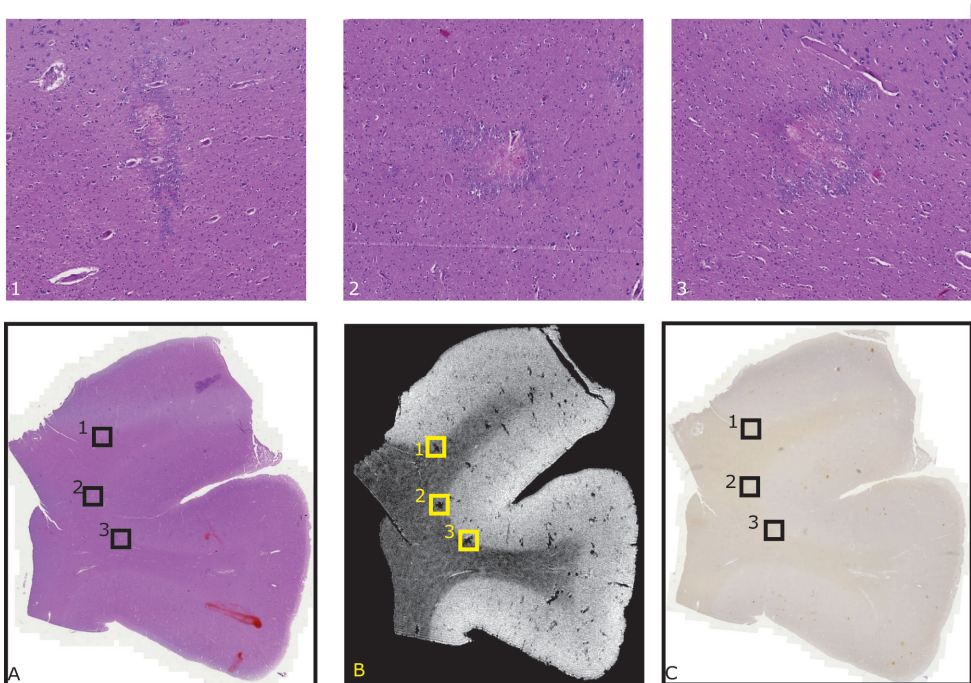


Figure 3: Images of subject 17. Comparison of MR image with HE staining and A β staining correlating the granular neuropil changes with the hypointensities in the MRI. The rectangles are the locations of 10x magnifications 1, 2 and 3. Showing that granular neuropil changes can be found at the same location as the hypo intensities but without amyloid deposition. Scale bars are given. A: HE staining; B: MR image; C: A β staining

coarse hypointensities. Three HE stained sections from the same level of the two sequential MRI slices were used to correlate MR images with histology. To perform these correlations, we used Adobe Photoshop 6.0 to visually overlay digitalized histological sections to their corresponding MR images. Of each patient, the same HE sections were used to score the amount of granular neuropil changes as follows: absent if no granular neuropil changes were found, present for 1-4 and extensive for ≥ 5 neuropil changes in at least one out of the three sections.

Subjects with similar score were combined for group analysis (Mann-Whitney) to find significant differences (P-value < 0.05) in fixation period and age (SPSS 17).

pH of formalin

Of five patients with widely variable fixation times (Table 3), the pH of the formalin around the brain slices in sealed plastic bags was determined using a logging pH meter (Hanna, H1 98230).

Results

Magnetic resonance imaging

High resolution T2*W images of 11 subjects showed irregularly contoured, elongated and stellate shaped hypointensities that were randomly distributed throughout the cortical gray matter and to a lesser degree in the white matter (Fig.1A). Their typical size (120 – 1200 μ m) and characteristic shape allowed clear distinction from possible other brain structures known to have a similar effect on T2*, e.g., blood vessels or small roundish hypointensities caused by amyloid- β (A β) plaques, especially when including their spatial orientation (Fig.4). Based on these characteristics, we defined them as “coarse hypointensities” and tissue was scored according to their presence (Table 1).

When comparing similar MR images of the same section at decreasing resolution (Fig.1A-D), these coarse hypointensities became less pronounced and harder to recognize as such. This depended on their actual size and shape being affected by partial volume effects due to increasing voxel size. High and low resolution data were compared with assess, if hypointense voxels on low resolution scans correlated with coarse hypointensities at high resolution. The largest coarse hypointensities were also visible at the lowest isotropic resolution of 400 μ m, which is comparable to the in vivo MRI resolution (Fig.1D). On quantitative T2* maps, areas containing coarse hypointensities caused a clearly noticeable decrease in T2* (Fig. 1E).

Pathology

Macroscopy

Only in brain tissue with coarse hypointensities on MRI, well circumscribed, white discolourations with similar size and distribution as the coarse MRI hypointensities were observed (Fig. 2, Table 1).

Histology

Microscopically, HE sections of tissue blocks with macroscopic white discolourations showed neuropil alterations with a close spatial correlation to the coarse MRI hypointensities (Fig. 3 and 4). These neuropil alterations comprised irregular, well circumscribed areas of granular, basophilic changes usually with some tissue rarefaction (Fig. 5). The corresponding Kluver’s staining within these areas was decreased with respect to sur-

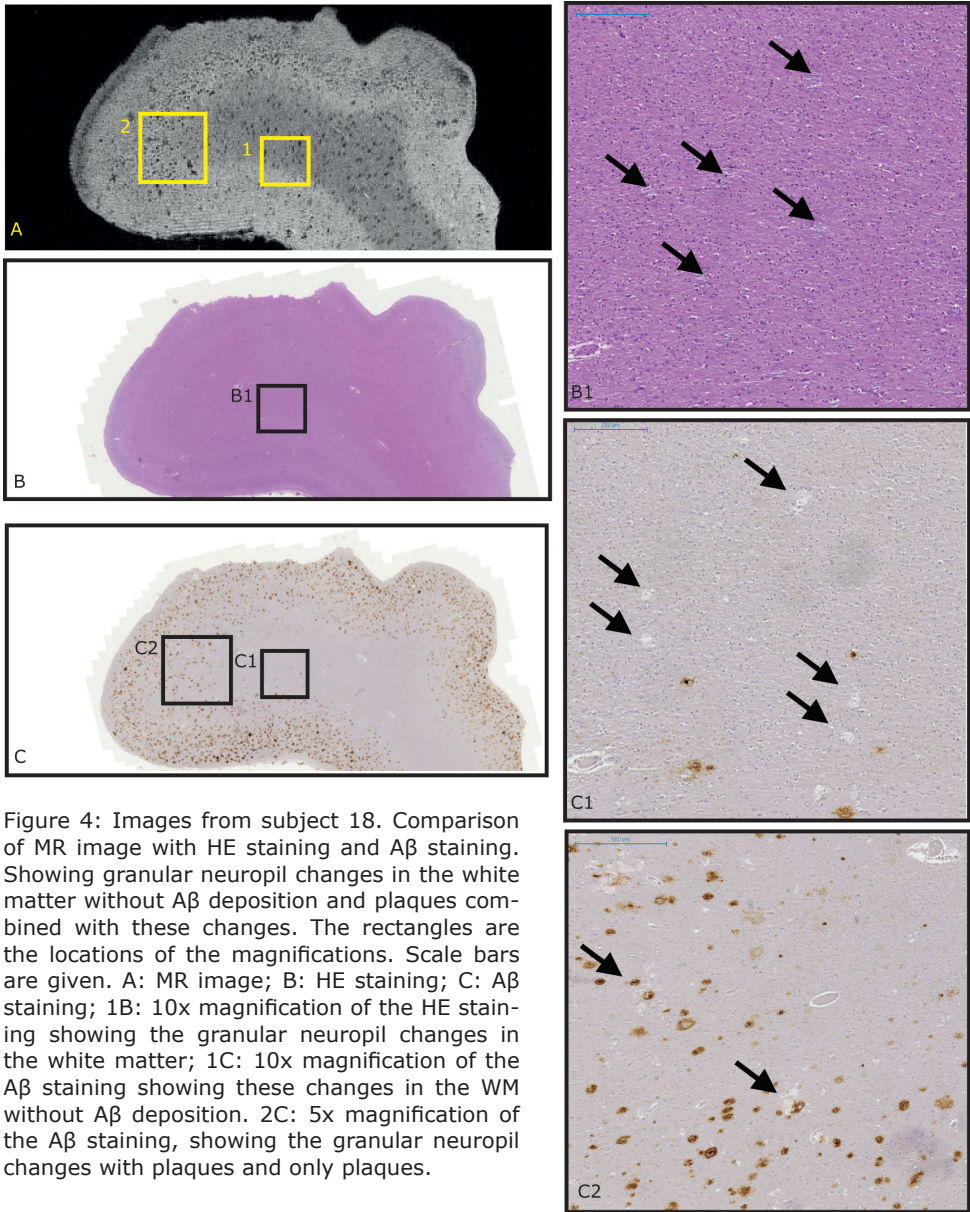


Figure 4: Images from subject 18. Comparison of MR image with HE staining and A β staining. Showing granular neuropil changes in the white matter without A β deposition and plaques combined with these changes. The rectangles are the locations of the magnifications. Scale bars are given. A: MR image; B: HE staining; C: A β staining; 1B: 10x magnification of the HE staining showing the granular neuropil changes in the white matter; 1C: 10x magnification of the A β staining showing these changes in the WM without A β deposition. 2C: 5x magnification of the A β staining, showing the granular neuropil changes with plaques and only plaques.

rounding cortex/white matter suggesting a lower density of myelin. Most of these areas showed birefringence under polarized light in the HE that was not seen in unstained sections or the Kluver's stain that excludes the presence of anorganic material. The areas of basophilic granular neuropil changes were randomly distributed throughout the cortex and increasingly present in the white matter of tissue with long fixation times. These areas were found around vessels but also apart from vessels. The basophilic granular neuropil changes showed no signs of gliosis, haemorrhages or infarcts. Neurons, astrocytes, microglia and vessels were normally distributed within these areas and morphologically unaltered. Gemistocytes were not present. Furthermore, all (immuno) histological stainings for iron, copper and amyloid- β were negative within these areas (Fig. 4). The basophilic granular neuropil changes were found not only in AD material but also in long fixated brain tissue of controls (Fig. 3 and 4). In contrast, these changes were not found in short fixated AD material. Apart from the coarse hypointensities that co-localized with neuropil degeneration, other small roundish hypointensities were observed on MRI that did correspond to amyloid plaques (Fig. 4).

Electron microscopy

Tissue with macroscopic white discolourations showed localized areas with absent neuropil, although vessels were often present in these spaces on 1 μm -thick, epoxy embedded tissue sections stained with toluidine blue. Electron microscopy of immediately adjacent ultrathin sections showed that these areas with absent neuropil actually consisted of spaces without any neuropil or only little neuropil remnants (Fig. 6A). However, in these spaces varying amounts of lamellar structures were

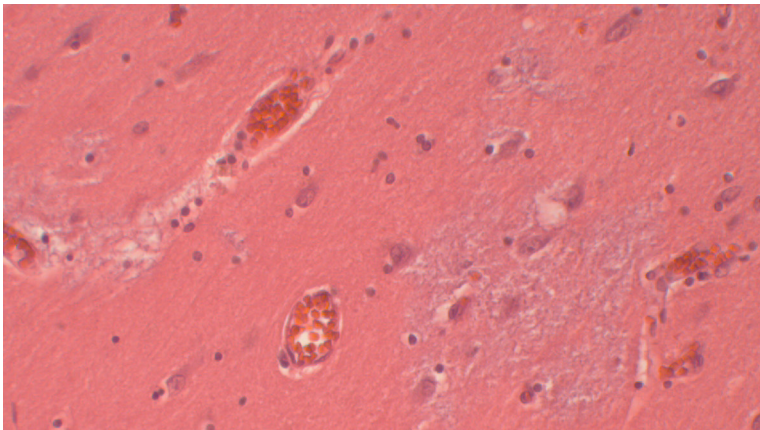


Figure 5: HE 20x
Granular neuropil
changes

found, which were interpreted as membrane remnants and/or swollen degenerated myelin sheaths (Fig. 6B-C). Outside these circumscribed areas, we observed variable splitting and swelling of myelin sheets ranging from little splitting in otherwise normal myelin sheaths around axons, to swollen myelin sheaths lining small empty spaces within the neuropil (Fig. 6D-E).

Relation of coarse MR hypointensities with fixation duration

The presence of coarse MR hypointensities, macroscopic and microscopic abnormalities were scored for each subject and the results are shown in Table 1. Subjects with similar scores were combined for group analysis.

With regard to coarse MR hypointensities, fixation periods were significantly shorter when scored "absent" compared to "present" (P-value = 0.017 / $r = -0.79$). Furthermore, with even longer fixation periods, the number of hypointensities significantly increases when comparing "present" with "extensive" (P-value = 0.018 / $r = -0.71$).

Similar results were obtained when comparing groups with different scores for granular neuropil changes. Fixation periods of those scored "absent" were significantly shorter when compared with those who scored "present" (P-value = 0.006 / $r = -0.82$), which was significantly shorter as compared to "extensive" cases (P-value = 0.008 / $r = -0.80$).

No significant differences in subject's age between groups were found for either coarse hypointensity, histological or macroscopic score. Furthermore, no correlation was found between coarse MR hypointensities and presence/absence of disease regardless of type of disease.

In summary, brain tissue showed no changes when fixed for a period of < 1 year in the same formalin solution, whereas changes were always present in tissue fixed for a period of > 6 year, and increasingly so with longer fixation periods.

To test the hypothesis that prolonged formalin fixation indeed leads to histological and MR detectable changes, brain tissue from the same subject that was formalin fixed for either a short or a much longer period was compared microscopically (Table 2). In the long-term fixed material, macroscopic white discolourations and granular neuropil changes were present, whereas short-term fixed material of the same subject completely lacked these findings, indeed supporting our hypothesis.

To obtain a complete picture, pH measurements were performed, because

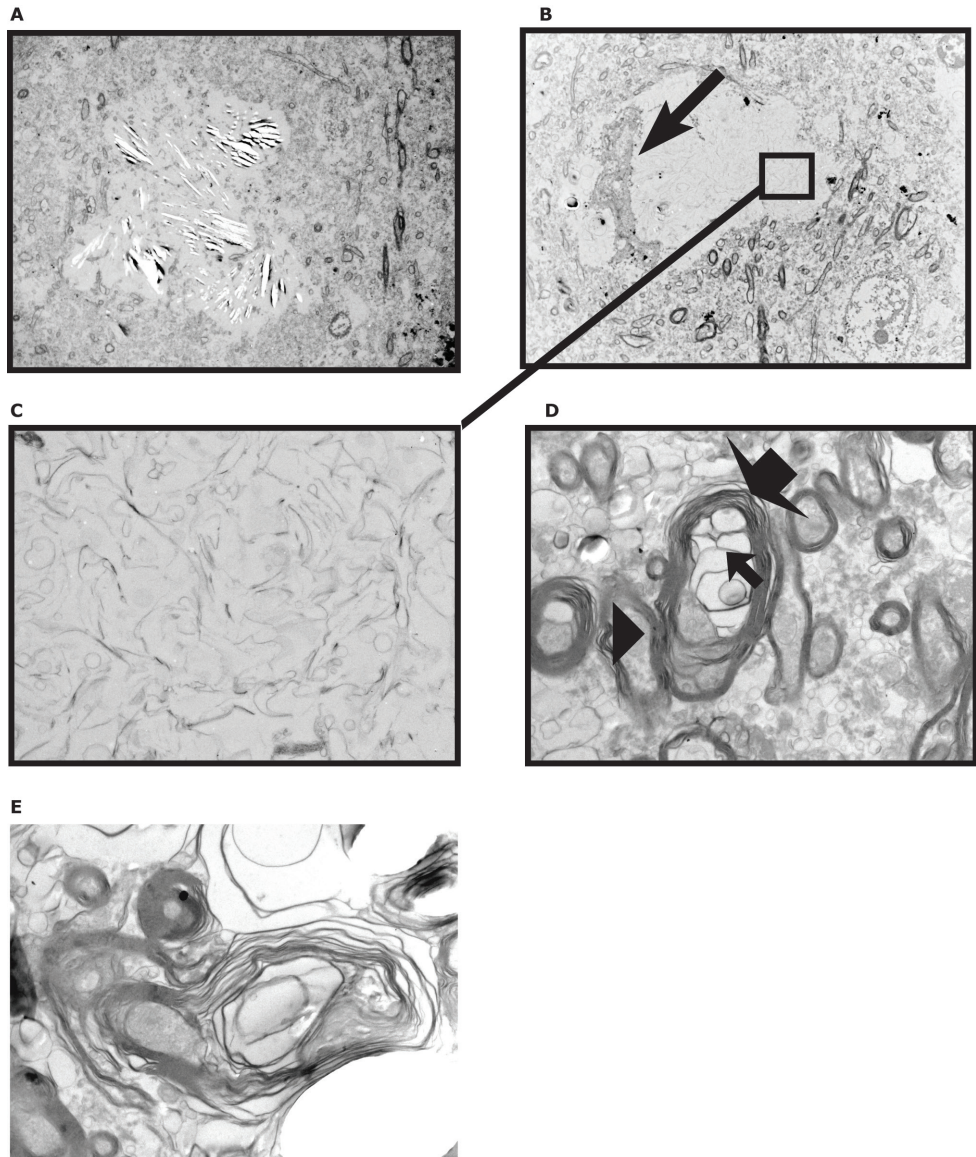


Figure 6: Ultrastructure of localized areas of nearly empty spaces on semithin sections in long term formalin fixed tissue with macroscopic white discolourations. A) These areas consisted of spaces without neuropil or only little neuropil remnants and often but not always contained a small blood vessel (1200X) B) Circumscribed area of absent neuropil showing lamellar structures and a capillary (arrow) (1200X). C) Lamellar structures in B (15000X). D) myelinated axons, some with splitting of the myelin sheath. One axon (arrowhead) shows myelin splitting (large arrow) with little expansion of the spaces between the myelin sheaths (small arrow) (15000X). E) myelinated axon partly with intact myelin sheath and partly with myelin splitting with transition to more laminated structures with increasing spaces between the lamellae.

formalin solutions are known to become more acidic over time. pH measurements indeed showed increased acidity after longer periods of formalin fixation, as observed in the sealed plastic bags used for tissue storage (Table 3).

Discussion and Conclusion

In this study, “coarse hypointensities” on postmortem brain MRI were seen corresponding to localized areas of neuropil destruction with remnants of membranes and myelin sheaths as observed by electron microscopy. These coarse hypointensities are mainly detected at high-resolution MR scans. Although brain tissue from A β -related diseases was used, the hypointensities were not related to deposits of iron, copper or A β correlating with these neurological diseases. Instead, these hypointensities appear to be an artifact associated with the duration of fixation within the same formalin. This can be concluded from the findings that these hypointensities were also detected in control tissue with long fixation times, and were not found in disease-related tissue fixated for a short period.

The exact mechanism of the described storage related artifacts is not known from previous studies, but formalin solutions are known to become more acidic over time (29). This was confirmed by pH measurements of the excess formalin around our sealed fixed brain tissue. Possibly neuropil destruction is caused by a local increase of acidity. However, continuous exposure to formalin and/or formic acid may form many other compounds that possibly play a role in causing artifactual tissue changes (29, 30). We were not able to study the effect of long term fixation in regularly refreshed formalin, and we can thus not exclude prolonged immersion in formalin itself as a cause of local neuropil destruction leading to MR hypointensities rather than the increasing acidity or the formation of aggressive metabolites. Postmortem autolysis does not appear to be the cause of the artifacts we have observed.

For this study, sufficient material fixed for a period of 1-6 years was lacking. Consequently, we can only conclude that neuropil artifacts occur in all tissue stored for a period of at least 6 years within the same formalin, whereas tissue stored for a period of <1 year showed no changes.

The coarse hypointensities correspond macroscopically to homogeneous white discolourations in the tissue, and microscopically in 8 μ m HE sections to granular neuropil alterations with slightly less density than the surrounding neuropil. The ultrathin sections (90 nm thick) used for EM re-

vealed that these areas represented absent neuropil with partial filling of the resulting spaces by membrane-like structures. We speculate that this degenerated membranous/proteineous material with weak birefringence causes hypointensities on MRI because of its solid-state-like properties. The low signal intensity on MRI may also result from replacement of formalin solution by proton free fluid in these relatively more empty spaces. However, a decrease in proton density would not cause a T2* decrease, as was observed in the T2* maps.

With respect to the induced MR changes, previous reports state that formalin fixation causes changes in relaxation and diffusion properties, thereby altering MR contrast, even though the exact mechanism remains unclear (16). However, these changes in MR properties occur throughout the entire sample and are partially reversible by rehydrating the sample in PBS. In contrast, the structural disruptions we found after prolonged formalin fixation are very localized and irreversible. Furthermore, detected changes were not related to any of the known possible changes due to prolonged PMI as described elsewhere (13,15,17,20,21). For this study brain tissue of all kinds of PMI periods was used, and no correlation was found with either the tissue changes or MRI hypointensities (Table 1).

The conclusion of this study suggests that data of several earlier published studies, using postmortem brain tissue of patients with AD for MRI (1-12), should be cautiously interpret. In these studies, hypointense spots were observed on T2* or T2-weighted scans that co-localized with dense amyloid plaques and iron accumulations (1-12). However, brain tissue in these studies was collected within a short period, and fixed for a maximum period of a few months.

With regard to the detection of amyloid plaques, we also observed hypointense spots on MRI that corresponded to the presence of amyloid plaques. However, these did not correlate with the larger stellar shape coarse hypointensities (Fig.4). The possible A β plaque detection indicates that the basic mechanisms for MR contrast (iron accumulation and dense protein aggregates) are still present. On ultrahigh resolution scans, these different hypointensities can be easily distinguished. However, on scans with a lower resolution, e.g., those comparable with resolutions that can be achieved on clinical MRI systems, both forms might become indistinguishable, and based on their size the coarse hypointensities because of fixation artifacts are more likely to remain visible (Fig. 1D). In our

study, these low resolution images were acquired at relatively short echo times; when a stronger T2*-weighting would be used, more hypointensities would be observable at these lower resolutions. Furthermore, it is important to realize that although these neuropil changes are beyond the anatomical resolution of scans with clinical resolutions, they could still be visible on such scans because their signal differs so strongly from surrounding tissue.

Other known sources for hypointensities on T2*-weighted images, like calcifications, iron deposits, microbleeds or cavernous malformations (31) could be easily disregarded within this study, whereas their presence could not be confirmed on histology. However, especially when conducting similar ex vivo MR studies for either one of these pathologies using old brain material and clinically relevant resolutions, one should be aware that the described formalin fixation artifacts could possibly lead to similar hypointensities and thus a misinterpretation of the data.

To put our findings into a broader perspective, a small survey was conducted among eight other brain banks and neuropathology departments regarding their brain storage protocol. Three of these centres store their formalin-fixed brain tissue in sealed plastic bags with little excess formalin similar to the tissue used in this study, whereas four other centres store fixed brain tissue floating in formalin, two without a protocol for regularly refreshing it, one renewing formalin "when necessary" and the fourth every few years. The last centre stores brains in polyethylene glycol. How the different storage protocols affect the general tissue quality with respect to ex vivo MRI research after long term storage remains to be further investigated, but this small survey shows that the fixation protocol for our study is common practice among brain banks, and therefore the findings will have implications for future research on brain bank tissue.

In conclusion, our results demonstrate that fixed brain tissue stored for prolonged periods gives rise to structural tissue changes that are associated with hypo intensities on T2*-weighted MR images. When brain tissue from pathology archives or brain banks is used to study (rare) disorders with ex vivo MRI, it is of vital importance to take the storage protocol into account and to check for the macroscopic and microscopic alterations that have been described and illustrated in this study.

Acknowledgements

Authors want to thank I. Hegeman-Kleinn and C. Welling-Graafland for technical assistance.

Reference List

1. Benveniste H, Einstein G, Kim KR, Hulette C, Johnson GA. Detection of neuritic plaques in Alzheimer's disease by magnetic resonance microscopy. *Proc Natl Acad Sci U S A* 1999;96(24):14079-14084.
2. Bobinski M, de Leon MJ, Wegiel J, DeSanti S, Convit A, Saint Louis LA, Rusinek H, Wisniewski HM. The histological validation of post mortem magnetic resonance imaging-determined hippocampal volume in Alzheimer's disease. *Neuroscience* 2000;95(3):721-725.
3. Bronge L, Bogdanovic N, Wahlund LO. Postmortem MRI and histopathology of white matter changes in Alzheimer brains. A quantitative, comparative study. *Dement Geriatr Cogn Disord* 2002;13(4):205-212.
4. Englund E, Sjobeck M, Brockstedt S, Latt J, Larsson EM. Diffusion tensor MRI post mortem demonstrated cerebral white matter pathology. *J Neurol* 2004;251(3):350-352.
5. Fernando MS, O'Brien JT, Perry RH, English P, Forster G, McMeekin W, Slade JY, Golkhar A, Matthews FE, Barber R, Kalaria RN, Ince PG. Comparison of the pathology of cerebral white matter with post-mortem magnetic resonance imaging (MRI) in the elderly brain. *Neuropathol App Neurobiol* 2004;30(4):385-395.
6. Geurts JJ, Bo L, Pouwels PJ, Castelijns JA, Polman CH, Barkhof F. Cortical lesions in multiple sclerosis: combined postmortem MR imaging and histopathology. *AJNR Am J Neuroradiol* 2005;26(3):572-577.
7. Gouw AA, Seewann A, Vrenken H, van der Flier WM, Rozemuller JM, Barkhof F, Scheltens P, Geurts JJ. Heterogeneity of white matter hypointensities in Alzheimer's disease: post-mortem quantitative MRI and neuropathology. *Brain* 2008;131(Pt 12):3286-3298.
8. House MJ, St Pierre TG, Kowdley KV, Montine T, Connor J, Beard J, Berger J, Siddaiah N, Shankland E, Jin LW. Correlation of proton transverse relaxation rates (R2) with iron concentrations in postmortem brain tissue from alzheimer's disease patients. *Magn Reson Med* 2007;57(1):172-180.

9. Kangarlu A, Bourekas EC, Ray-Chaudhury A, Rammohan KW. Cerebral cortical lesions in multiple sclerosis detected by MR imaging at 8 Tesla. *AJNR Am J Neuroradiol* 2007;28(2):262-266.
10. Larsson EM, Englund E, Sjobeck M, Latt J, Brockstedt S. MRI with diffusion tensor imaging post-mortem at 3.0 T in a patient with fronto-temporal dementia. *Dement Geriatr Cogn Disord* 2004;17(4):316-319.
11. Schmierer K, Parkes HG, So PW, An SF, Brandner S, Ordidge RJ, Yousry TA, Miller DH. High field (9.4 Tesla) magnetic resonance imaging of cortical grey matter lesions in multiple sclerosis. *Brain* 2010;133(Pt 3):858-867.
12. van Rooden S, Maat-Schieman ML, Nabuurs RJ, van der Weerd L, van Duijn S, van Duinen SG, Natte R, van Buchem MA, van der Grond J. Cerebral amyloidosis: postmortem detection with human 7.0-T MR imaging system. *Radiology* 2009;253(3):788-796.
13. Blamire AM, Rowe JG, Styles P, McDonald B. Optimising imaging parameters for post mortem MR imaging of the human brain. *Acta Radiol* 1999;40(6):593-597.
14. Dawe RJ, Bennett DA, Schneider JA, Vasireddi SK, Arfanakis K. Postmortem MRI of human brain hemispheres: T2 relaxation times during formaldehyde fixation. *Magn Reson Med* 2009;61(4):810-818.
15. Pfefferbaum A, Sullivan EV, Adalsteinsson E, Garrick T, Harper C. Postmortem MR imaging of formalin-fixed human brain. *Neuroimage* 2004;21(4):1585-1595.
16. Shepherd TM, Thelwall PE, Stanisz GJ, Blackband SJ. Aldehyde fixative solutions alter the water relaxation and diffusion properties of nervous tissue. *Magn Reson Med* 2009;62(1):26-34.
17. Shepherd TM, Flint JJ, Thelwall PE, Stanisz GJ, Mareci TH, Yachnis AT, Blackband SJ. Postmortem interval alters the water relaxation and diffusion properties of rat nervous tissue--implications for MRI studies of human autopsy samples. *Neuroimage* 2009;44(3):820-826.

18. Tovi M, Ericsson A. Measurements of T1 and T2 over time in formalin-fixed human whole-brain specimens. *Acta Radiol* 1992;33(5):400-404.
19. Yong-Hing CJ, Obenaus A, Stryker R, Tong K, Sarty GE. Magnetic resonance imaging and mathematical modeling of progressive formalin fixation of the human brain. *Magn Reson Med* 2005;54(2):324-332.
20. Nagara H, Inoue T, Koga T, Kitaguchi T, Tateishi J, Goto I. Formalin fixed brains are useful for magnetic resonance imaging (MRI) study. *J Neurol Sci* 1987;81(1):67-77.
21. D'Arceuil HE, Westmoreland S, de Crespigny AJ. An approach to high resolution diffusion tensor imaging in fixed primate brain. *Neuroimage* 2007;35(2):553-565.
22. Metz B, Kersten GF, Hoogerhout P, Brugghe HF, Timmermans HA, de JA, Meiring H, ten HJ, Hennink WE, Crommelin DJ, Jiskoot W. Identification of formaldehyde-induced modifications in proteins: reactions with model peptides. *J Biol Chem* 2004;279(8):6235-6243.
23. Puchtler H, Meloan SN. On the chemistry of formaldehyde fixation and its effects on immunohistochemical reactions. *Histochemistry* 1985;82(3):201-204.
24. LeVine SM. Oligodendrocytes and myelin sheaths in normal, quaking and shiverer brains are enriched in iron. *J Neurosci Res* 1991;29(3):413-419.
25. Smith MA, Harris PL, Sayre LM, Perry G. Iron accumulation in Alzheimer disease is a source of redox-generated free radicals. *Proc Natl Acad Sci U S A* 1997;94(18):9866-9868.
26. Natte R, Maat-Schieman ML, Haan J, Bornebroek M, Roos RA, van Duinen SG. Dementia in hereditary cerebral haemorrhage with amyloidosis-Dutch type is associated with cerebral amyloid angiopathy but is independent of plaques and neurofibrillary tangles. *Ann Neurol* 2001;50(6):765-772.

27. Viale G, Gambacorta M, Coggi G, Dell'Orto P, Milani M, Doglioni C. Glial fibrillary acidic protein immunoreactivity in normal and diseased human breast. *Virchows Arch A Pathol Anat Histopathol* 1991;418(4):339-348.
28. Natte R, Yamaguchi H, Maat-Schieman ML, Prins FA, Neeskens P, Roos RA, van Duinen SG. Ultrastructural evidence of early non-fibrillar Abeta42 in the capillary basement membrane of patients with hereditary cerebral haemorrhage with amyloidosis, Dutch type. *Acta Neuropathol* 1999;98(6):577-582.
29. Matubayasi N, Nakahara M. Hydrothermal reactions of formaldehyde and formic acid: free-energy analysis of equilibrium. *J Chem Phys* 2005;122(7):074509.
30. Schrag M, Dickson A, Jiffry A, Kirsch D, Vinters HV, Kirsch W. The effect of formalin fixation on the levels of brain transition metals in archived samples. *Biometals* 2010.(Epub ahead of print)
31. Greenberg SM, Vernooij MW, Cordonnier C, Viswanathan A, Al-Shahi SR, Warach S, Launer LJ, van Buchem MA, Breteler MM. Cerebral microbleeds: a guide to detection and interpretation. *Lancet Neurol* 2009;8(2):165-174.

Chapter 3

Comparison of histological techniques to visualize iron in paraffin embedded brain tissue of patients with Alzheimer's disease.

Sara van Duijn, MSc 1, Rob J.A. Nabuurs, MD, PhD 2, Sjoerd G. van Duinen, MD, PhD 1, Remco Natté, MD, PhD 1

1. Department of Pathology, Leiden University Medical Centre, Leiden, Netherlands
2. Department of Radiology, Leiden University Medical Centre, Leiden, Netherlands

J. Histochem. Cytochem. 2013 Nov; 61 (11): 785-792

Abstract

Better knowledge of the distribution of iron in the brains of Alzheimer's disease (AD) patients may facilitate the development of an in vivo magnetic resonance (MR) marker for AD and may cast light on the role of this potentially toxic molecule in the pathogenesis of AD. Several histological iron staining techniques have been used in the past but they have not been systematically tested for sensitivity and specificity.

This article compares three histochemical techniques and ferritin immunohistochemistry to visualize iron in paraffin embedded human AD brain tissue. The specificity of the histochemical techniques was tested by staining sections after iron extraction.

Iron was demonstrated in the white matter, in layers IV/V of the frontal neocortex, in iron containing plaques, and in microglia. In our hands these structures were best visualized using the Meguro iron stain, a method that has not been described for iron staining in human brain or AD in particular. Ferritin immunohistochemistry stained microglia and iron containing plaques similar to the Meguro method but was less intense in myelin associated iron. The Meguro method is most suitable for identifying iron positive structures in paraffin-embedded human AD brain tissue.

Keywords: iron, Alzheimer's disease, ferritin, brain, plaques, microglia

Introduction

There is growing evidence that iron plays an important role in the development of neurodegenerative diseases such as Alzheimer's disease (AD). One of the reasons is an altered brain iron distribution with iron accumulation in AD plaques (LeVine 1991; Smith et al. 1997; Crichton et al. 2002; Haacke et al. 2005; Meadowcroft et al. 2009; Bartzokis 2011). These disease-related changes in brain iron distribution are a potential marker for early in vivo diagnosis using MRI, especially because recent advances in human magnetic resonance imaging (MRI), systems operating at an ultra-high magnetic field (7 Tesla and higher) show increased sensitivity to iron-based susceptibility contrast in the human brain that have not been observed before (Nabuurs et al. submitted). A validated histological method to stain iron in brain tissue is required to correlate the MRI findings with histological changes in iron distribution and to study the role of iron in the development of neurodegenerative diseases like AD.

Iron (Fe) is essential for the proper functioning of many cellular processes. Due to its capability to catalyze oxidation-reduction reactions, iron serves as an active site in molecules with critical biological functions. However, this also requires a strict regulation to prevent uncontrolled spreading of catalytic active iron and its potential (neuro) toxicity (Meguro et al. 2007). This regulation is achieved by strong binding between iron and the proteins transferrin and ferritin. Transferrin, a transporter protein, can bind two Fe³⁺ ions. Ferritin serves as the principle iron storage protein capable of binding up to 4500 iron atoms in different mineral forms, predominantly as Fe³⁺ and small amounts of Fe²⁺ (Meguro et al. 2007). In organisms iron can be categorized as heme or non-heme iron. Heme iron is a Fe²⁺ protoporphyrin complex found in, for instance, haemoglobin. Non-heme iron consists of Fe³⁺ bound to ferritin or transferrin and very small amounts of Fe³⁺ and Fe²⁺ loosely bound to organic bases, enzymes, iron sulphur proteins and nucleotides. In general, nearly all non-heme iron found in the human body is bound to ferritin as Fe³⁺. The distribution of ferritin closely resembles the distribution of iron and therefore may act as a surrogate marker for iron (Grundke-Iqbal et al. 1990; Meguro et al. 2007).

In the normal brain, most iron is present in myelin and oligodendrocytes which require iron-dependent enzymes to produce and maintain myelin. Myelin-rich areas such as white matter thus contain large amounts of iron. In the cerebral cortex, iron is also expected in the myelin-rich layers

IV and V (Fatterpekar et al. 2002). In damaged brain tissue, microglial cells have been shown to accumulate iron (Schonberg et al. 2012). Non-heme iron (predominantly in the Fe³⁺ form) can be visualized in paraffin embedded tissue by the classic Perl's iron stain, in which soluble ferrocyanide reacts with the tissue Fe³⁺ to form crystals that make an insoluble Prussian blue dye. Further enhancement can be obtained by allowing the Prussian blue crystal to catalyze the H₂O₂-dependent oxidation of diaminobenzidine (DAB) (Meguro et al. 2007). Several protocols for DAB-enhanced iron stains, using different pre-treatment, slide thickness, endogenous blocking and reagent concentrations have been published but these different methodologies have never been directly compared with one and another and only some staining patterns have been related to ferritin immunohistochemistry (IHC) (Barbeito et al. 2009; Butt et al. 2010; Fukunaga et al. 2010; Chen-Roetling et al. 2011; Shpyleva et al. 2011) or checked for false positive results in iron depleted sections (Smith et al. 2007). The DAB enhanced histochemical iron stains described by Smith (Smith et al. 1997) and LeVine (LeVine 1991) have been reported to label AD plaques. The Meguro method (Meguro et al. 2007) has not been described in human brain tissue or animal models of AD but has been widely used in other organs in rat, mice and monkey (Meguro et al. 2005; Meguro et al. 2007; Freret et al. 2008; Iwatsuki et al. 2008; Meguro et al. 2008; Butt et al. 2010; Winter et al. 2010; Butt et al. 2011; Shpyleva et al. 2011).

The purpose of the present study is to compare the Meguro, Smith, and LeVine iron staining methods for detection of non-heme iron in brain tissue with AD pathology. In addition, we investigated their correlation with the distribution of ferritin by IHC.

Materials and methods

Brain tissue samples

One block of formalin-fixed, paraffin embedded brain tissue of the frontal cortex of 4 AD patients (60-87 y; Braak 6: N = 2; Braak 5: N = 1; Braak 4: N = 1) and 4 control patients without dementia of evidence of AD (62-76 y; Braak 0) was used. Samples were handled in a coded fashion to maintain anonymity according to Dutch national ethical guidelines. The brain tissue had been routinely immersed in buffered 10% formalin for a maximum of 6 months.

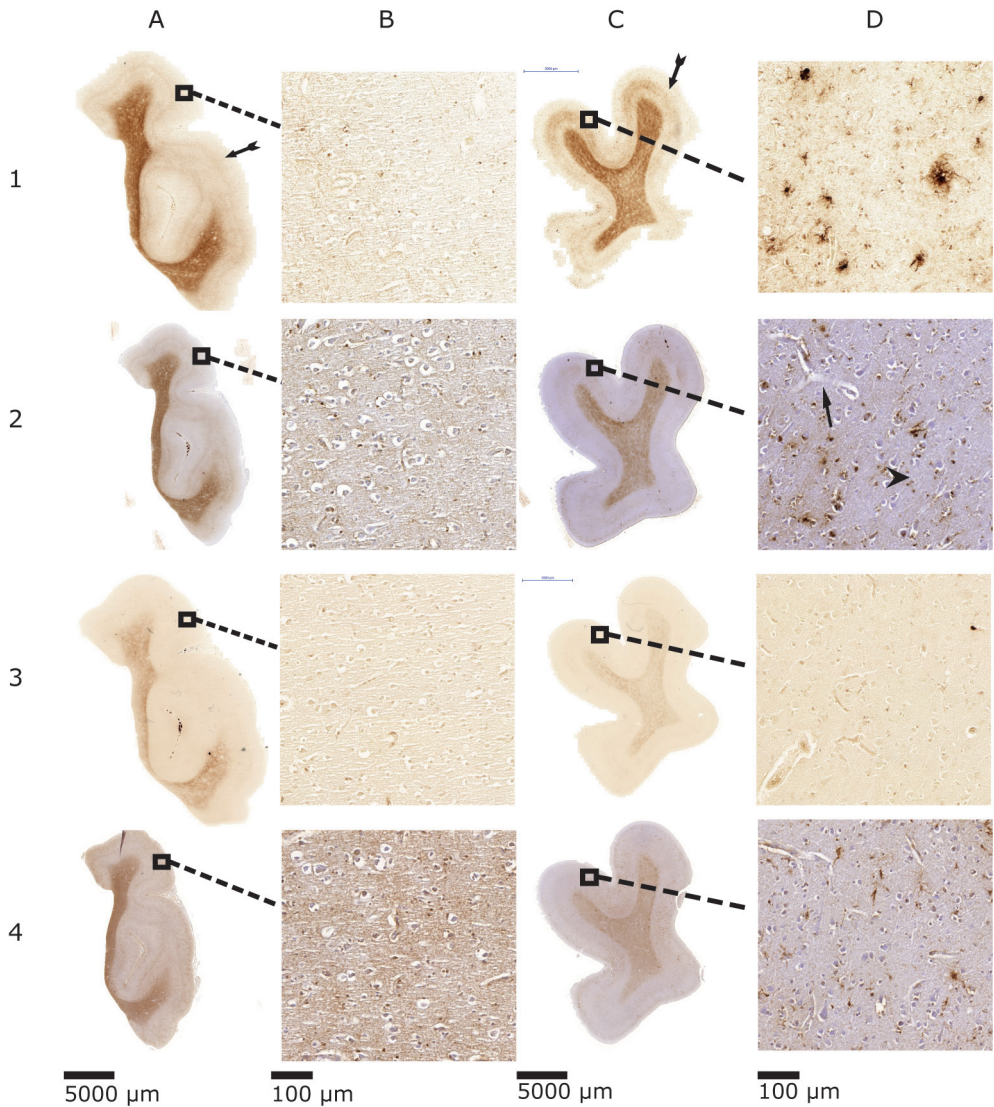


Figure 1: Comparison of the Meguro (1), Smith (2), LeVine (3) and ferritin IHC (4) in control patients (A and B) and AD patients (C and D). A: whole section of a control patient (scale bar 5000 μm); B: 20x magnification of A (scale bar 100 μm); C: whole section of an AD patient (scale bar 5000 μm); D: 20x magnification of C (scale bar 100 μm). Arrows indicate examples of iron positive plaques; arrowheads indicate examples of microglia; double arrows show layer IV/V of the cortex.

Iron extraction

In the first experiment, the tissue of AD patients was used to examine the effect of iron extraction on the different stainings. For each patient

sample 7 serially cut 10 µm thick sections were mounted onto slides. Of each of these series, section 1, 3 and 5 were incubated with 250 µl 0,1 M Na-citrate/HCL pH 1,0 buffer (Boom BV, Meppel, The Netherlands). After overnight incubation, the buffer was aspirated from the section and its iron concentration was measured using the Cobas Integra 400/800 method (Roche Diagnostics, Mannheim, Germany). As a control, the iron concentration was tested in the native buffer, in buffer incubated on a glass slide without tissue and in buffer with Fe³⁺ (Menck BV, Amsterdam, The Netherlands) added as a positive control. The limits of sensitivity of the Fe elution assay are 0,9-179 µmol/L (Roche Diagnostics).

As a control experiment the tissue of AD patients was used to test the iron extraction capability of Na-citrate/HCL buffer. Of each patient sample a section was incubated with 250 µl 0,05 M TRIS/HCL pH 1,0 buffer (Menck BV) and an adjacent section was incubated with 250 µl 0,1 M Na-citrate pH 1,0 buffer to extract iron. After overnight incubation, the buffer was aspirated from the section and its iron concentrations was measured as described above.

Histological procedures for iron staining

For the first experiment, the sections of AD tissue as described above were used. Of each patient sections 1 and 2 were stained as described by Meguro et al. (Meguro et al. 2007) with an increase in incubation times of 25%: after de-waxing/rehydration the paraffin sections were incubated for 40 min in 1% potassium ferrocyanide, washed and treated in methanol containing 0.01 M NaN₃ and 0,3% H₂O₂ for 75 min. Then the sections were treated in 0.1 M phosphate buffer, followed by a solution containing 0.025% 3,3'-DAB-4HCL (DAB, Sigma, St Louis, MO, USA) and 0.005% H₂O₂ in a 0.1 M phosphate buffer for 40 min. The reaction was stopped by washing.

The third and fourth sections were stained according to Smith et al. (Smith et al., 1997) In short, after deparaffinization in xylene and rehydration through graded ethanol, sections were incubated for 15 hrs in 7% potassium ferrocyanide in aqueous hydrochloric acid (3%) and subsequently incubated in 0.075 % 3,3'-DAB and 0.015% H₂O₂ for 5–10 min.

The fifth and sixth sections were stained according to Levine et al. (LeVine 1991) but with an increased DAB incubation time of 1 hour and 45 minutes. Briefly, after deparaffinization and rehydration the sections were incubated in 10 mg NaBH₄/ml PBS, 30 min, washed in PBS and incubated in 30 µg protK/ml PB S with 0.1% Triton X-100, 20 min, at room temper-

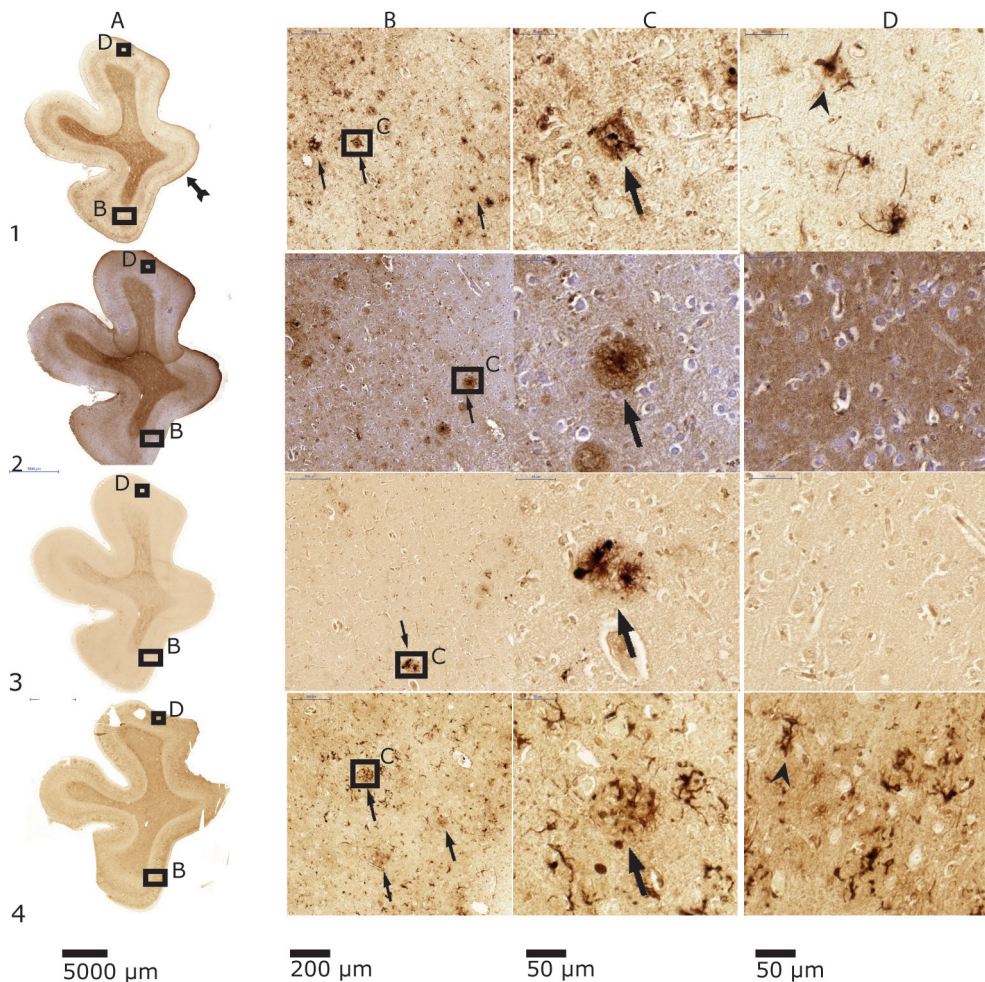


Figure 2: Comparison of the Meguro (1), Smith (2), LeVine (3) to ferritin IHC (4) on AD tissue. A: whole section (scale bar 5000 μm); B: 10x magnification (scale bar 200 μm); C: 40x magnification of 2 (scale bar 50 μm); D: 40x magnification (scale bar 50 μm). Arrows indicate examples of iron positive plaques; arrowheads indicate examples of microglia; double arrows show layer IV/V of the cortex.

ature. Sections were washed in PBS and incubated in 1% potassium ferrocyanide/1% Triton X-100/0.125 N HCL, 30 min. Sections were washed in PBS and incubated in a mixture of 1 mg DAB: 5 ml 0.01M Tris HCl pH 7.6: 10 μl 30% H₂O₂ for 2 hours in the dark followed by washing in PBS. The seventh section was stained immunohistochemically for ferritin using polyclonal anti-ferritin rabbit antibody at 1:10000 (Bethyl, Montgomery, Texas, USA) overnight, followed by a swine anti-rabbit biotin (Dako) 1:600 for 1 hour at room temperature. After washing with PBS, immunolabelling

followed using an ABC kit (Vectastain) according to the manufacturer's instructions and visualized with DAB (3'3 diaminobenzidine, Sigma). The concentration of ferritin rabbit antibody 1:10000 was chosen after a series of 7 different concentrations. 1:100, 1:500, 1:1000, 1:5000, 1:10000, 1:20000, 1:40000. The dilution of 1:10000 gave the most optimal signal compared to the higher and lower concentrations.

In the second experiment the three different methods and the ferritin IHC were performed on tissue of AD patients and on tissue of control patients. The tissue was cut in 10 µm thick sections and mounted onto slides. Adjacent sections were stained with the Meguro, Smith and LeVine method and the ferritin IHC as described above.

Scoring

All sections were scored for iron/ferritin labelling of plaques, microglia, white matter and cortical layers IV and V. Microglia cells were defined as iron positive cells with dilated cell bodies and dilated cellular processes. We and others have shown that iron positive cells with this morphology label for microglial immunohistochemical markers (Nabuurs et al. 2011; Schonberg et al. 2012). The intensity of iron and ferritin staining in plaques and microglia was scored as: no staining (-), intermediate staining (+) or strong staining (++). Labelling of myelin-associated iron in the white matter and the myelin rich cortical layers IV and V was scored as no contrast (-), intermediate contrast (+) and strong contrast (++) versus the rest of the cortex. Scoring was performed independently by the authors (SvD, SGvD,RN).

Results

Iron histochemistry.

The Meguro method showed the strongest contrast between gray and white matter in AD and control tissue (fig 1 and 2). This contrast was also seen using the Smith and LeVine staining, however, it was less pronounced. Cortical layers IV and V showed the most intense labelling by the Meguro stain, and labelling of these layers was more pronounced in AD than in controls. These layers were also seen to a lesser extent in the Smith staining but not in the LeVine staining. Iron-containing plaques and microglia in AD tissue were most frequently and most intensely labelled by the Meguro stain. The Smith method detected less microglia and fewer iron containing plaques in the cortices of AD patients. The LeVine meth-

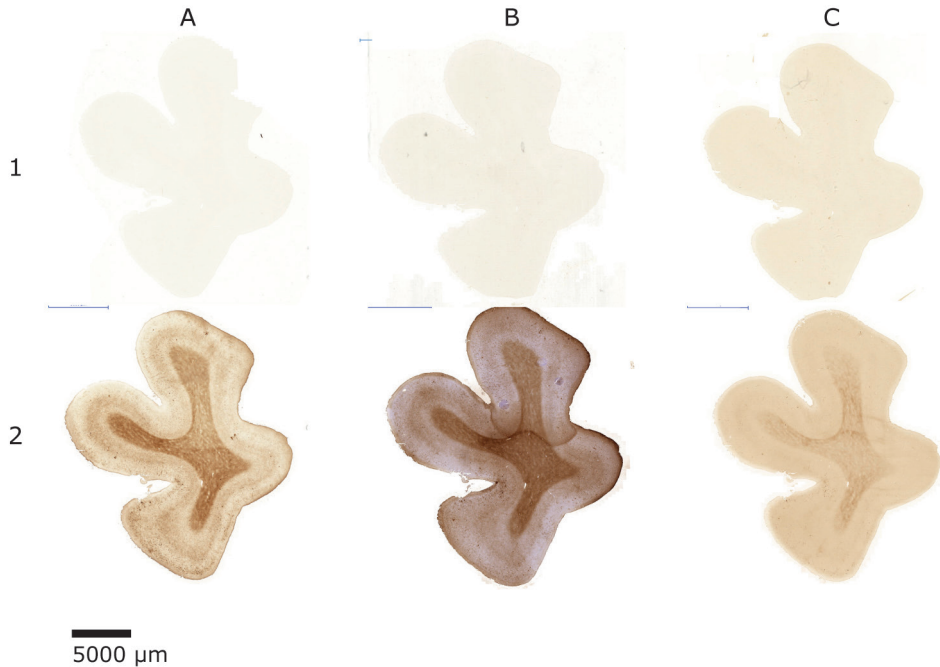


Figure 3: The Meguro (A), Smith (B), LeVine (C) method with iron extraction as pre-treatment (1) and without iron extraction as pre-treatment (2) on AD tissue; scale bars 5000 μm .

od was clearly the least sensitive, showing no enhanced labelling of the cortical layers IV/V, only a few plaques and no microglia. No iron positive plaques or microglia were found, with any of the iron staining methods, in control tissue.

Comparison with ferritin IHC

The Meguro method and ferritin IHC showed a comparable distribution and frequency of iron-positive plaques and microglia in AD tissue but the plaques looked different. Both methods showed plaques with clustered iron positive microglia, but the extracellular parenchymal plaque deposits were labelled differently. The Meguro method showed intense and sharply circumscribed labelling of extracellular plaque deposits, whereas ferritin IHC showed weak, diffuse labelling of these deposits (fig 2). The contrast between white matter and cortex and the visibility of cortical layers IV/V was better using the Meguro iron stain than in ferritin IHC in both AD tissue and control tissue. Higher concentrations of the antibody gave more background with less contrast between the different layers in the cortex and between white and grey matter.

Table 1: Comparison of LeVine, Smith, Meguro iron stain and ferritin Immunohistochemistry.

| | Plaques | Microglia | Layer IV/V AD tissue | White matter AD tissue | Layer IV/V control tissue | White matter control tissue |
|----------|---------|-----------|-------------------------|---------------------------|------------------------------|--------------------------------|
| Meguro | +/++ | ++ | +++ | ++ | ++ | +++ |
| Smith | + | + | + | + | ++ | + |
| LeVine | + | - | - | + | - | + |
| Ferritin | +/+++ | ++ | + | + | + | + |

Each score represents the aggregated result of the 4 patients. For iron positive plaques and microglia: - = no staining; + = intermediate staining; ++ = strong staining. For contrast between cortical layers IV/V and the other cortical layers and for contrast between white and grey matter: - = no contrast; + = intermediate contrast; ++ = strong contrast.

Iron extraction

None of the three investigated procedures showed staining of any cell or structure in tissue after iron extraction (fig 3), but all showed their usual staining pattern in the parallel section without iron extraction as a pre-treatment. Only the LeVine method showed a light background staining and lacked contrast between white matter and grey matter.

The buffer incubated with tissue showed much higher iron concentrations, than buffer incubated on a glass slide without tissue, confirming iron extraction (table 2).

Iron extraction with Na-citrate/HCL buffer gave better results compared with the TRIS/HCL buffer on the tissue. However, after adding Fe³⁺ to the buffer the results were better using TRIS/HCL as a buffer.

Discussion

To our knowledge, this is the first study to provide a direct comparison of three frequently used histochemical iron stains on human paraffin-embedded AD brain tissue and simultaneously investigates changes in the distribution of ferritin. We evaluated their ability to stain iron-containing plaques and microglia as well as myelin-associated iron. The method according to Meguro et al. (Meguro et al. 2007) resulted in the most robust and intense labelling of these iron containing structures.

We are not aware of earlier studies using the Meguro method to visualize iron in human brain tissue, but it has been described for the detection of iron in paraffin-embedded tissue of rat, mice, monkey and guinea pig (Meguro et al. 2005; Freret et al. 2008; Iwatsuki et al. 2008; Meguro et al. 2008; Butt et al. 2010; Winter et al. 2010; Butt et al. 2011; Shpyleva et al. 2011).

The Smith method (Smith et al. 1997) showed moderate amounts of microglia and plaques with less intensity than the Meguro stain. The staining of cortical layers IV and V was weak. With this method plaques have been demonstrated on 6 to 8 μm paraffin sections (Smith et al. 1997; van Duijn et al. 2011). Labelling of iron in microglia has not been described in earlier reports. This method differs to that described by Meguro et al. in its exclusion of the methanol-Na₃N- H_2O_2 treatment step between the ferrocyanide and DAB amplification step as well as the much longer (overnight versus 30 minutes) incubation time, with a 7 fold higher concentration of ferrocyanide and a shorter incubation with DAB in a 3x higher concentration. How these differences result in a less intense labelling of iron-positive structures than that by the Meguro method remains unclear. For the protocol used by Smith et al. methacarn fixation has been described to result in better iron labelling than formalin fixation. We performed the Smith protocol on formalin-fixed tissue because in our and most other laboratories tissue is routinely fixed by formalin; thus a general iron staining should be optimized preferably for formalin fixed tissue.

The last technique, published by LeVine (LeVine 1991), showed the least intense staining of the scored characteristics or no staining at all. Earlier studies showed plaques using this method on 60- to 100- μm free-floating sections (LeVine 1997; Meadowcroft et al. 2009) and iron-containing microglia in multiple sclerosis brains (LeVine 1997). No results of iron in layers IV/V have been reported using this method. The most likely explanation for the inferior labelling of plaques in the LeVine method compared to the other stains is our use of 10- μm de-paraffinized sections on glass slides whereas the LeVine method has been developed for 60- to 100- μm

Table 2: quantification of iron present in the extraction buffer after incubation;

| | Fe ($\mu\text{mol/L}$) | |
|--|--------------------------|----------|
| | Na-citrate | TRIS/HCL |
| Patient 1 | 4,7 | 2,3 |
| Patient 2 | 5,3 | 1,7 |
| Patient 3 | 4,7 | 2,3 |
| Patient 4 | 4,4 | 1,7 |
| Slide without tissue | 1,5 | 0,9 |
| Native buffer | 0,9 | 0,9 |
| Buffer + 10 $\mu\text{g Fe}^{3+}/\text{ml}$ | 191,9 | 217,4 |
| Buffer + 1 $\mu\text{g Fe}^{3+}/\text{ml}$ | 20,1 | 20,9 |
| Buffer + 0,1 $\mu\text{g Fe}^{3+}/\text{ml}$ | 3,1 | 2,9 |

These results were not corrected for the amount of tissue that was incubated.

free-floating sections (LeVine 1991; LeVine et al. 1992; LeVine et al. 1993). The absence of labelling of cortical layers IV and V may be due to the aggressive pre-treatment releasing iron from the myelin which is slightly increased compared to the other layers.

Using the Meguro technique, the contrast between white and grey matter and between cortical layers IV/V and the other cortical layers was more intense than using ferritin IHC. This may be due to problems with antigen retrieval in myelin-containing tissue. A problem of antibody sensitivity seems unlikely because intracellular microglial staining is very strong and frequent in ferritin IHC, similar to that observed with the Meguro iron stain. The differences between the Meguro iron stain and the ferritin IHC remained when higher or lower ferritin antibody concentrations were used. Alternatively, there may be a true difference between the presence of iron and ferritin in myelin due to a relatively high non-ferritin bound iron pool in the white matter and in cortical layers IV/V. Oligodendrocyte differentiation from oligodendrocyte precursor cells and myelin synthesis requires high iron concentrations, presumably because high amounts of enzymes with iron at their active sites are necessary (Todorich et al. 2009). The different labelling of plaques by the Meguro method and ferritin IHC is possibly caused by binding of iron to some of the many molecules other than ferritin in the extracellular compartment of plaques (Grundke-Iqbal et al. 1990; Connor et al. 1995).

The specificity of the tested histochemical iron stains was checked by using sections depleted of iron in acid buffer as a negative control. The absence of iron staining in these iron-depleted sections confirms the results of another study using the Smith protocol on iron depleted sections (Smith et al., 2007). Staining of other metals in brain is not completely excluded by these experiments, but other studies report the absence of DAB oxidation in reaction products of ferrocyanide with copper, zinc or magnesium (Meguro et al., 2007; Meguro et al. 2003; Roschztardt et al. 2009). All this information supports that the modified, DAB enhanced Perl's stainings used in this study are specific for iron ions.

Detailed knowledge of iron distribution in brain tissue may be of value for improving in vivo (MRI) diagnostics in AD and for a more complete picture of the pathogenesis of AD. In addition, it may also reflect normal brain ageing (Bartzokis et al. 2007b; Pfefferbaum et al. 2010) and the presence of other neurodegenerative diseases such as Parkinson's disease (Loeffler et al. 1995; Brar et al. 2009), Lewy body disease (Tuite et al. 1996; Golts et al. 2002) and Huntington's disease (Bartzokis et al. 2007a; Rosas et al. 2012). Although the present study was done on AD brain tissue, the results may be of use for the choice of iron stain in these other neurode-

generative diseases.

In conclusion, the results of this study suggest that the Meguro method is the best technique to stain iron in 10- μm formalin fixed paraffin sections of human brain tissue. Ferritin IHC is a good alternative for demonstrating iron in microglia and, to a lesser amount, plaques, but somewhat less suitable for staining myelin-associated iron.

Acknowledgment

The authors thank I. Hegeman-Kleinn for her excellent technical assistance.

Reference List

Barbeito, A.G., Garringer, H.J., Baraibar, M.A., Gao, X.Y., Arredondo, M., Nunez, M.T., Smith, M.A., Ghetti, B., & Vidal, R. 2009. Abnormal iron metabolism and oxidative stress in mice expressing a mutant form of the ferritin light polypeptide gene. *Journal of Neurochemistry*, 109, (4) 1067-1078

Bartzokis, G. 2011. Alzheimer's disease as homeostatic responses to age-related myelin breakdown. *Neurobiol.Aging*, 32, (8) 1341-1371

Bartzokis, G., Lu, P.H., Tishler, T.A., Fong, S.M., Oluwadara, B., Finn, J.P., Huang, D., Bordelon, Y., Mintz, J., & Perlman, S. 2007a. Myelin breakdown and iron changes in Huntington's disease: pathogenesis and treatment implications. *Neurochem. Res.*, 32, (10) 1655-1664

Bartzokis, G., Tishler, T.A., Lu, P.H., Villablanca, P., Altshuler, L.L., Carter, M., Huang, D., Edwards, N., & Mintz, J. 2007b. Brain ferritin iron may influence age- and gender-related risks of neurodegeneration. *Neurobiol. Aging*, 28, (3) 414-423

Brar, S., Henderson, D., Schenck, J., & Zimmerman, E.A. 2009. Iron accumulation in the substantia nigra of patients with Alzheimer disease and Parkinsonism. *Archives of Neurology*, 66, (3) 371-374

Butt, O.I., Buehler, P.W., & D'Agnillo, F. 2010. Differential induction of renal heme oxygenase and ferritin in ascorbate and nonascorbate producing species transfused with modified cell-free haemoglobin. *Antioxidants & Redox Signaling*, 12, (2) 199-208

Butt, O.I., Buehler, P.W., & D'Agnillo, F. 2011. Blood-brain barrier disruption and oxidative stress in guinea pig after systemic exposure to modified cell-free haemoglobin. *American Journal of Pathology*, 178, (3) 1316-1328

Chen-Roetling, J., Chen, L.F., & Regan, R.F. 2011. Apotransferrin protects cortical neurons from haemoglobin toxicity. *Neuropharmacology*, 60, (2-3) 423-431

Connor, J.R., Snyder, B.S., Arosio, P., Loeffler, D.A., & Lewitt, P. 1995. A

quantitative-analysis of isoferritins in select regions of aged, parkinsonian, and, Alzheimers diseased brains. *Journal of Neurochemistry*, 65, (2) 717-724

Crichton, R.R., Wilmet, S., Legssyer, R., & Ward, R.J. 2002. Molecular and cellular mechanisms of iron homeostasis and toxicity in mammalian cells. *J. Inorg. Biochem.*, 91, (1) 9-18

Fatterpekar, G.M., Naidich, T.P., Delman, B.N., Aguinaldo, J.G., Gultekin, S.H., Sherwood, C.C., Hof, P.R., Drayer, B.P., & Fayad, Z.A. 2002. Cytoarchitecture of the human cerebral cortex: MR microscopy of excised specimens at 9.4 Tesla. *AJNR Am. J. Neuroradiol.*, 23, (8) 1313-1321

Freret, T., Bouet, V., Toutain, J., Saulnier, R., Pro-Sistiaga, P., Bihel, E., MacKenzie, E.T., Roussel, S., Schumann-Bard, P., & Touzani, O. 2008. Intraluminal thread model of focal stroke in the non-human primate. *Journal of Cerebral Blood Flow and Metabolism*, 28, (4) 786-796

Fukunaga, M., Li, T.Q., van, G.P., de Zwart, J.A., Shmueli, K., Yao, B., Lee, J., Maric, D., Aronova, M.A., Zhang, G., Leapman, R.D., Schenck, J.F., Merkle, H., & Duyn, J.H. 2010. Layer-specific variation of iron content in cerebral cortex as a source of MRI contrast. *Proc. Natl. Acad. Sci. U.S.A*, 107, (8) 3834-3839

Golts, N., Snyder, H., Frasier, M., Theisler, C., Choi, P., & Wolozin, B. 2002. Magnesium inhibits spontaneous and iron-induced aggregation of alpha-synuclein. *Journal of Biological Chemistry*, 277, (18) 16116-16123

Grundke-Iqbal, I., Fleming, J., Tung, Y.C., Lassmann, H., Iqbal, K., & Joshi, J.G. 1990. Ferritin is a component of the neuritic (senile) plaque in Alzheimer dementia. *Acta Neuropathol.*, 81, (2) 105-110

Haacke, E.M., Cheng, N.Y., House, M.J., Liu, Q., Neelavalli, J., Ogg, R.J., Khan, A., Ayaz, M., Kirsch, W., & Obenaus, A. 2005. Imaging iron stores in the brain using magnetic resonance imaging. *Magn Reson. Imaging*, 23, (1) 1-25

Iwatsuki, H., Meguro, R., Asano, Y., Odagiri, S., Li, C.T., & Shoumura, K. 2008. Chelatable Fe (II) is generated in the rat kidneys exposed to is-

chemia and reperfusion, and a divalent metal chelator, 2, 2'-dipyridyl, attenuates the acute ischemia/reperfusion-injury of the kidneys: a histochemical study by the perfusion-Perls and -Turnbull methods. *Archives of Histology and Cytology*, 71, (2) 101-114

LeVine, S.M. 1991. Oligodendrocytes and myelin sheaths in normal, quaking and shiverer brains are enriched in iron. *J. Neurosci. Res.*, 29, (3) 413-419

LeVine, S.M. 1997. Iron deposits in multiple sclerosis and Alzheimer's disease brains. *Brain Research*, 760, (1-2) 298-303

LeVine, S.M. & Torres, M.V. 1992. Morphological features of degenerating oligodendrocytes in twitcher mice. *Brain Research*, 587, (2) 348-352

LeVine, S.M. & Torres, M.V. 1993. Satellite oligodendrocytes and myelin are displaced in the cortex of the reeler mouse. *Developmental Brain Research*, 75, (2) 279-284

Loeffler, D.A., Connor, J.R., Juneau, P.L., Snyder, B.S., Kanaley, L., Demaggio, A.J., Nguyen, H., Brickman, C.M., & Lewitt, P.A. 1995. Transferrin and iron in normal, Alzheimers disease, and Parkinsons disease brain regions. *Journal of Neurochemistry*, 65, (2) 710-716

Meadowcroft, M.D., Connor, J.R., Smith, M.B., & Yang, Q.X. 2009. MRI and histological analysis of beta-amyloid plaques in both human Alzheimer's disease and APP/PS1 transgenic mice. *Journal of Magnetic Resonance Imaging*, 29, (5) 997-1007

Meguro, R., Asano, Y., Iwatsuki, H., & Shoumura, K. 2003. Perfusion-Perls and -Turnbull methods supplemented by DAB intensification for non-heme iron histochemistry: demonstration of the superior sensitivity of the methods in the liver, spleen, and stomach of the rat. *Histochem. Cell Biol.*, 120, (1) 73-82

Meguro, R., Asano, Y., Odagiri, S., Li, C., Iwatsuki, H., & Shoumura, K. 2005. The presence of ferric and ferrous iron in the nonheme iron store of resident macrophages in different tissues and organs: histochemical demonstrations by the perfusion-Perls and -Turnbull methods in the rat.

Arch. Histol. Cytol., 68, (3) 171-183

Meguro, R., Asano, Y., Odagiri, S., Li, C., Iwatsuki, H., & Shoumura, K. 2007. Nonheme-iron histochemistry for light and electron microscopy: a historical, theoretical and technical review. Arch. Histol. Cytol., 70, (1) 1-19

Meguro, R., Asano, Y., Odagiri, S., Li, C.T., & Shoumura, K. 2008. Cellular and subcellular localizations of nonheme ferric and ferrous iron in the rat brain: a light and electron microscopic study by the perfusion-Perls and -Turnbull methods. Archives of Histology and Cytology, 71, (4) 205-222

Nabuurs, R.J., Hegeman, I., Natte, R., van Duinen, S.G., van Buchem, M.A., van der Weerd, L., & Webb, A.G. 2011. High-field MRI of single histological slices using an inductively coupled, self-resonant microcoil: application to ex vivo samples of patients with Alzheimer's disease. NMR Biomed., 24, (4) 351-357

Nabuurs, R. J. A., van Rooden, S., van Duijn, S., Versluis, M. J., Emmer, B. J., Liem, M. K., Milles, J. R. R, Webb, A., Frosch, M., van Duinen, S., Natte, R., van der Grond, J., van der Weerd, L., & van Buchem, M. A. 2013. Cortical changes in Alzheimer's disease at ultra-high field MRI. Submitted

Pfefferbaum, A., Adalsteinsson, E., Rohlfing, T., & Sullivan, E.V. 2010. Diffusion tensor imaging of deep gray matter brain structures: effects of age and iron concentration. Neurobiol.Aging, 31, (3) 482-493

Rosas, H.D., Chen, Y.I., Doros, G., Salat, D.H., Chen, N.K., Kwong, K.K., Bush, A., Fox, J., & Hersch, S.M. 2012. Alterations in brain transition metals in Huntington disease: an evolving and intricate story. Arch. Neurol., 69, (7) 887-893

Roschztardt H., Conéjéro G., Curie C., Mari S. 2009. Identification of the endodermal vacuole as the iron storage compartment in the arabidopsis embryo. Plant Physiology, 151, 1329-1338

Schonberg, D.L., Goldstein, E.Z., Sahinkaya, F.R., Wei, P., Popovich, P.G., & McTigue, D.M. 2012. Ferritin stimulates oligodendrocyte genesis in the adult spinal cord and can be transferred from macrophages to NG2 cells

in vivo. *Journal of Neuroscience*, 32, (16) 5374-5384

Shpyleva, S.I., Muskhelishvili, L., Tryndyak, V.P., Koturbash, I., Tokar, E.J., Waalkes, M.P., Beland, F.A., & Pogribny, I.P. 2011. Chronic administration of 2-acetylaminofluorene alters the cellular iron metabolism in rat liver. *Toxicological Sciences*, 123, (2) 433-440

Smith, K.D., Kallhoff, V., Zheng, H., & Pautler, R.G. 2007. In vivo axonal transport rates decrease in a mouse model of Alzheimer's disease. *Neuroimage.*, 35, (4) 1401-1408

Smith, M.A., Harris, P.L., Sayre, L.M., & Perry, G. 1997. Iron accumulation in Alzheimer disease is a source of redox-generated free radicals. *Proc. Natl. Acad. Sci. U.S.A.*, 94, (18) 9866-9868

Todorich, B., Pasquini, J.M., Garcia, C.I., Paez, P.M., & Connor, J.R. 2009. Oligodendrocytes and myelination: the role of iron. *Glia*, 57, (5) 467-478

Tuite, P.J., Provias, J.P., & Lang, A.E. 1996. Atypical dopa responsive parkinsonism in a patient with megalencephaly, mid-brain Lewy body disease, and some pathological features of Hallervorden-Spatz disease. *Journal of Neurology Neurosurgery and Psychiatry*, 61, (5) 523-527

van Duijn, S., Nabuurs, R.J., van, R.S., Maat-Schieman, M.L., van Duinen, S.G., van Buchem, M.A., van der Weerd, L., & Natta, R. 2011. MRI artifacts in human brain tissue after prolonged formalin storage. *Magn Reson. Med.*, 65, (6) 1750-1758

Winter, E.M., Hogers, B., van der Graaf, L.M., Gittenberger-de Groot, A.C., Poelmann, R.E., & van der Weerd, L. 2010. Cell tracking using iron oxide fails to distinguish dead from living transplanted cells in the infarcted heart. *Magnetic Resonance in Medicine*, 63, (3) 817-821

Chapter 4

Cortical iron reflects severity of Alzheimer's Disease

Sara van Duijn MSc 1, Marjolein Bulk, MSc 2,3,4, Sjoerd G. van Duinen MD PhD 1, Rob J.A. Nabuurs MD PhD 2,5*, Mark A. van Buchem MD PhD 2, Louise van der Weerd PhD 2,3, and Remco Natté MD PhD 1.

1Department of Pathology, Leiden University Medical Centre, Leiden, the Netherlands

2Department of Radiology, Leiden University Medical Centre, Leiden, the Netherlands

3Department of human genetics, Leiden University Medical Centre, the Netherlands

4Pecuros BV, Leiden, The Netherlands

5*Current address: Department of Neurology, VU-University Medical Centre, Amsterdam, the Netherlands

J. Alz. Dis. August 2017; 60 (4): 1533-1545

Abstract

Abnormal iron distribution in the isocortex is increasingly recognized as an in vivo marker for Alzheimer's disease (AD). However, the contribution of iron accumulation to the AD pathology is still poorly understood. In this study, we investigated: 1) frontal cortical iron distribution in AD and normal aging and 2) the relation between iron distribution and degree of AD pathology. We used formalin-fixed paraffin-embedded frontal cortex from 10 AD patients, 10 elder, 10 middle aged, and 10 young controls and visualized iron with a modified Perl's histochemical procedure. AD and elderly subjects were not different with respect to age and sex distribution. Iron distribution in the frontal cortex was not affected by normal aging but was clearly different between AD and controls. AD showed accumulation of iron in plaques, activated microglia, and, in the most severe cases, in the mid-cortical layers along myelinated fibres. The degree of altered iron accumulations was correlated to the amount of amyloid β plaques and tau pathology in the same block, as well as to Braak stage ($p < 0.001$).

AD and normal aging show different iron and myelin distribution in the frontal cortex. These changes appear to occur after the development of AD pathological hallmarks. These findings may help the interpretation of high resolution in vivo MRI and suggest the potential of using changes in iron-based MRI contrast to indirectly determine the degree of AD pathology in the frontal cortex.

Keywords: Alzheimer's disease, iron, myelin, magnetic resonance imaging

Introduction

Future therapeutic interventions for Alzheimer's disease (AD) require early and preferably non-invasive clinical tests. A promising approach is in vivo detection of amyloid β ($A\beta$) plaques, neuropil threads (NT) and neurofibrillary tangles (NFT), since these histological hallmarks of AD occur 10-20 years before cognitive decline [1, 2]. In vivo visualization of $A\beta$ plaque burden is already possible using positron emission tomography (PET) [3-6], but this technique requires the use of a radioactive tracer and a highly-specialized infrastructure. Recent advances in PET tracers for tau are promising to study the spatial and temporal relation between amyloid and tau accumulation in vivo. Nevertheless, our understanding of AD is incomplete, and the role of other modulators of the disease such as microglia activation and iron accumulation is only partially understood. Recently, high field (7T) Magnetic Resonance Imaging (MRI) has been reported to discriminate AD from control neocortex by changes in phase shift, which is a reliable indication of iron content in the brain [7, 8]. Other MRI studies show susceptibility induced changes in vivo in AD transgenic mice [9-11] and in postmortem human AD brain tissue [12, 13] that correlate to $A\beta$ plaques histologically. $A\beta$ plaques show iron accumulation [14-20] and it has been suggested that this iron causes the high T2* susceptibility effects [11, 21-23]. However, there may be additional pathological substrates for iron-related MRI changes in AD. A subset of histological studies report iron accumulation in microglia in the cortex and hippocampus of AD patients [14, 16, 19]. In contrast, Smith et al shows iron accumulation in NFT but explicitly report absence of iron labelling in glial cells [20]. AD-related iron accumulation in other tissue compartments than $A\beta$ plaques is also suggested by the presence of diffuse MRI hypointensities in postmortem AD cortex [19, 24], but the pathologic substrate of these diffuse MRI hypointensities is not known. Moreover, we found a diffusely increased iron labelling in layers III-V of the frontal cortex of AD patients in a study comparing different histological iron stains [25].

The value of iron-based MRI changes for the diagnosis and staging of AD depends on an association between cortical iron accumulation and AD pathology. However, we are not aware of studies that have correlated the degree of cortical iron accumulation to Braak stage, local $A\beta$ plaque load or local tau pathology. For the interpretation of iron-based cortical MRI changes as a biomarker for AD, it is also necessary to know the effect of

Table 1: Demographics and pathology of subjects.

| No. | age/ sex | AD/ control | Braak stage | Tau | A β plaque | Fe plaque/ mcg | band Fe/PLP | other brain pathology |
|-----|-------------|----------------|----------------|-----|------------------|-------------------|----------------|--|
| 1 | 17/M | C | 0 | - | - | - | - | No |
| 2 | 18/M | C | 0 | - | - | - | - | Colloid cyst 3rd ventricular moderate hydrocephalus |
| 3 | 21/M | C | 0 | - | - | - | - | Colloid cyst 3rd ventricular with brain herniation |
| 4 | 25/M | C | 0 | - | - | - | - | No |
| 5 | 31/M | C | 0 | - | - | - | - | No |
| 6 | 30/M | C | 0 | - | - | - | - | No |
| 7 | 33/M | C | + | - | - | - | - | Old lacunair infarct periventrically |
| 8 | 36/F | C | 0 | - | - | - | - | No |
| 9 | 37/M | C | 0 | - | + | - | - | No |
| 10 | 38/F | C | 0 | - | - | - | - | No |
| 11 | 51/M | C | + | - | - | - | - | No |
| 12 | 52/M | C | I | + | ++ | ++ | - | No |
| 13 | 53/M | C | + | - | - | - | - | Old meningo-ventriculitis Old lacunair infarct caudate nucleus |
| 14 | 53/M | C | + | - | - | - | - | No |
| 15 | 54/M | C | 0 | - | - | - | - | No |
| 16 | 56/M | C | 0 | - | - | - | - | No |
| 17 | 56/M | C | + | - | + | - | - | No |
| 18 | 58/F | C | + | - | - | - | - | No |
| 19 | 58/M | C | + | - | - | - | - | No |
| 20 | 57/F | C | + | + | + | - | - | No |
| 21 | 74/M | C | + | - | - | - | - | Capillary teleangiectasia pons |
| 22 | 75/F | C | + | - | + | + | - | No |
| 23 | 76/M | C | + | - | - | - | - | No |
| 24 | 76/M | C | I | - | - | - | - | Small old hemorrhagic infarct temporal lobe |
| 25 | 77/F | C | I | - | + | + | - | No |
| 26 | 80/F | C | + | + | + | - | - | No |
| 27 | 83/F | C | I | + | + | + | - | No |
| 28 | 84/M | C | + | - | - | - | - | No |
| 29 | 89/F | C | II | + | + | - | - | No |
| 30 | 89/F | C | III | + | +++ | +++ | - | No |
| 31 | 65/F | AD | VI | +++ | +++ | +++ | + | No |
| 32 | 66/F | AD | IV | +++ | +++ | +++ | - | No |
| 33 | 74/M | AD | V | +++ | +++ | +++ | + | No |
| 34 | 77/F | AD | IV | ++ | +++ | ++ | - | No |
| 35 | 78/M | AD | V | +++ | +++ | +++ | + | Meningioma, 1cm, parietal |
| 36 | 79/F | AD | V | +++ | +++ | ++ | - | No |
| 37 | 86/M | AD | IV | ++ | +++ | ++ | - | No |
| 38 | 88/F | AD | IV | ++ | +++ | ++ | - | No |
| 39 | 89/M | AD | IV | ++ | +++ | ++ | - | No |
| 40 | 90/M | AD | V | +++ | +++ | +++ | - | No |

Abbreviations: M = male; F = female; AD = Alzheimer Disease; FE = iron, mcg = microglia; PLP = proteolipid protein.

Symbols: - = absent, + = mild, ++ = moderate, +++ = severe. See Methods for definitions.

aging on cortical iron accumulation. Aging itself leads to increased iron and ferritin concentrations in the cortex [26, 27], but the microscopically distribution of this age-related increase is unknown.

Our previous finding of increased cortical phase shift changes as a possible non-invasive clinical biomarker for AD [7] led us to investigate the following questions: 1) is the pathological substrate of iron based MRI changes in AD cortex limited to iron accumulation in A β plaques or is iron also accumulating in other tissue compartments? 2) Is cortical iron accumulation related to Braak stage, local A β plaques and local tau pathology? 3) How does iron accumulation in AD compare to normal aging?

Materials and Methods

Patients

We included autopsy material of 10 AD patients (age 65-90 years old, 5 male and 5 female) with a clinical diagnosis of dementia and histological changes of at least Braak stage IV. Other neuropathological changes were absent, except for one patient with a 1 cm large meningioma in the parietal lobe which had not been noticed during life. We also included autopsy material of 10 young (17-38 years old, 8 male, 2 female), 10 middle aged (51-57, 8 male, 2 female) and 10 old (74-89, 4 male, 6 female) controls. No difference was found in sex distribution between the four groups ($P > 0.05$). By definition, AD and old age controls were significantly older compared to the middle aged and young controls ($P < 0.05$). The tissue was selected from the archive of the Department of Pathology, without knowledge of the degree of AD pathology in these blocks. All tissue samples were handled in a coded fashion, according to Dutch national ethical guidelines (Code for proper secondary use of human tissue, Dutch Federation of Medical Scientific Societies). Controls were included if the autopsy request file did not mention cognitive disorders, movement disorders, or extensive cerebrovascular disease. For all patients and controls, Braak stage was determined by two experienced neuropathologists (SGvD en RN) according to Alafuzoff [28] investigating the relevant brain areas. Patient characteristics, including Braak stage and additional neuropathological findings are presented in Table 1.

Tissue

Of each patient and control 1 block of formalin fixed paraffin embedded frontal cortex was taken. We choose the frontal cortex because increased diffuse iron in layers III-V was found earlier in a study designed to compare different histological iron stains [25]. Tissue was fixed in standard formalin for a minimum of 1 week and a maximum of 6, on average 1-2 weeks for both AD patients and controls. From each block, sequential 10- μ m thick sections were cut and stained consecutively for myelin - iron and A β - iron-tau. In addition, 20- μ m thick sections were stained for iron paralleled by a 10- μ m section of A β immunohistochemistry. The iron stained 20- μ m sections were used to count iron positive plaques (and in addition iron positive activated microglia) because at 20- μ m the iron stain labelled much more plaques and labelled them more reproducibly.

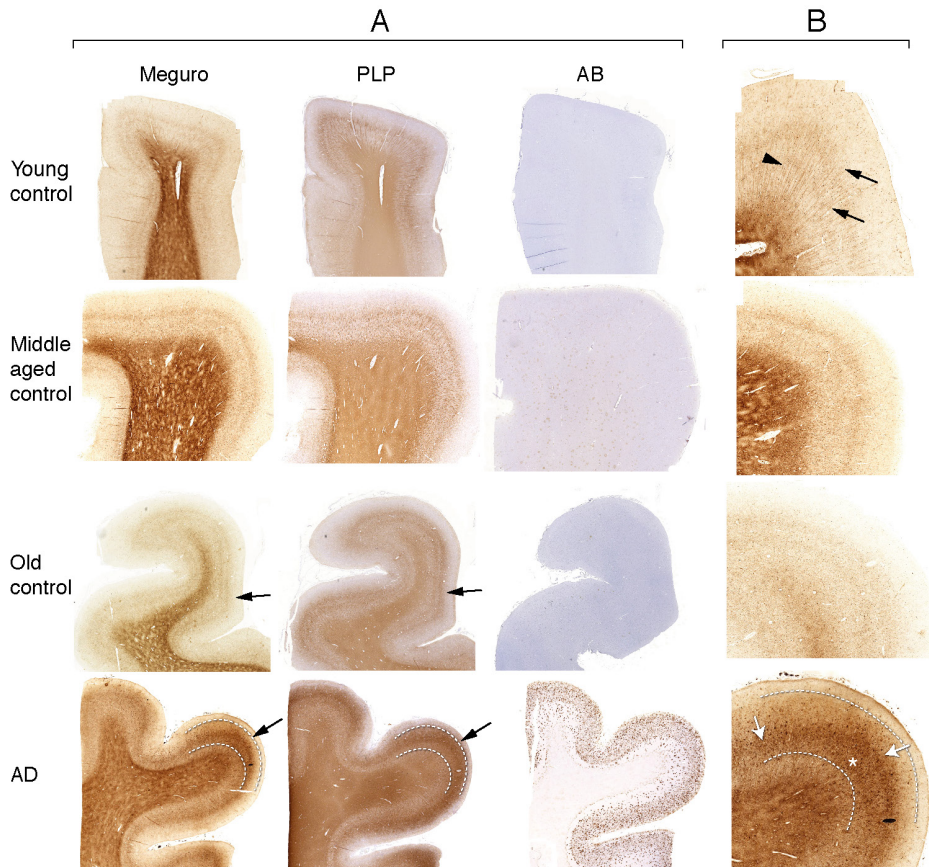


Figure 1: A: Each row represents consecutive sections of frontal cortex stained for iron, myelin (PLP immunohistochemistry) and A β immunohistochemistry. Controls show a similar iron distribution, irrespective of age, with increased amounts in the myelin rich areas: white matter and the inner and outer line of Baillarger (arrows). AD cortex (bottom row) shows a diffuse band shaped iron and PLP increase in cortical layer IV/V, extending to the inner part of layer III (arrow, and indicated by lines).

B: higher magnification of A, Meguro iron stain. Controls show evenly distributed iron concentration in myelinated fibres and a good distinction between the lines of Baillarger. AD cortex shows diffuse iron increase in the middle cortical layers (arrows), as well as iron positive plaques (asterisk), also concentrated in the middle cortical layers.

Histochemistry

Iron was detected using a modified diaminobenzidine (DAB)enhanced Perl's protocol as described previously [22, 25]. Sections of 10 μ m were incubated for 40 min in 1% potassium ferrocyanide (pH 1) and washed, followed by 75 minutes incubation with methanol containing 0.01 M sodium azide (NaN₃) and 0,3% H₂O₂. Then the sections were washed in 0.1 M phosphate buffered saline (PBS), before visualization by 0.025% 3,3'-diaminobenzidine (Sigma, St Louis, MO, USA) and 0.005% H₂O₂ in

0.1 M PBS for 40 min. The reaction was stopped by washing. For the 20 μ m sections incubation times were modified to: potassium ferrocyanide 80 minutes, methanol-NaN₃-H₂O₂ 100 minutes and DAB 80 minutes. A slightly adapted protocol was used to compare the potential impact of using fixed versus fresh-frozen post-mortem tissue on the detection of iron. Frozen sections (20 μ m) of the contralateral hemisphere of two AD patients were post fixed for 1 minute to prevent floating of the frozen sections from the slide during the staining procedure. The rest of the protocol was identical as described above apart from the 75 minutes incubation in methanol containing 0.01 M NaN₃ and 0.3% H₂O₂: PBS was used instead of methanol.

Immunohistochemistry

Immunohistochemistry (IHC) was used to detect A β protein, hyperphosphorylated tau, , proteolipid protein (PLP), myelin basic protein (MBP), myelin oligodendrocyte glycoprotein (MOG) and HLA-DR. Specific information regarding the antibodies and the dilutions used can be found in Table 2.

After de-paraffination, all 10 μ m sections were blocked with methanol and H₂O₂ (0,3%) for 20 minutes at room temperature. Slides for A β IHC were pre-treated by 85% formic acid at room temperature for 1 hour, followed by 30 minutes in trypsin at 37°C. Pre-treatment for MBP and MOG was citrate buffer, pH 6, at boiling temperature for 20 minutes and cooling down for an hour. No pre-treatment was performed for tau and PLP IHC. All incubations with primary antibodies were overnight at room temperature. For A β , tau, PLP, MBP the second step was performed with rabbit anti mouse biotin (DAKO, dilution 1:200) for 1 hour at room temperature. For MOG swine anti-rabbit biotin was used (DAKO, dilution 1:600) for 1 hour at room temperature. The third step was performed by avidin biotin complex (Vectastain, Vector, Burlingame CA, USA), according to the manufacturer's instructions (incubation for 30 minutes at room temperature). DAB (0,05%) with H₂O₂ (0,005%) was used as a chromogen with an incubation time of 10 minutes at room temperature. Double labelling for ferritin and HLA-DR was performed by pre-treatment with boiled citrate buffer pH 6.0 for 20 minutes and cooling down for one hour. Then, tissue was incubated overnight with a 1:1 cocktail of the antibodies for ferritin and HLA-DR (Table 2). The second step was performed by 2 hours incubation with a 1:1 cocktail of goat anti rabbit biotin (resulting dilution of 1:800) and goat-anti mouse alkaline phosphatase (resulting dilution 1:60), followed

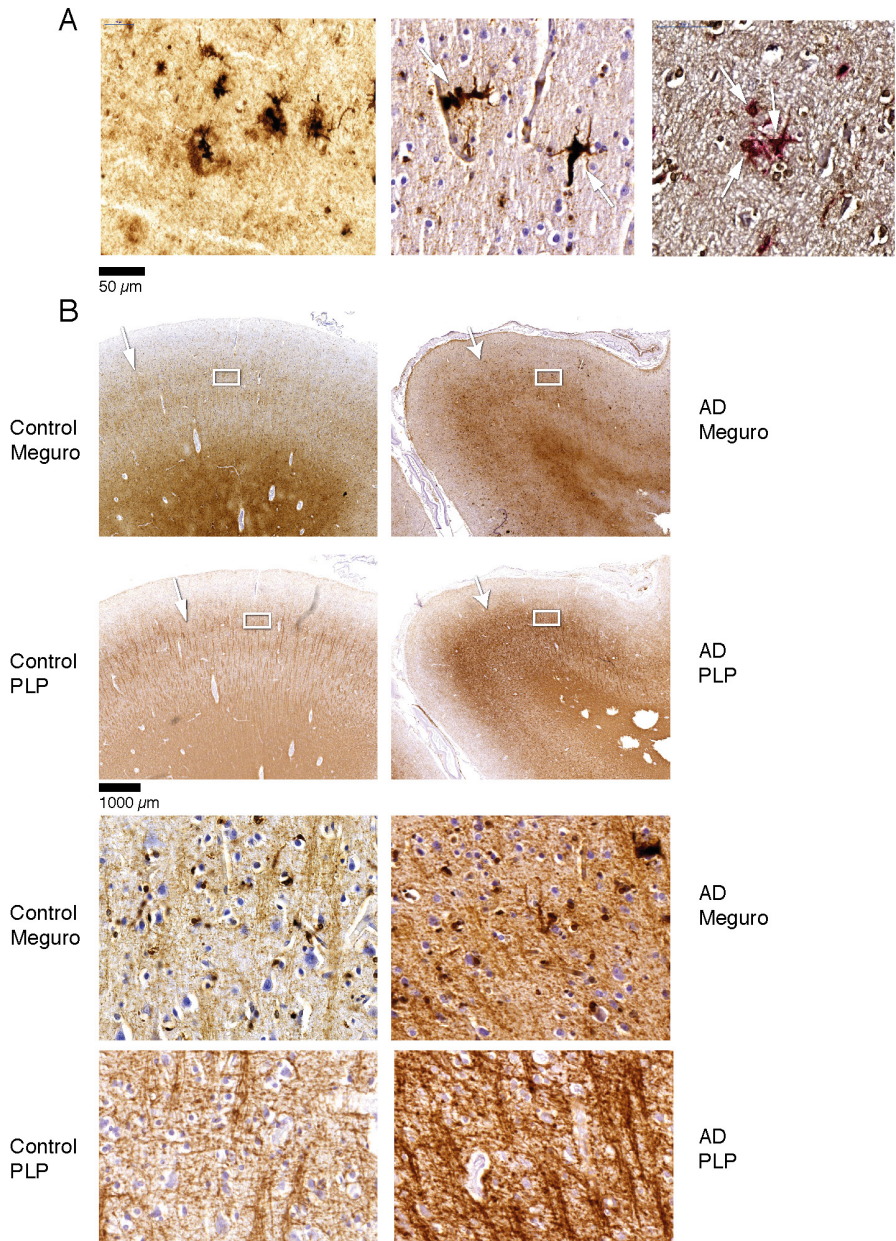


Figure 2: A: iron accumulation in plaques (left) and microglia (middle) (both Meguro stain). On the right double labelling of iron positive cells by ferritin (brown) and MHCII (red).

B: band shaped increase of iron and PLP labelling in AD (right column) compared to an old control (left column). The right column illustrates that the normal distinction of the lines of Baillarger (arrow) is blurred by a band shaped iron/PLP increase in cortical layer IV/V extending to layer III (arrow heads). This is due to darker and thicker iron/PLP labelling of more crowded myelinated fibres (bottom panel).

by 30 minutes incubation with avidin-biotin complex (Vectastain, Vector, Burlingame CA, USA), according to the manufacturer's instructions. First, ferritin was visualized by 10 minutes incubation with DAB (0,05%) with H₂O₂ (0,005%) and 1% cobalt-chloride, followed by visualization of HLA-DR by 25 minutes incubation with liquid permanent red (DAKO, 1:60), both at room temperature.

Semi-quantitative scoring of AD pathology and iron accumulation

Severity of the different pathological features in the frontal cortex was assessed semi-quantitatively by an experienced neuropathologist (RN). Tau pathology was scored as: absent (-): no AT8 immunoreactivity; mild (+): any AT8 immunoreactive structures up to occasional AT8 positive NT/NFT; moderate (++) : microscopic diffuse AT8 positive NT up to visible cortical layer V; severe (+++) : macroscopically visible layer V and other cortical layers, especially layers II/III.

A β pathology was scored as: absent (-): no A β plaques; mild (+): 1 A β plaque up to 10 fields with >50 plaques/ 100X field; moderate (++) : >10 fields of >50 plaques/100X field; severe (+++) : all cortical areas show >100 plaques/100X field.

The degree of abnormal iron accumulation was scored by counting the amount of iron positive plaques and iron positive microglia with activated morphology outside plaques in the cortical 100X field with the highest density and by assessing the presence or absence of a band like increase of PLP and myelin associated iron labelling in cortical layers III-V. Scoring categories were defined as: absent (-): no plaque/microglial iron accumulations; mild (+): 1-30 plaque/microglial iron accumulations; moderate (++) : 31-100 plaque/microglial iron accumulations; severe (+++) : > 100 plaque/microglial iron accumulations. Abnormal iron accumulation in the cortex was scored as ++++ when the tissue showed a band of diffusely increased PLP and iron in layer III-V in addition to > 100 plaque/microglial iron accumulations

Statistical methods

Age was compared between groups using a one-way ANOVA followed by a Bonferonni post hoc test. A chi-square test was used to compare sex distribution between groups. Semiquantitative iron score was correlated to Braak stage, and semiquantitative scores for A β plaques and tau pathology by a linear by linear association test for ordinal variables [29]. All statistical analyses were performed using Statistical Package of Social

Sciences (SPSS, version 23; SPSS, Chicago, USA). A significant level of 0.05 was used.

Results

Iron distribution in aging and AD

For histochemical visualization of iron, we used a modified Perl's procedure described by Meguro [22]. With this method, only non-heme iron is stained, mostly Fe³⁺ but also some Fe²⁺ [22]. Thus, if we refer to iron in this study, this is DAB enhanced Perl's detectable iron meaning non-heme iron, mostly Fe³⁺ and some Fe²⁺. In the absence of A β plaques and tau pathology (20 out of 30 controls), iron distribution in the frontal cortex was identical in young (9), middle aged (7), and old (4) controls. These samples showed a finely diffuse, regular iron distribution with evenly increased density in myelin-rich areas: the white matter, the lines of Baillarger and the radially projecting thickly myelinated fibres from the white matter into the cortex (Fig. 1). 5 Controls (1 young, 2 middle aged and 2 old) had minimal A β plaques with or without minimal tau pathology and showed the same iron distribution as controls without these AD lesions. The last 5 controls (1 middle aged, 4 old) showed variable iron accumulation in plaques and cells, directly correlating to the amount of A β plaques (Table 1). All 10 AD patients showed iron accumulation in plaques and cells (Table 1, Fig. 2A), most frequent in cortical layers III-V (Fig 1, bottom row). Intracellular iron was mainly localized in rounded microglia

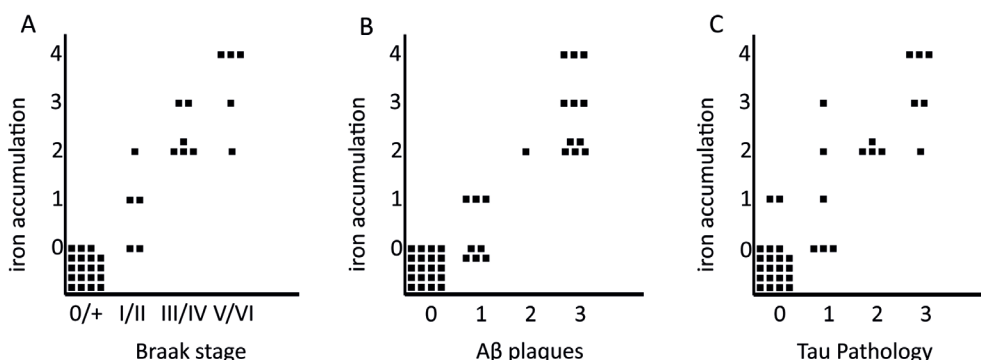


Figure 3: Semi-quantitative relation between iron accumulation and Braak stage (A), A β plaques (B) and tau pathology (C). Iron accumulation: 0: no iron accumulation, 1: low, 2: intermediate and 3: high iron accumulation in plaques and microglia, 4: high iron accumulation in plaques and microglia and a band shaped iron/PLP increase in the middle cortical layers. For grading definitions see Methods.

with dilated cell-branches (Fig 2A), morphologically identified as activated microglia [30, 31]. Iron laden microglia were often seen in or directly around A β plaques but also apart from A β plaques. Iron accumulation was not observed in neurofibrillary tangles. In 3 out of 10 AD patients, we observed a diffuse band-shaped increase of both iron and PLP labelling in cortical layers IV/ V, and part of layer III, blurring the normal distinction between the lines of Baillarger (Fig. 1, 2B). At higher magnification, we observed darker and thicker labelling of neuropil fibres by iron and myelin proteins (PLP, MOG, and MBP) in a more crowded network (Fig. 2B). The band of increased mid-cortical iron and myelin labelling is not reflected by A β plaques, which are most dense in cortical layers I-IV.

Correlation between iron accumulation, myelin changes, plaques and tau pathology.

Iron accumulations were scored from 0-3 depending on the amount of iron positive plaques and microglia together (see "Materials and Methods"). In the presence of an increased iron band in the mid-cortical layers the degree of iron change was scored as 4. This histological iron score correlated with Braak stage ($P < 0.001$) and with the semi-quantitatively scored amount of A β plaques ($P < 0.001$) and degree of tau pathology ($P < 0.001$). This level of statistical significance was the same for stratification by age as well as comparison of AD with the old age controls only (Fig. 3). Note that absence or low (score 0-1) iron accumulation in plaques and microglia excluded advanced Braak stage, significant A β plaques or significant tau pathology. A band-shaped increase of diffuse iron and PLP/MBP/MOG labelling was only present in AD frontal cortex with the severest tau pathology (Fig. 3 and 4), despite comparable amounts of A β plaques for all AD patients (Fig. 4, Table 1).

Discussion

Technical Considerations

In the present study, we show non-heme iron accumulation in A β plaques and activated microglia in the frontal cortex of AD patients. This is in line with earlier studies showing iron in human A β plaques [17, 19, 20], and in activated microglia [14, 17, 30-33]. We did not identify iron accumulation in NFT or NT and this is in line with most [14, 17, 19], but not all [20], previous reports. The modified Perl's protocol we employed was also used in other studies [17, 20] and principally stains Fe 3+ but also some Fe 2+

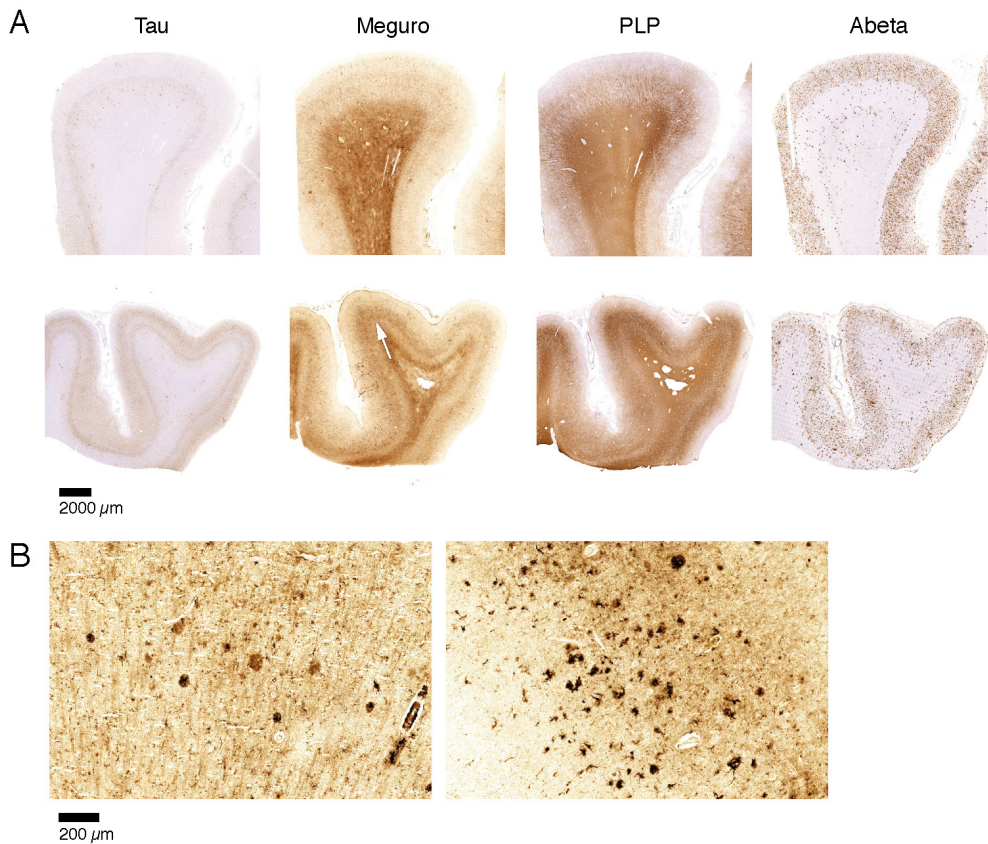


Figure 4: Iron accumulation in AD, related to tau pathology and plaques. A: Both patients (first and second row) show similar amounts of plaques but only the tissue with the most severe tau pathology shows a diffuse band shaped increase of iron/PLP labelling in the middle cortical layers (arrows). B: 20µm sections of the same blocks. Cortex with the most severe tau pathology shows more iron accumulation in plaques and microglia.

[22, 34]. In addition to iron, other metals like copper, zinc, magnesium and aluminium have been shown in plaques and have also been implicated in AD and plaque pathogenesis [18, 35-37]. Although the ferrocyanide that is applied in the Perl's staining can also bind to other metals apart from iron, the precipitation of ferrocyanide with these metals does not appear to catalyze polymerization of DAB [22]. Indeed, ferrocyanide in combination with DAB, detects iron with much higher sensitivity than copper, magnesium, zinc, or calcium [34]. This excludes a significant contribution of other metals to our visualization of iron in the tissue.

Fixation and storage of tissue in formalin could lead to leakage of iron [38]. We took care not to include tissue that had been stored for prolonged

periods of time. Nevertheless, we investigated the potential impact using fixed versus fresh-frozen postmortem tissue of the same patients on the histochemical detection of iron. Briefly-fixed frozen sections qualitatively showed a similar band of increased iron staining as in the paraffin sections. Also, iron-laden plaques and microglia could be observed, but visual comparison showed that this was not more prominent than in the paraffin sections. Therefore, we conclude that a qualitative assessment of iron accumulation in different cell types is reliable in our selected samples.

Iron and Myelin

In addition to iron in A β plaques and microglia of AD cortex, we confirmed our preliminary observation [25] of a band-shaped increase of iron and PLP labelling in cortical layers III-V in a subset of AD patients with the most severe tau pathology, a finding we have not seen reported before.

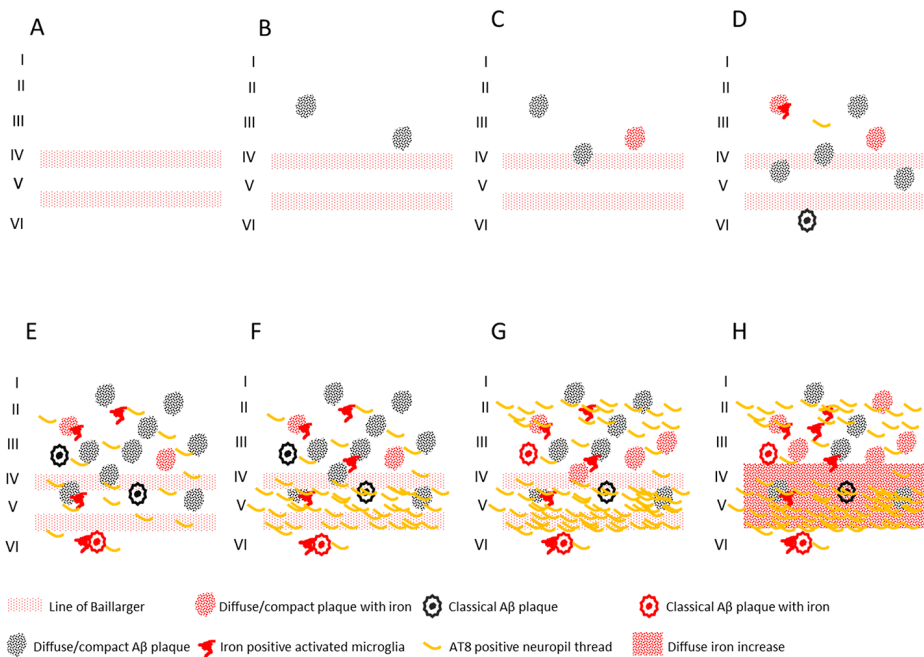


Figure 5: Schematic representation of the observed combinations of AD pathology and iron accumulation in frontal cortex. A: aging without plaques or tau pathology. B: controls with little diffuse plaques without iron accumulation. C and D: controls with increasing iron accumulation in plaques and microglia depending on the amount of plaques. E: AD with high A β plaque load and diffuse limited increase of tau pathology with increased iron accumulation. F-H: Similar high plaque load with increasing tau pathology and iron accumulation.

This band reflected a more crowded network of neuropil fibres with thicker and darker staining for iron and several different myelin proteins. This finding is in line with a meta-analysis by Tao et al. [39] and a recent laser-ablation inductively coupled plasma-mass spectrometry imaging study [40], both showing increased iron levels in the cortex of AD patients compared to controls. Interestingly, the investigators also showed a trend of increased iron along white matter fibres, including myelinated fibres in the lines of Baillarger, in AD patients [40]. This is in line with our observations of increased iron along neuropil fibres in the mid cortical layers. This qualitative observation of increased myelin staining in a late stage of AD, a neurodegenerative disease, is counter-intuitive. This study was not designed to prove this observation quantitatively, and therefore we cannot exclude the possibility that atrophy or other disease-associated tissue changes may result in better antigen retrieval or compaction of myelinated fibres. Furthermore, increased labelling of myelin proteins does not prove an increased amount of functional myelin or myelinated fibres. However, we found a consistent increase of several myelin proteins by different antibodies, making a true local myelin increase more likely. The mechanism by which severe AD may lead to increased cortical myelin proteins is open for speculation. Re-myelination is an almost default reaction of the brain to demyelination caused by myelin damage and/or death of oligodendrocytes [41-44]. Thus, maybe the continuous severe tissue and cell damage in late stage AD leads to unbalanced de- and re-myelination. Indeed, myelin damage and restoration with increased oligodendrocyte proliferating cells (OPC) has been shown in an AD mouse model, although in the same study a decrease of OPC was found in the brains of human AD patients [45]. We observed a band shaped increase of iron/myelin proteins in cortical layers III-V in a context of increased iron laden microglia. This is in line with the close relationship between iron and myelin synthesis extensively described in the literature [46, 47]. For example, activated microglia have been described to drive the recruitment and proliferation of OPC and their differentiation to oligodendrocytes, as well as the formation of a myelin sheath around available axons [41, 42, 48]. Moreover, it is thought that microglia provide the high iron concentrations needed for myelination and oligodendrocyte differentiation [47, 49, 50]. We observed increased labelling of myelin proteins as a late phenomenon, occurring only in cortices severely affected by both A β plaques and tau pathology. This does not support the hypothesis of an early role of myelin dyshomeostasis in the pathogenesis of AD [1]. However, disruption of

cortical myelin may contribute to the ongoing neurological deterioration in late stage AD.

Iron and Microglia

In our cases, there was a clear presence of activated and iron laden microglial cells around A β plaques. The polarization of microglia, as in macrophages, plays an important role in the neuroinflammatory response [51]. Classically activated, or M1, microglia drive the pro-inflammatory response, whereas the alternative activation state, or M2, is apparently an anti-inflammatory state, mediating tissue maintenance and repair. In macrophages, iron accumulation can directly activate the M1 phenotype. Conversely, M2-polarized cells are thought to be involved in iron recycling by expressing molecules involved in iron uptake and export [52]. However, recent evidence shows that increased intracellular iron can alter microglia polarization to a pro-inflammatory M1 phenotype [53].

Iron and Neurodegeneration

Iron accumulation is not merely a marker of neurodegeneration, but has been shown to play a crucial role in the progression of neurodegeneration through several mechanisms [54-56]. Production of reactive oxygen species (ROS) leading to DNA damage and cell death is a well-known consequence of iron overload and a common feature in many neurodegenerative diseases [56]. The mechanisms behind iron dyshomeostasis are still not fully understood, but several key processes in AD have been found to be of importance. A β processing and regulation of intracellular iron are e.g. both modulated by furin, thus mutually activating pro-amylogenic and intracellular iron accumulation pathways [57].

In addition, apart from driving the amyloid cascade, the intracellular complexation of a certain iron species, magnetite, with A β appears to have an adverse effect on neuronal network function to a much larger extent than A β alone [54]. Also iron has been implicated in lipid metabolism through an interaction with Apolipoprotein E (ApoE); with the APOE- ϵ 4 allele inducing high levels of cerebrospinal fluid ferritin [58] and brain iron levels on MRI [55], possibly due to reduced clearance of iron because of the low affinity of APOE- ϵ 4 to high-density lipoprotein [58]. As such, locally high iron concentrations in AD are likely the result of an intricate disbalance of iron uptake, mediated by furin and iron-regulating elements and iron clearance through microglial lysosomal degradation and ApoE-mediated transport [36, 59], see also further reviews on this topic. The fact that

transferrin and HFE mutations have a higher incidence in AD patients stresses the self-perpetuating loop caused by iron and amyloid deposition. In this context, a recent paper by Maher et al. raised the intriguing concept that iron deposition as an initiator of AD pathogenesis may not only be the result of iron-regulation gone haywire, but may also be caused by environmental factors such as airborne iron-bearing nanoparticles entering the brain through the olfactory bulb, [60]. In conclusion, at this moment it appears that iron toxicity in the brain is a complex phenomenon, which may be both the cause and consequence of neurodegenerative processes. Further research should focus on the cellular localization of iron and its interaction with other mediators of AD, such as A β , as well as on the characterization of different iron species in the brain [61].

Iron and ageing

Some [27, 62] but not all [26] quantitative studies show increased frontal cortical iron concentrations with aging. The present study was not designed to quantify iron load, but we found no changes in frontal cortical iron distribution from young to old controls without A β plaques. This suggests that, although there may be increased iron load in aging cortex, the distribution of frontal cortical iron remains the same. This finding is helpful if iron based MRI changes may be used in the differentiation between an aging related disease like AD and aging.

Iron and APOE

APOE- ϵ 4 is a well-known risk factor for AD and has recently been shown to correlate with ferritin levels in cerebrospinal fluid of APOE- ϵ 4 carriers [58]. Van Bergen et al. (2016) demonstrated that magnetic susceptibility, as measured with MRI, was significantly higher in APOE- ϵ 4 carriers with mild cognitive impairment (MCI) compared to MCI patients with other APOE variants [55]. These results confirm the hypothesis that the APOE- ϵ 4 allele may increase the risk of developing AD via brain iron accumulation. In our study, we unfortunately only had DNA available for 8/10 of our AD patients, of which 2 were ϵ 4/ ϵ 4, 5 were ϵ 4/ ϵ 3 and only 1 ϵ 3/ ϵ 3. As expected, APOE- ϵ 4 was highly prevalent in these patients and the APOE- ϵ 3/ ϵ 3 patient showed frontal cortical iron accumulations similar to the others. However, our sample size was too small and thus our data do not allow any conclusion to be drawn about a relation between APOE status and frontal cortical iron accumulations. Lastly, besides APOE status, mutations in some iron-regulating genes, such as HFE (hemochromato-

sis), are also known to associate with age of onset in AD [63]. Future studies correlating iron-related genetic variants to brain iron accumulation would be of interest.

Iron and AD pathology

Finally, we showed a statistically significant correlation between iron accumulations (in A β plaques/microglia and myelinated fibres in the mid cortical layers) and the amount of A β plaques and tau pathology, as well as between these iron accumulations and Braak stage. To our knowledge this is the first report that correlates frontal cortical iron accumulations with Braak stage and local tau pathology. This opens the possibility to grade the severity of AD pathology by MR in vivo. In Fig 5 we schematically represent the different combinations of AD pathology and pathological iron accumulations we encountered. These combinations suggest that histochemically detectable iron accumulation is secondary to A β plaques and tau pathology and follows its progression. In controls, iron accumulation only occurs in the presence of A β plaques and the amount of iron accumulation is correlated to the amount of A β plaques. For AD, A β plaque load does not increase much from Braak IV to VI, but iron accumulation and tau pathology both progress. The band shaped increase of diffuse iron-/myelin protein labelling in cortical layers III-V especially appears to be a late phenomenon, occurring when several cortical layers, especially layer V and II/outer III are heavily involved by tau pathology.

Conclusion

The presented data show a correlation between frontal cortical iron accumulation and AD pathology independent of age. Iron is not only accumulated in A β plaques but also in activated microglia and in myelinated fibres in the middle cortical layers with increased labelling of myelin proteins. Ex vivo MRI has shown iron related hypointensities in iron rich cortical myelin tracts and iron accumulation in microglia and A β plaques [13, 64, 65], suggesting the potential to detect these iron rich cortical areas with in vivo MRI. Complementary work from our lab showed that changes in iron and in myelin organization co-localize on a pixel-by-pixel basis to MRI contrast changes, demonstrating that iron is a major source of cortical MRI contrast in AD (data submitted for publication). The direct clinical relevance of these findings is supported by an earlier study in which high field susceptibility-weighted MR already demonstrated that iron-related MR contrast was detectable in human subjects, and shows different con-

trast between controls, patients with cognitive impairment and patients with clinically diagnosed AD [7]. Thus, iron imaging with MR reflects multiple aspects of AD pathology beyond A β plaques and therefore offers complementary in vivo imaging possibilities beyond PiB-PET amyloid and tau-PET imaging.

Acknowledgements

This work was in part supported by a project grant from the EU Seventh Framework Programme: FP7-PEOPLE-2013-IAPP (612360 – BRAINPATH)

Conflict of Interest

The authors have no conflict of interest to report.

References

- [1] Jack CR, Jr., Knopman DS, Jagust WJ, Shaw LM, Aisen PS, Weiner MW, Petersen RC, Trojanowski JQ (2010) Hypothetical model of dynamic biomarkers of the Alzheimer's pathological cascade. *Lancet Neurol* 9, 119-128.
- [2] Nelson PT, Braak H, Markesbery WR (2009) Neuropathology and cognitive impairment in Alzheimer disease: a complex but coherent relationship. *J Neuropathol Exp Neurol* 68, 1-14.
- [3] Engler H, Forsberg A, Almkvist O, Blomquist G, Larsson E, Savitcheva I, Wall A, Ringheim A, Langstrom B, Nordberg A (2006) Two-year follow-up of amyloid deposition in patients with Alzheimer's disease. *Brain* 129, 2856-2866.
- [4] Klunk WE, Engler H, Nordberg A, Wang YM, Blomqvist G, Holt DP, Bergstrom M, Savitcheva I, Huang GF, Estrada S, Ausen B, Debnath ML, Barletta J, Price JC, Sandell J, Lopresti BJ, Wall A, Koivisto P, Antoni G, Mathis CA, Langstrom B (2004) Imaging brain amyloid in Alzheimer's disease with Pittsburgh Compound-B. *Annals of Neurology* 55, 306-319.
- [5] Rowe CC, Ng S, Ackermann U, Gong SJ, Pike K, Savage G, Cowie TF, Dickinson KL, Maruff P, Darby D, Smith C, Woodward M, Merory J, Tochon-Danguy H, O'Keefe G, Klunk WE, Mathis CA, Price JC, Masters CL, Villemagne VL (2007) Imaging beta-amyloid burden in aging and dementia. *Neurology* 68, 1718-1725.
- [6] Rowe CC, Villemagne VL (2011) Brain Amyloid Imaging. *Journal of Nuclear Medicine* 52, 1733-1740.
- [7] van Rooden S, Versluis MJ, Liem MK, Milles J, Maier AB, Oleksik AM, Webb AG, van Buchem MA, van der Grond J (2014) Cortical phase changes in Alzheimer's disease at 7T MRI: a novel imaging marker. *Alzheimers Dement* 10, e19-26.
- [8] Ogg RJ, Langston JW, Haacke EM, Steen RG, Taylor JS (1999) The correlation between phase shifts in gradient-echo MR images and regional brain iron concentration. *Magn Reson Imaging* 17, 1141-1148.
- [9] Jack CR, Jr., Garwood M, Wengenack TM, Borowski B, Curran GL, Lin J, Adriany G, Grohn OH, Grimm R, Poduslo JF (2004) In vivo visualization of Alzheimer's amyloid plaques by magnetic resonance imaging in transgenic mice without a contrast agent. *Magn Reson Med* 52, 1263-1271.
- [10] Jack CR, Jr., Wengenack TM, Reyes DA, Garwood M, Curran GL, Borowski BJ, Lin J, Preboske GM, Holasek SS, Adriany G, Poduslo JF

- (2005) In vivo magnetic resonance microimaging of individual amyloid plaques in Alzheimer's transgenic mice. *J Neurosci* 25, 10041-10048.
- [11] Vanhoutte G, Dewachter I, Borghgraef P, Van Leuven F, Van der Linden A (2005) Non-invasive in vivo MRI detection of neuritic plaques associated with iron in APP[V717I] transgenic mice, a model for Alzheimer's disease. *Magn Reson Med* 53, 607-613.
- [12] Benveniste H, Einstein G, Kim KR, Hulette C, Johnson GA (1999) Detection of neuritic plaques in Alzheimer's disease by magnetic resonance microscopy. *Proc Natl Acad Sci U S A* 96, 14079-14084.
- [13] Meadowcroft MD, Connor JR, Smith MB, Yang QX (2009) MRI and histological analysis of beta-amyloid plaques in both human Alzheimer's disease and APP/PS1 transgenic mice. *J Magn Reson Imaging* 29, 997-1007.
- [14] Connor JR, Menzies SL, St Martin SM, Mufson EJ (1992) A histochemical study of iron, transferrin, and ferritin in Alzheimer's diseased brains. *J Neurosci Res* 31, 75-83.
- [15] Falangola MF, Lee SP, Nixon RA, Duff K, Helpert JA (2005) Histological co-localization of iron in Abeta plaques of PS/APP transgenic mice. *Neurochem Res* 30, 201-205.
- [16] Grundke-Iqbal I, Fleming J, Tung YC, Lassmann H, Iqbal K, Joshi JG (1990) Ferritin is a component of the neuritic (senile) plaque in Alzheimer dementia. *Acta Neuropathol* 81, 105-110.
- [17] LeVine SM (1997) Iron deposits in multiple sclerosis and Alzheimer's disease brains. *Brain Res* 760, 298-303.
- [18] Lovell MA, Robertson JD, Teesdale WJ, Campbell JL, Markesbery WR (1998) Copper, iron and zinc in Alzheimer's disease senile plaques. *J Neurol Sci* 158, 47-52.
- [19] Nabuurs RJ, Hegeman I, Natta R, van Duinen SG, van Buchem MA, van der Weerd L, Webb AG (2011) High-field MRI of single histological slices using an inductively coupled, self-resonant microcoil: application to ex vivo samples of patients with Alzheimer's disease. *NMR Biomed* 24, 351-357.
- [20] Smith MA, Harris PL, Sayre LM, Perry G (1997) Iron accumulation in Alzheimer disease is a source of redox-generated free radicals. *Proc Natl Acad Sci U S A* 94, 9866-9868.
- [21] El Tannir El Tayara N, Delatour B, Le Cudennec C, Guegan M, Volk A, Dhenain M (2006) Age-related evolution of amyloid burden, iron load, and MR relaxation times in a transgenic mouse model of Alzheimer's disease. *Neurobiol Dis* 22, 199-208.

- [22] Meguro R, Asano Y, Odagiri S, Li C, Iwatsuki H, Shoumura K (2007) Nonheme-iron histochemistry for light and electron microscopy: a historical, theoretical and technical review. *Arch Histol Cytol* 70, 1-19.
- [23] House MJ, St Pierre TG, Kowdley KV, Montine T, Connor J, Beard J, Berger J, Siddaiah N, Shankland E, Jin LW (2007) Correlation of proton transverse relaxation rates (R2) with iron concentrations in postmortem brain tissue from Alzheimer's disease patients. *Magn Reson Med* 57, 172-180.
- [24] van Rooden S, Maat-Schieman ML, Nabuurs RJ, van der Weerd L, van Duijn S, van Duinen SG, Natta R, van Buchem MA, van der Grond J (2009) Cerebral amyloidosis: postmortem detection with human 7.0-T MR imaging system. *Radiology* 253, 788-796.
- [25] van Duijn S, Nabuurs RJ, van Duinen SG, Natta R (2013) Comparison of histological techniques to visualize iron in paraffin-embedded brain tissue of patients with Alzheimer's disease. *J Histochem Cytochem* 61, 785-792.
- [26] Hallgren B, Sourander P (1958) The effect of age on the non-haemin iron in the human brain. *J Neurochem* 3, 41-51.
- [27] Ramos P, Santos A, Pinto NR, Mendes R, Magalhaes T, Almeida A (2014) Iron levels in the human brain: a post-mortem study of anatomical region differences and age-related changes. *J Trace Elem Med Biol* 28, 13-17.
- [28] Alafuzoff I, Arzberger T, Al-Sarraj S, Bodi I, Bogdanovic N, Braak H, Bugiani O, Del-Tredici K, Ferrer I, Gelpi E, Giaccone G, Graeber MB, Ince P, Kamphorst W, King A, Korkolopoulou P, Kovacs GG, Larionov S, Meyronet D, Monoranu C, Parchi P, Patsouris E, Roggendorf W, Seilhean D, Tagliavini F, Stadelmann C, Streichenberger N, Thal DR, Wharton SB, Kretschmar H (2008) Staging of neurofibrillary pathology in Alzheimer's disease: a study of the BrainNet Europe Consortium. *Brain Pathol* 18, 484-496.
- [29] Hothorn T, Hornik K, van de Wiel MAV, Zeileis A (2008) Implementing a Class of Permutation Tests: The coin Package. *Journal of Statistical Software* 28, 1-23.
- [30] Hughes V (2012) Microglia: The constant gardeners. *Nature* 485, 570-572.
- [31] Lue LF, Kuo YM, Beach T, Walker DG (2010) Microglia activation and anti-inflammatory regulation in Alzheimer's disease. *Mol Neurobiol* 41, 115-128.
- [32] Carpenter AF, Carpenter PW, Markesbery WR (1993) Morphometric

analysis of microglia in Alzheimer's disease. *J Neuropathol Exp Neurol* 52, 601-608.

[33] Kreutzberg GW (1996) Microglia: a sensor for pathological events in the CNS. *Trends Neurosci* 19, 312-318.

[34] Roschzttardtz H, Conejero G, Curie C, Mari S (2009) Identification of the endodermal vacuole as the iron storage compartment in the *Arabidopsis* embryo. *Plant Physiol* 151, 1329-1338.

[35] Leskovjan AC, Lanzirotti A, Miller LM (2009) Amyloid plaques in PSAPP mice bind less metal than plaques in human Alzheimer's disease. *Neuroimage* 47, 1215-1220.

[36] Meadowcroft MD, Connor JR, Yang QX (2015) Cortical iron regulation and inflammatory response in Alzheimer's disease and APPSWE/PS1DeltaE9 mice: a histological perspective. *Front Neurosci* 9, 255.

[37] Miller LM, Wang Q, Telivala TP, Smith RJ, Lanzirotti A, Miklossy J (2006) Synchrotron-based infrared and X-ray imaging shows focalized accumulation of Cu and Zn co-localized with beta-amyloid deposits in Alzheimer's disease. *Journal of Structural Biology* 155, 30-37.

[38] Hare DJ, George JL, Bray L, Volitakis I, Vais A, Ryan TM, Cherny RA, Bush AI, Masters CL, Adlard PA, Doble PA, Finkelstein DI (2014) The effect of paraformaldehyde fixation and sucrose cryoprotection on metal concentration in murine neurological tissue (vol 29, pg 565, 2014). *Journal of Analytical Atomic Spectrometry* 29, 1726-1726.

[39] Tao Y, Wang Y, Rogers JT, Wang F (2014) Perturbed iron distribution in Alzheimer's disease serum, cerebrospinal fluid, and selected brain regions: a systematic review and meta-analysis. *J Alzheimers Dis* 42, 679-690.

[40] Hare DJ, Raven EP, Roberts BR, Bogeski M, Portbury SD, McLean CA, Masters CL, Connor JR, Bush AI, Crouch PJ, Doble PA (2016) Laser ablation-inductively coupled plasma-mass spectrometry imaging of white and gray matter iron distribution in Alzheimer's disease frontal cortex. *Neuroimage* 137, 124-131.

[41] Crawford AH, Chambers C, Franklin RJ (2013) Remyelination: the true regeneration of the central nervous system. *J Comp Pathol* 149, 242-254.

[42] Gudi V, Gingele S, Skripuletz T, Stangel M (2014) Glial response during cuprizone-induced de- and remyelination in the CNS: lessons learned. *Front Cell Neurosci* 8, 73.

[43] Nave KA (2010) Myelination and the trophic support of long axons. *Nat Rev Neurosci* 11, 275-283.

- [44] Franklin RJ, Ffrench-Constant C (2008) Remyelination in the CNS: from biology to therapy. *Nat Rev Neurosci* 9, 839-855.
- [45] Behrendt G, Baer K, Buffo A, Curtis MA, Faull RL, Rees MI, Gotz M, Dimou L (2013) Dynamic changes in myelin aberrations and oligodendrocyte generation in chronic amyloidosis in mice and men. *Glia* 61, 273-286.
- [46] Connor JR, Menzies SL (1996) Relationship of iron to oligodendrocytes and myelination. *Glia* 17, 83-93.
- [47] Todorich B, Pasquini JM, Garcia CI, Paez PM, Connor JR (2009) Oligodendrocytes and myelination: the role of iron. *Glia* 57, 467-478.
- [48] Miron VE, Franklin RJ (2014) Macrophages and CNS remyelination. *J Neurochem* 130, 165-171.
- [49] Schonberg DL, Goldstein EZ, Sahinkaya FR, Wei P, Popovich PG, McTigue DM (2012) Ferritin stimulates oligodendrocyte genesis in the adult spinal cord and can be transferred from macrophages to NG2 cells in vivo. *J Neurosci* 32, 5374-5384.
- [50] Schonberg DL, McTigue DM (2009) Iron is essential for oligodendrocyte genesis following intraspinal macrophage activation. *Exp Neurol* 218, 64-74.
- [51] Cherry JD, Olschowka JA, O'Banion MK (2014) Neuroinflammation and M2 microglia: the good, the bad, and the inflamed. *J Neuroinflammation* 11, 98.
- [52] Corna G, Campana L, Pignatti E, Castiglioni A, Tagliafico E, Bosurgi L, Campanella A, Brunelli S, Manfredi AA, Apostoli P, Silvestri L, Camaschella C, Rovere-Querini P (2010) Polarization dictates iron handling by inflammatory and alternatively activated macrophages. *Haematologica* 95, 1814-1822.
- [53] Kroner A, Greenhalgh AD, Zarruk JG, Passos Dos Santos R, Gaestel M, David S (2014) TNF and increased intracellular iron alter macrophage polarization to a detrimental M1 phenotype in the injured spinal cord. *Neuron* 83, 1098-1116.
- [54] Teller S, Tahirbegi IB, Mir M, Samitier J, Soriano J (2015) Magnetite-Amyloid-beta deteriorates activity and functional organization in an in vitro model for Alzheimer's disease. *Sci Rep* 5, 17261.
- [55] van Bergen JM, Li X, Hua J, Schreiner SJ, Steininger SC, Quevenco FC, Wyss M, Gietl AF, Treyer V, Leh SE, Buck F, Nitsch RM, Pruessmann KP, van Zijl PC, Hock C, Unschuld PG (2016) Colocalization of cerebral iron with Amyloid beta in Mild Cognitive Impairment. *Sci Rep* 6, 35514.
- [56] Zecca L, Youdim MB, Riederer P, Connor JR, Crichton RR (2004) Iron, brain ageing and neurodegenerative disorders. *Nat Rev Neurosci* 5,

863-873.

- [57] Silvestri L, Pagani A, Camaschella C (2008) Furin-mediated release of soluble hemojuvelin: a new link between hypoxia and iron homeostasis. *Blood* 111, 924-931.
- [58] Ayton S, Faux NG, Bush AI, Alzheimer's Disease Neuroimaging I (2015) Ferritin levels in the cerebrospinal fluid predict Alzheimer's disease outcomes and are regulated by APOE. *Nat Commun* 6, 6760.
- [59] Ward RJ, Zucca FA, Duyn JH, Crichton RR, Zecca L (2014) The role of iron in brain ageing and neurodegenerative disorders. *Lancet Neurol* 13, 1045-1060.
- [60] Maher BA, Ahmed IA, Karloukovski V, MacLaren DA, Foulds PG, Allsop D, Mann DM, Torres-Jardon R, Calderon-Garciduenas L (2016) Magnetite pollution nanoparticles in the human brain. *Proc Natl Acad Sci U S A* 113, 10797-10801.
- [61] Kumar P, Bulk M, Webb A, van der Weerd L, Oosterkamp TH, Huber M, Bossoni L (2016) A novel approach to quantify different iron forms in ex-vivo human brain tissue. *Sci Rep* 6, 38916.
- [62] Connor JR, Snyder BS, Arosio P, Loeffler DA, LeWitt P (1995) A quantitative analysis of isoferritins in select regions of aged, parkinsonian, and Alzheimer's diseased brains. *J Neurochem* 65, 717-724.
- [63] Ali-Rahmani F, Schengrund CL, Connor JR (2014) HFE gene variants, iron, and lipids: a novel connection in Alzheimer's disease. *Front Pharmacol* 5, 165.
- [64] Fukunaga M, Li TQ, van Gelderen P, de Zwart JA, Shmueli K, Yao B, Lee J, Maric D, Aronova MA, Zhang G, Leapman RD, Schenck JF, Merkle H, Duyn JH (2010) Layer-specific variation of iron content in cerebral cortex as a source of MRI contrast. *Proc Natl Acad Sci U S A* 107, 3834-3839.
- [65] Zeineh MM, Chen Y, Kitzler HH, Hammond R, Vogel H, Rutt BK (2015) Activated iron-containing microglia in the human hippocampus identified by magnetic resonance imaging in Alzheimer disease. *Neurobiol Aging* 36, 2483-2500.

Chapter 5

Detection of cortical changes in Alzheimer's disease patients at ultra-high field MRI

R.J.A. Nabuurs, MD PhD #1, S van Rooden, MSc #1, S van Duijn, MSc 2, M.J. Versluis, PhD 1, B.J. Emmer, MD, PhD 1, M.K. Liem, MD, PhD 1, J.R. Milles, PhD 3, A.G. Webb, PhD 1, M.P. Frosch, MD, PhD 4, S.G. van Duinen, MD, PhD 2, R Natté, MD, PhD 2, J van der Grond, PhD 1, L van der Weerd, PhD 1,5, M.A. van Buchem, MD, PhD 1

Authors have contributed to this work equally.

1. Department of Radiology, Leiden University Medical Centre, Albinusdreef 2, 2333 ZA, Leiden, Netherlands
2. Department of Pathology, Leiden University Medical Centre, Albinusdreef 2, 2333 ZA, Leiden, Netherlands
3. Division of Image Processing (LKEB), Department of Radiology, Leiden University Medical Centre, Albinusdreef 2, 2333 ZA, Leiden, Netherlands
4. C.S. Kubik Laboratory for Neuropathology, Massachusetts General Hospital and Harvard Medical School, 55 Fruit Street, Boston, MA 02114, USA
5. Department of Human Genetics, Leiden University Medical Centre, 2333 ZA, Albinusdreef 2, Leiden, Netherlands

Abstract

Non-invasive methods to detect Alzheimer's disease (AD) in vivo at an early stage are important to increase our still-incomplete understanding of the pathophysiology of the disease. In this study we assessed whether differences in cortical appearance could be observed in AD patients using 7T magnetic resonance imaging in vivo and to assess the nature of these changes by a histological-radiological correlation ex vivo. In vivo regional cortical differences between probable AD patients (n=14, mean age 76.4 years (range: 68 - 86), 9 males) and healthy control subjects (n=15, mean age 75.1 years (range: 69 - 80), 10 males), visible on 7T susceptibility-weighted images, were analyzed after defining a novel scoring method based on the cortical appearance. In addition, postmortem magnetic resonance imaging of confirmed AD cases (n=6) was performed to assess the histological correlates of the changes observed in vivo in AD patients. A chi-square test showed that diffuse hypointense bands were frequently found in the cortex of the frontal lobes of AD patients (57%), but not in controls, $p = 0.001$. Histologic correlation revealed that the pattern of the susceptibility-weighted contrast in the cortex of AD patients does not primarily co-localize with amyloid plaques or neurofibrillary tangles, but with microglia- and myelin-associated iron accumulation and with an altered myelin cytoarchitecture. Our observation of disturbed iron accumulation and myelin architecture in AD has important implications for the understanding of the pathophysiological mechanisms underlying this disease, and also for in vivo diagnosis of AD.

Keywords: Alzheimer's disease, cortex, beta-amyloid, magnetic resonance imaging, iron.

Abbreviations: amyloid-beta ($A\beta$), diaminobenzidine-tetrahydrochloride (DAB), echo time (TE), electron microscopy (EM), gray matter (GM), Mini Mental State Examination (MMSE), National Institute of Neurological and Communicative Disorders and Stroke and Alzheimer's disease and Related Disorders Association (NINCDS-ADRDA), paired helical filament-tau (AT8), protolipid-protein (PLP), repetition time (TR), susceptibility-weighted (SW), white matter (WM).

Introduction

For the definitive diagnosis of Alzheimer's disease (AD) histological post-mortem detection of amyloid plaques and neurofibrillary tangles is required. During life, only a probable diagnosis can be made that is based primarily on clinical signs and symptoms (Montine et al., 2012). However, recently it has been proposed to use biomarkers based on CSF analysis, structural MRI and amyloid imaging using PET, as supporting diagnostic criteria in research settings (Jack, Jr. et al., 2010).

Over the past few years, the feasibility of detecting the histological hallmarks of AD using MRI has been explored by many research groups. In general these efforts have focused on detecting individual amyloid plaques: increased iron accumulation around amyloid plaques induces a magnetic susceptibility effect, which is visible as hypointense foci on T2*-weighted or susceptibility-weighted (SW) MRI in the cerebral cortex of transgenic AD mouse models and in human post-mortem brain slices (van Rooden et al., 2009; Meadowcroft et al., 2009; Chamberlain et al., 2011). However, these findings have not yet been convincingly replicated in vivo in patients, and it is doubtful whether detecting individual amyloid plaques with MRI will be possible in a clinical setting given the required high anatomical resolution, limited scanning time, and physiological motion of the patient. Furthermore, the central role of amyloid in the pathophysiology of AD remains a topic of debate. Although amyloid is still considered to be a hallmark as well as an initiating factor in the progression of the disease, there is increasing evidence that other primary or interacting causes, including changes in iron metabolism, may exist (Karran et al., 2011; Fjell and Walhovd, 2012).

Recent advances in human MRI systems operating at an ultra-high magnetic field strength (7 Tesla and higher) show that the increased sensitivity to susceptibility effects generates iron-based contrasts in the human brain that have not been observed at lower fields (Fukunaga et al., 2010). The aim of our study was to establish whether 7T MRI allows in vivo detection of differences in the cerebral cortex between probable Alzheimer's disease patients and healthy age-matched controls. Having observed a difference, we then determined the histological substrate of the changes by comparing MRI to light- and electron microscopy (EM) of human post-mortem material of Alzheimer's disease patients and controls.

Table 1: Characteristics of patients and controls and scoring results of *in vivo* the SW imaging study

| | Alzheimer's disease (n = 14) | Controls (n = 15) | p-value |
|--------------------------------------|---------------------------------|----------------------|---------|
| <u>Characteristics:</u> | | | |
| Male / female | 9/5 | 10/5 | 0.893 |
| Mean age (range, yrs) | 76.4 (68 – 86) | 75.1 (69 – 80) | 0.497 |
| MMSE (range) | 22.5 (19 - 26) | 29.2 (27 – 30) | 0.000 |
| <u>Presence of homogeneous layer</u> | | | |
| Superior frontal lobe | 12/14 (85.7%) | 15/15 (100%) | 0.224 |
| Middle and inferior frontal lobe | 5/14 (35.7%) | 9/15 (60%) | 0.006 |
| <u>Presence of two layers</u> | | | |
| Superior frontal lobe | 2/14 (14.3%) | 5/15 (33.3%) | 0.390 |
| Middle and inferior frontal lobe | 10/14 (71.4%) | 13/15 (86.6%) | 0.390 |
| <u>Presence of three layers</u> | | | |
| Superior frontal lobe | 0/14 (0%) | 2/15 (13.3%) | 0.483 |
| Middle and inferior frontal lobe | 3/14 (21.4%) | 3/15 (20%) | 1.000 |
| <u>Presence of diffuse band</u> | | | |
| Superior frontal lobe | 2/14 (14.3%) | 0/15 (0%) | 0.224 |
| Middle and inferior frontal lobe | 8/14 (57.1%) | 0/15 (0%) | 0.001 |
| <u>Hypo-intense foci</u> | | | |
| Superior frontal lobe | 0/14 (0%) | 0/15 (0%) | - |
| Middle and inferior frontal lobe | 0/14 (0%) | 0/15 (0%) | - |

Materials and Methods

A. In vivo MRI study:

Participants

This study was approved by the institutional review board. In all cases, informed consent was obtained according to the declaration of Helsinki. Fourteen probable AD patients (mean age 76.4 years (range: 68 - 86), 9 males) and fifteen control subjects (mean age 75.1 years (range: 69 - 80), 10 males) were included (table 1). Alzheimer's disease patients were recruited from the memory outpatient clinic of our institution. Memory outpatient clinic patients were referred to the hospital by their general practitioner or a medical specialist. Prior to the 7T MRI study these patients all underwent a routine clinical protocol, comprising a whole brain MRI (performed on a clinical 3 Tesla platform), a battery of neuropsychological tests, and a general medical and neurological examination performed by a neurologist, psychiatrist or internist-geriatrician. The diagnosis was made in a multidisciplinary consensus meeting using the National Institute of Neurological and Communicative Disorders and Stroke and AD and Related Disorders Association (NINCDS-ADRDA) criteria for diagnosing probable AD (McKhann et al., 1984). Participants with the diagnosis 'probable Alzheimer's disease', who were capable of giving informed consent and who had a Mini Mental State Examination (MMSE) of ≥ 19 were selected for inclusion in the 7T study, either retrospectively within one year after attending the memory clinic, or prospectively. Healthy control subjects were recruited by focused advertisements. Subjects between 69 and 80 years of age, who were living independently and had an MMSE of ≥ 25 and a Geriatric Depression Scale (GDS) of ≤ 4 were selected for inclusion. Control subjects with the following diseases were excluded: stroke, Parkinson's disease, diabetes mellitus, rheumatoid arthritis, polymyalgia rheumatica, cancer, heart failure, and chronic obstructive pulmonary disease.

MRI data acquisition

Our study was performed on a human whole-body MRI system operating at a magnetic field strength of 7 Tesla (Philips Healthcare, Best, The Netherlands) using a quadrature transmit and 16-channel receive head coil (Nova Medical, Wilmington, MA, USA). Alzheimer's disease-related pathology spreads throughout almost the entire brain, but macroscopically

Table 2: Post-mortem subject characteristics and SW imaging analysis.

| <u>Subject characteristics</u> | | | | <u>9.4 T SW imaging analysis</u> | | | | | |
|--------------------------------|-----------|----------|--|----------------------------------|---------|------------------------------|--------------|--------------|--------|
| No. | Age / Sex | Diagnose | Cause(s) of death | Braak | Amyloid | Homogenous | Diffuse band | Hypo-intense | Clouds |
| | | | | | | with cortical layers foci | | | |
| 1 | 83 / F | Control | Arrhythmia | II | 0 | Yes | - | - | - |
| 2 | 93 / F | Control | Acute death | I | A | Yes | - | - | - |
| 3 | 89 / F | Control | Myocardial infarct / Pneumonia | III | A | No | + | + | + |
| 4 | 77 / M | AD | Cachexia / dehydration by advanced dementia syndrome | VI | C | No | + | + | - |
| 5 | 85 / F | AD | Aspiration pneumonia by advanced dementia syndrome | IV | C | No | + | - | + |
| 6 | 87 / F | AD | Respiratory tract infection / cerebrovascular accident | VI | C | No | + | - | + |
| 7 | 87 / M | AD | Cachexia / dehydration by advanced dementia syndrome | V | C | No | + | + | - |
| 8 | 87 / F | AD | Sepsis | V | C | No | - | - | + |
| 9 | 88 / F | AD | Unknown | IV | C | No | + | - | + |

typically involves the fronto-temporal association cortices (Duyckaerts et al., 2009; Bartzokis, 2011; Alves et al., 2012). Participants were scanned using a 2D flow-compensated axial T2*-weighted gradient-echo sequence which included the frontal lobe for detection of Alzheimer’s disease pathology with a total imaging duration of 10 minutes. Imaging parameters were: repetition time (TR)/echo time (TE) 794/25 ms, flip angle 45°, slice thickness 1.0 mm with a 0.1 mm interslice gap, 20 slices, 240 x 180 x 22 mm field of view, 1024x768 matrix size – resulting in an in-plane spatial resolution of 0.24 x 0.24 mm². The bandwidth per pixel was 46 Hz, corresponding to a readout length of approximately 22 ms. Frequency and phase encoding directions were along the anterior-posterior and right-left axes, respectively. This sequence is very sensitive to image artifacts arising from resonance frequency fluctuations within the brain caused by slight patient movements, even in areas significantly away from the head, and so a navigator echo was included to correct for these artifacts. (Versluis et al., 2010) Shimming up to third order was performed using an image based shimming approach (Schar et al., 2004). Phase images were unwrapped by high-pass filtering with a 92x92 kernel size. SW images were constructed by applying four phase mask multiplications (Haacke et al., 2004).

Whole brain imaging at this high spatial resolution (0.24 x 0.24 x 1 mm³) however would result in an impractically long imaging duration, particularly for Alzheimer’s disease patients (Versluis et al., 2010). Since susceptibility artifacts induced by the temporal bone hampered the imaging of the temporal lobe, the final imaging volume focused on the frontal lobe, which is less prone to atrophy than the temporal lobe, but is known to accumulate high amyloid loads (Rowe and Villemagne, 2011), to have a lower metabolic rate (Langbaum et al., 2009), and to have an altered

resting state network connectivity in Alzheimer's disease (Rombouts et al., 2005).

Image analysis

Based on previous 7T MRI studies of the human cortex in post-mortem brain specimens of Alzheimer's disease patients (van Rooden et al., 2009) and in vivo imaging of healthy volunteers (Duyn et al., 2007) we developed a scoring method to capture the appearance of the cortex on SW images. We defined a normal cortex based on the following criteria: a) a cortical ribbon containing one homogeneous layer with a higher signal intensity as compared to the adjacent white matter (WM), b) a cortical ribbon containing two well-defined, homogeneous layers, with the superficial layer demonstrating a higher signal intensity compared to the deepest layer (the layer adjacent to the WM) and the WM, or c) a cortical ribbon with three layers: the same layers as previously described separated by a third thin layer with a lower signal intensity than the other two layers (fig. 1). Abnormal cortex was classified as a deviation from the normal patterns described above, showing the presence of well-defined foci of signal loss (hypointense foci) and/or more diffuse areas with lower signal intensity in the superficial layer as compared to the adjacent WM (a diffuse band) (fig. 1). Features were scored as present or absent per subject in several predefined gyri of the frontal lobe (table 1). Uniform window settings were used for all images. Images were scored by two neuroradiologists (B.E. and M.L.) who were blinded for the diagnosis in a consensus reading.

Statistics

A Mann-Whitney U-test was used to assess differences in age and MMSE, and a chi-square test was used to assess differences in gender between Alzheimer's disease and control groups. For each feature (hypointense foci and/or a diffuse band), a Fisher's exact test was performed per brain region. Positive and negative predictive values of the features to detect Alzheimer's disease were calculated per brain region. All statistical analyses were performed with the Statistical Package of Social Sciences (SPSS 17.0.1; SPSS, Chicago, Ill).

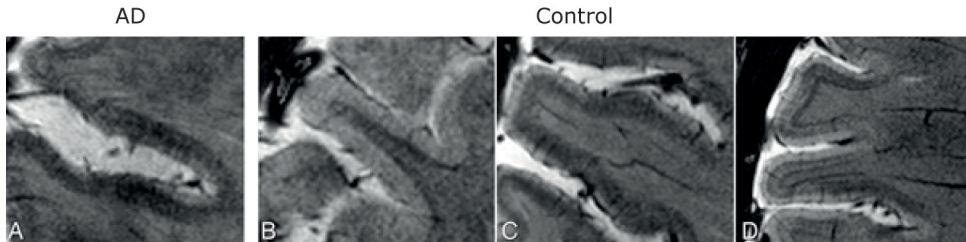


Figure 1: The observed variations of in vivo 7T SW imaging appearance of the human cortex. Shown are the middle/inferior frontal brain area of an Alzheimer's disease patient (A) and healthy elderly controls (B, C, D). A clear example of a cortical ribbon containing a hypointense diffuse band is observed in the Alzheimer's disease patient (A). Please note the blurring of the edges of the layers. (B) shows an example of a cortical ribbon containing one regular layer with higher signal intensity than the adjacent WM. In (C) a cortical ribbon is shown containing two well-defined layers. (D) shows a cortical ribbon containing three well-defined layers.

B. Post-mortem MRI study:

Study design

To investigate the histological substrates responsible for the observed in vivo MRI changes at 7T, we applied similar scan methods on post-mortem material of Alzheimer's disease patients and controls using a vertical-bore 9.4 T system (Bruker Biospin, Ettlingen, Germany). For each sample high-resolution (isotropic 40 μm voxels) images were acquired, as well as images with a similar resolution (isotropic 200 μm voxels) as were used in the in vivo study. The lower resolution MR images were acquired to help the translation between the in vivo and ex vivo MR data sets. The high-resolution MR images helped to identify the particular MR images that matched best with the 8- μm thick histological sections.

Sample preparation

Brain tissue was obtained from the tissue bank of the Department of Pathology at our institution and from the Netherlands Brain Bank (NBB, Netherlands Institute for Neuroscience, Amsterdam). Following a post-mortem interval of <19 hours, brains were resected and stored in 4% paraformaldehyde. At both institutions brain tissue was examined histologically for the presence of Alzheimer's disease-related pathology and scored using the Braak classification (Braak et al., 2006). Based on availability 6 samples with a clinical diagnosis of Alzheimer's disease by histological confirmation were selected, as well as 3 age-matched non-demented controls (table 2). Patient anonymity was strictly maintained. All tissue samples were handled in a coded fashion, according to Dutch national ethical

guidelines (Code for Proper Secondary Use of Human Tissue, Dutch Federation of Medical Scientific Societies). To avoid formalin-induced artifacts in the MR images only material fixed for a period of between 3 months and 2 years was used (van Duijn et al., 2011). From each subject 1 tissue block of approximately 4 x 15 x 15 mm³ was resected from the medial temporal lobe using a vibratome (VT1000S, Leica, Germany). Care was taken to ensure that the samples were resected with a similar gyral orientation. Residual formalin was washed out by placing the samples in phosphate buffered saline (PBS) for >24 hours to partially restore MR relaxation parameters (Shepherd et al., 2009). For MRI, each sample was placed in a customized tissue container and immersed in a proton-free fluid (Fomblin LC08, Solvay). Air was removed by application of a vacuum for several minutes (van Duijn et al., 2011).

Post-mortem MRI

Scans were acquired on a 9.4 Tesla vertical bore MRI system, equipped with a 1 T/m actively-shielded gradient insert and Paravision 5.0 imaging software (Bruker Biospin, Ettlingen, Germany). A 20-mm diameter bird-

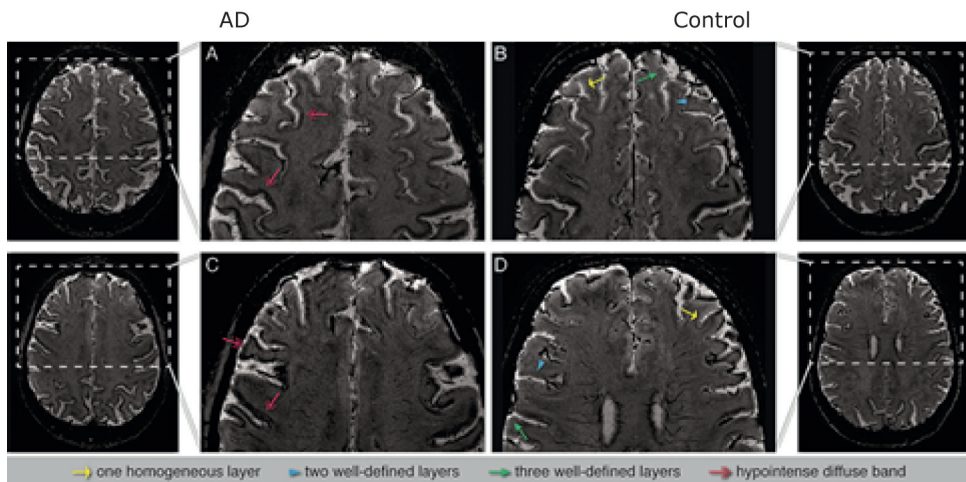


Figure 2. In vivo cortical differences seen on SW images in Alzheimer's disease patients versus age-matched control subjects. Regional distribution of the observed variations of in vivo 7T SW imaging appearance as presented in fig. 1, shown in an Alzheimer's disease patient and a control subject. The left two columns (A and C) show an Alzheimer's disease patient and the right two columns (B and D) a control subject. The upper row (A and B) shows the superior frontal region, the lower row (C and D) the middle and inferior frontal region. In the Alzheimer's disease patient a diffuse band is seen in both regions of the frontal lobe and the double arrows show several locations containing this band whereas in the control subject this diffuse band is absent and a regular layer (arrow), two-well defined layers (arrowhead) and three-well defined layers (small arrow) could be detected.

cage transmit/receive coil was used to acquire T2*-weighted 3D gradient echo images with TR = 75 ms; TE = 22.5 ms; flip angle = 25° at either 200 µm isotropic resolution with 20 signal averages, or 40 µm isotropic resolution with 28 signal averages. The average scan time per resolution was approximately 40 minutes (200 µm resolution) or 25 hours (40 µm resolution), with minor differences between samples of slightly different sizes. To create SW images comparable to in vivo scans, the 200 µm resolution phase images were unwrapped using a k-space Hanning filter with a width set to 50% of the image size (Wang et al., 2000). Final SW images were reconstructed from the original images by four phase mask multiplications (Haacke et al., 2004). All data processing was performed with MatLab (MathWorks, Natick, MA).

Postmortem image analysis

For assessment of ex vivo SW images we used the same criteria as were used in vivo for defining normal and abnormal cortex (hypointense bands and hypointense foci). In addition, since the ex vivo images showed increased anatomical detail compared to the in vivo scans (due to the absence of physiological motion), a third category of abnormal cortex could be added, namely diffuse areas with low signal intensity, not extending parallel to the cortical surface (as in healthy tissue) but instead expanding locally in an irregular fashion throughout the cortex, a feature which we have termed "clouds". Window settings were optimized for each sample based on the WM and gray matter (GM) histogram. The 200 µm SW images were scored blinded for diagnosis by a neuroradiologist (M.v.B) and MR-microscopy expert (L.v.d.W) in a consensus reading.

Histology and electron microscopy

All brain samples were paraffin-embedded and serially cut into 8-µm thick sections. Tissue morphology was assessed by standard hematoxylin-eosin (HE) staining. Iron was detected using a 3'3-diaminobenzidine-tetrahydrochloride (DAB) enhanced Perls' staining protocol for light microscopy and EM which has shown to be the most sensitive to detect iron-positive structures in paraffin-embedded human AD brain tissue (Meguro et al., 2007; van Duijn et al., 2013). Consecutive sections were (co-)stained for amyloid-beta (Aβ), paired helical filament-tau (AT8), myelin (protolipid-protein (PLP)), microglia (CD68 and HLA-DR) and activated astrocytes (GFAP) (Supplementary table 1). Endogenous peroxidase was blocked by 30 minutes of incubation in methanol with 0.02% H₂O₂. After these

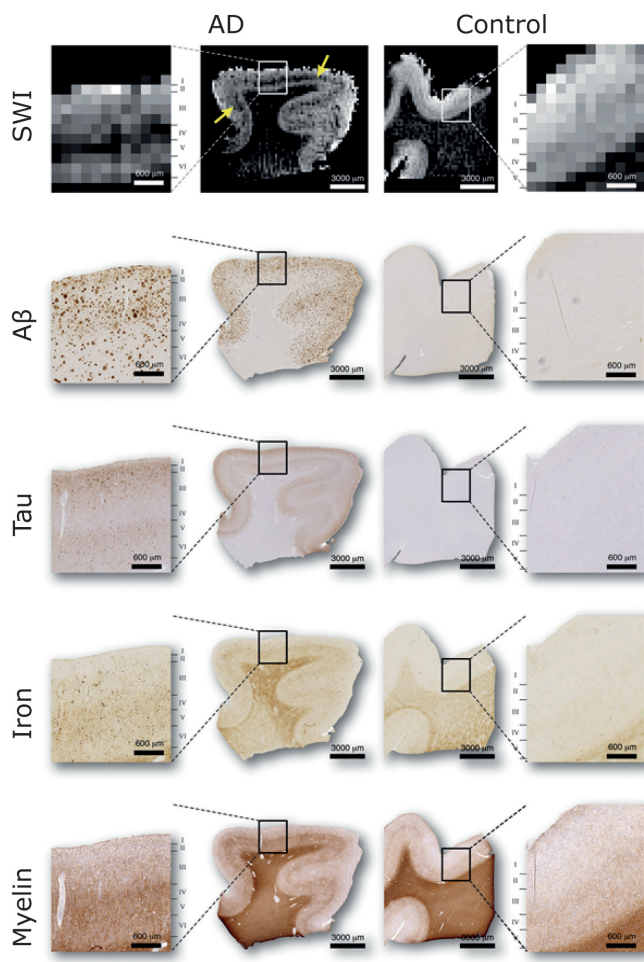


Figure 3. Comparison of post-mortem SW images with histology. The SW image of the Alzheimer's disease patient (table 2 subject 7) showed a midcortical hypointense band (yellow arrows) in addition to several focal hypointensities, as opposed to a clear homogeneous cortex as seen in the control subject (table 2 subject 1). For detailed evaluation similar regions of interest of the cortex are shown alongside each corresponding main image and the cortical layers have been assigned accordingly. Neither the cortical distribution of A β or tau matched the hypointense band. Tau typically showed a band-like pattern in cortical layers II – III and V, and so is not co-localized in the layer corresponding to MR signal decrease. Both iron and myelin correlated with the observed pattern of band-like hypointensities, including a diminished staining in the inner cortical layers V and VI. As compared to the control, the iron staining of the Alzheimer's disease subject showed an increase in cellular deposits and diffuse iron within the neuropil,

mainly centred around cortical layer IV spreading to both sides with overlap in layers III and IV. The myelin distribution visualized by the PLP-immunostaining showed a similar pattern of increased staining in the Alzheimer's disease subject resulting from a denser network of thin myelinated fibres. Similar to previous reports, in the Alzheimer's disease patient the cortex also contained several small roundish areas devoid of myelinated fibres suggesting the presence of amyloid plaques based on their morphological appearance (Mitew et al., 2010.)

pre-treatments, non-specific binding was minimized by incubation with 10% fetal calf serum (DakoCytomation). Labelling was visualized by DAB staining (DakoCytomation). All sections were digitized with a microscope scanner (Panoramic, 3DHistotech, Hungary) for global and microscopic evaluation. To assess co-localization of cellular iron with CD68, HLA-DR or GFAP-positive cells, sections stained for iron as described above were subsequently treated according to the previously described immunohistochemical procedures except for using an Alexa647-labeled secondary

anti-mouse antibody for immunofluorescence. Co-localization of these antigens with iron was assessed using a confocal fluorescence microscope (LSM 510, Zeiss, Germany). Iron-stained ultrathin (100 nm) sections were examined by electron microscopy (JEM-1011, JEOL, Germany) to assess the exact localization of the cortical iron in the neuropil.

Histology-MRI correlation

The digitized histological sections were matched with their corresponding high-resolution (40 μm) MR images by visual comparison of the contour and vascular architecture of each section. The corresponding low-resolution SW image that matched best with the histological section could then be identified directly since the two SW image datasets are inherently co-registered. To assess the histological substrate of the cortical changes observed on MR images, the digitized histological sections were first inspected at low magnification (2x) alongside the corresponding low-resolution SW image. Subsequently, these areas were further analyzed microscopically at higher magnification (40x) to look for the microscopic changes underlying the MR. All observations were independently verified by three neuropathologists (R.N., S.v.D., M.F.).

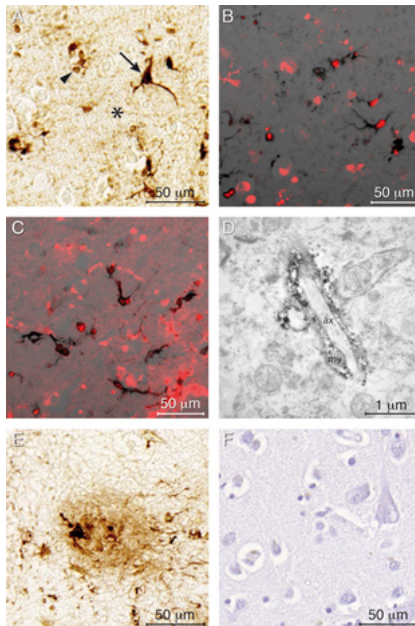


Figure 4. Characterization of intracortical iron distribution in Alzheimer's disease brain tissue. Shown are the different types of cellular and neuropilar intracortical iron in the medial temporal lobe of an Alzheimer's disease patient (table 2 subject 7). (A) Indicated by the brown colour due to the modified 3'3-DAB enhanced Perls' iron staining, iron is present as perinuclear (arrow head) and stellate cellular deposits (arrow), and as diffuse iron spread throughout the neuropil (asterix). Morphologically the cellular iron was attributed to oligodendrocyte or microglia cells. The latter was further verified by the co-localization of iron (black) with (B) CD68 (red) and (C) HLA-DR (red) immunostaining. As indicated by both stainings, even in close proximity to these iron-bearing microglia, several microglia were present that were completely devoid of iron. (D) Ultrastructurally, as shown by EM, neuropil iron was found to be located in the myelin sheets folded around an axon. (E) A example of iron found associated with an amyloid plaque. (F) The negative iron staining of a consecutive section did not result in any DAB enhancement, thereby confirming specificity of the iron stain (axon, ax; myelin sheet, my)

Results

The characteristics of the participants for in vivo MRI are shown in table 1. No difference in age ($p = 0.497$) or gender ($p = 0.893$) was found between patient and control groups. Scores for global cognitive functioning (MMSE score) were significantly higher in controls (29.2 points; range 27-30) than in patients with Alzheimer's disease (22.5 points, range 19-26), $p < 0.001$. 7T SW images of the frontal lobe of probable Alzheimer's disease patients ($n=14$) were visually compared to those of control subjects ($n=15$).

We developed a scoring method to rate the cortical appearance based on previous 7T observations in normal brain and postmortem observations in Alzheimer's disease patients, distinguishing normal-appearing cortical patterns with one or more homogeneous layers from hypointense foci or hypointense diffuse bands (fig. 1). Clear in vivo differences between Alzheimer's disease patients and controls were seen in terms of the presence of diffuse hypointense bands on the SW images (table 1, fig. 2). Within the frontal lobe, these patterns were found in the middle and inferior frontal gyri in eight out of 14 patients, whereas these diffuse bands were not observed in any of the control subjects. In these frontal gyri, the diffuse hypointense band was significantly more prevalent in Alzheimer's disease patients as compared to controls ($p = 0.001$), with positive predictive and negative values of 100% and 71%, respectively. In the superior frontal gyrus, a similar hypointense band was observed in only two out of the 14 Alzheimer's disease patients and in none of the control subjects: there was no significant difference between the two groups ($p = 0.224$). For this specific cortical region, corresponding positive and negative predictive values were 100% and 55%, respectively. Foci of signal loss were not observed in the frontal lobe in either Alzheimer's disease patients or control subjects.

Post-mortem cerebral cortex samples of six Alzheimer's disease cases and three age-matched controls were scanned with a similar SWI protocol as for the in vivo MRI. Two of the controls showed a normal cortex. The control subject with an abnormal cortex revealed Alzheimer's disease-type pathology (Braak stage III), despite the absence of an ante-mortem clinical Alzheimer's disease diagnosis. We therefore discuss the findings in this case separately.

In all postmortem AD samples (6 out of 6), an abnormal cortex was observed on SW images (table 2). Hypointense bands were observed in five out of six AD cases, and in the control with Braak III. Due to the lack of

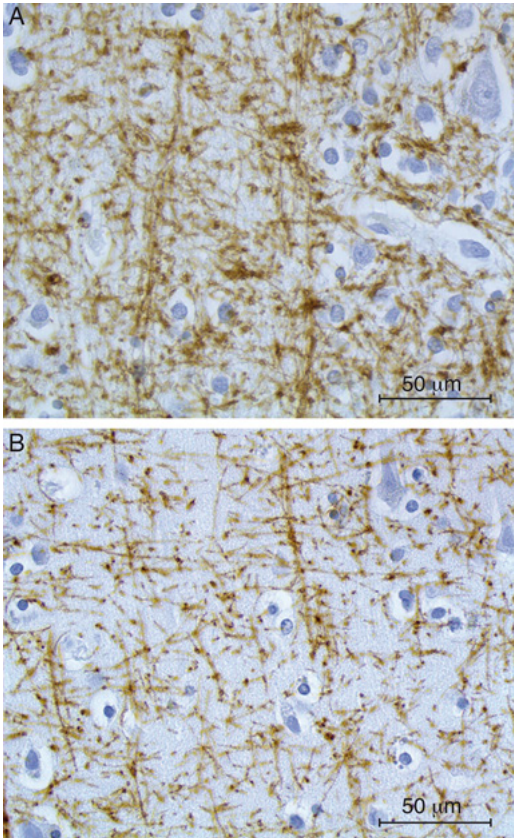


Figure 5. Structural alterations of intracortical myelin. In addition to the observed differences in myelin highlighted by fig. 3, this figure presents a more detailed comparison of the intracortical myelin of the medial temporal lobe of (A) an Alzheimer's disease patient (table 2 subject 4) and (B) a non-demented age-matched control (table 2 subject 1). Shown are midcortical regions (layer IV) with a comparable orientation assessed by a PLP-immunostaining (brown). At this higher magnification, the intracortical myelin in the Alzheimer's disease subjects was characterized by an accentuated PLP staining due to changes in myelin structure comprising fragmentation, increased segmental tortuosity and bead-like varicosities. As a result the PLP staining of the Alzheimer's disease cortex appeared disorganized with loss of individually discernable fibres and orientation when compared to the cortex of the control subjects.

physiological movements, the ex vivo images that were acquired with a similar resolution as the in vivo images provided more anatomical detail, and demonstrated that the hypointense bands did not cover the full width of the cortex, but were located centrally in the cortex (fig. 3). Hypointense foci were observed in 2 out of 6 AD cases, and in the 1 control specimen with Braak III. In addition to the scoring criteria defined for the in vivo scans, in these post-mortem samples a third category of cortical disturbance could be observed, consisting of cloud-like areas of low signal intensity with less alignment along, and more expansion through, the cortical layers (4 out of 6 AD cases, and in the control subject with Braak III). Comparing radiological and histological data of the same sample, the epicentre of the hypointense bands and clouds observed on the ex vivo MR images could be localized in cortical layer IV. Subsequently, we assessed which of the histological markers ($A\beta$, tau, iron, and myelin) showed a similar distribution over the cortical layers to the hypointense bands and clouds. We observed that the hypointense bands and clouds on MRI co-lo-

calized with areas characterized by an increased presence of iron and changes in myelin structure (fig. 3). Only cortices that were scored as abnormal on SW images demonstrated these accentuated local patterns for iron and myelin on histological examination. Interestingly, no co-localization was observed between the hypointense bands and clouds on MRI and areas staining for A β or tau. Tau pathology typically affected cortical layers II – III and V. A β staining was present to an equal extent across all cortical layers. Microscopically, some of the hypointense foci observed on the ex vivo images corresponded to large amyloid plaques, but these focal signal voids barely contributed to the observed hypointense cortical bands.

Since the pattern of the abnormalities observed on MRI corresponded best with the patterns observed on iron and myelin-stained tissue, we examined these stainings in more detail. Microscopically, using higher magnification, four different types of iron accumulation were observed in the cortex: 1) diffuse neuropil deposition associated with myelinated fibres, 2) dense stellate cytoplasmic iron accumulation in microglial cells, 3) a dense thin line of perinuclear iron accumulation in oligodendroglial and microglial cells, and 4) iron associated with amyloid plaques (fig. 4). All 4 types of iron deposits were more abundant in the subjects with an abnormally appearing cortex on postmortem MRI, including the control subject with Braak III. The first 3 types of iron deposits were localized differently in the cortical layers: neuropil iron accumulation was centered in layer IV, extending into layers III and V of the cortex; stellate glial aggregates were most abundant in the middle cortical layers (layers III and IV), but were also present to a lesser extent in the deep cortical layers (layers V and VI), and perinuclear glial iron accumulation was most abundant in layers V and VI, followed by layers IV and III (fig. 3). In addition, increased microglial and neuropil iron accumulations were also observed in areas characterized by cloud-like hypointensities on MRI. EM analysis revealed that the diffuse iron in the neuropil was located predominantly in oligodendrocytic myelin sheaths (fig. 4D).

The association of iron with myelin sheaths in the neuropil led us to examine the cortical myelin in more detail using a PLP staining. Interestingly, the intensity of myelin staining also showed a colocalization with the low signal intensity bands and clouds on MRI (fig. 3). Histologically, these areas were characterized by an accentuated PLP staining due to changes in myelin structure comprising fragmentation, increased segmental tortuosity and bead-like varicosities, centralized in layer IV, but extending to

layers III and V in the AD patients (fig. 3 and 5). Furthermore, as expected, small round plaque-like areas that were devoid of any myelin fibres were observed in cortical areas containing a high number of A β deposits.

Discussion

Using 7T MRI we observed striking differences in vivo in the frontal cortex between AD patients and age-matched controls. In patients with probable AD we found a disturbance of the layered structure of the cortex. Previous studies in healthy subjects demonstrated that cortical lamination at 7T reflects intracortical myeloarchitecture (Duyn et al., 2007; Fukunaga et al., 2010; Cohen-Adad et al., 2012), and this normal pattern of cortical lamination was attributed to differences in myelin-associated iron and myelin lipids in the different cortical layers (Duyn et al., 2007). Our current study shows that in AD patients the cortical areas of altered SW contrast co-localize with areas of increased microglia- and myelin-associated iron accumulation and also with changes in myelin cytoarchitecture. However, our data also demonstrate that the pattern of the changes observed on MRI does not correspond to the pattern of amyloid deposits. These observations are not in line with the previous assumption, mostly based on animal experiments, that T2*-weighted and SW imaging contrast in Alzheimer's disease primarily reflects the presence of iron associated with amyloid plaques (Duyn et al., 2007; van Rooden et al., 2009; Meadowcroft et al., 2009; Chamberlain et al., 2011). Our observations of disturbed iron accumulation and myelin architecture have important implications for in vivo diagnosis of AD, and also for the understanding of the pathophysiological mechanisms underlying this disease.

According to the amyloid hypothesis oligomeric forms of A β are the trigger for a cascade of events that ultimately results in dementia. However, there is increasing evidence that a range of other ethological factors have an important impact on this cascade, presumably by interacting with the A β aggregates or by subsequent cellular changes which follow it (Herrup, 2010; Bartzokis, 2011; Fjell and Walhovd, 2012). In our study, we found a close correlation between SW MRI contrast changes, myelin changes and increased iron accumulation in cortices with Alzheimer's disease pathology. Interestingly, changes in iron metabolism and myelin breakdown have both been mentioned as potential upstream mechanisms for Alzheimer's disease (Herrup, 2010; Bartzokis, 2011).

Iron and myelin are closely associated in the brain. Seventy percent of the brain's iron is located in oligodendrocytes. Maturation of oligodendro-

cytes and myelin synthesis are both dependent on the availability of iron (Todorich et al., 2009; Bartzokis, 2011). During demyelination processes in disease, as well as during normal myelin turnover, iron is assumed to be released from myelin into the brain tissue (Bartzokis, 2011). Our observation of increased iron in microglial cells (which have an important phagocytic role) in areas of altered myelin structure suggests that the observed MRI changes are a reflection of increased demyelination.

Cortical demyelination has been observed previously in AD, but mainly as areas of focal myelin loss in the immediate vicinity of amyloid plaques (Mitew et al., 2010; Serrano-Pozo et al., 2010). We also observed this pattern of myelin loss in our samples, but it was much less prominent than the more diffuse changes in myelin structure (increased fragmentation, tortuosity, and bead-like varicosities) which we report here. To our knowledge, these findings have not been reported before in human Alzheimer's disease, but strikingly similar myelin alterations were recently discovered in a mouse model of Alzheimer's disease (Chen et al., 2011). Apart from its role in myelin metabolism, iron is an important upstream and downstream modulator of several molecular pathways in Alzheimer's disease. Recently it was demonstrated that APP plays a physiological role in preventing iron-mediated oxidative stress in the brain (Duce et al., 2010). In Alzheimer's disease, zinc accumulation in amyloid plaques and loss of soluble tau interfere with APP's ferroxidase activity, causing increased neuronal iron accumulation. Furthermore, there is evidence that APP processing through the amyloidogenic and non-amyloidogenic pathways is affected by iron (Duce et al., 2010; Lei et al., 2012). Finally, experimental data have demonstrated that iron may accelerate A β oligomerization (Roberts et al., 2012). Based on these observations, it has been suggested that iron could be an important biomarker of AD (Collingwood and Dobson 2006; Zhu et al., 2009).

The data presented here show convincing evidence that the cortical myelin cytoarchitecture and iron distribution are disturbed in Alzheimer's disease patients. Although these changes might not be central to the pathogenesis of Alzheimer's disease, the ability to visualize them by MRI creates a putative novel biomarker with the potential to reflect an as yet under-appreciated change that may accompany the progression of Alzheimer's disease. However, our data are preliminary since they have been generated in a limited number of patients and healthy controls, and cover only a limited part of the brain. Postmortem, we observed these changes in SWI contrast in all patients with confirmed Alzheimer's dis-

ease. In vivo, we observed these changes in cortical appearance only in a sub-set of patients; one reason for this discrepancy may be that the patients have been included based on a clinical diagnosis (NINCDS-ADRDA criteria), which is known to have a limited diagnostic accuracy (77 - 85%) (Jobst et al., 1998). Further studies, comprising larger patient series and additional controls populations of patients with different types of dementia are required to assess the potential of the cortical changes we observed to constitute true diagnostic biomarkers for AD. There are many other important and related questions, such as whether the presence of cortical changes is associated with reduced cognitive function, whether the changes appear early in the course of AD, and whether the frontal lobes are the best regions in which to detect these early changes. Additional in vivo and postmortem research on the correlation between ultra-high field MRI and pathology will allow us to further elucidate the role of iron and myelin in the pathogenesis of Alzheimer's disease. Overall, the analysis of the cortical changes via visual inspection and simple scoring criteria, without the need for quantitative measurements or sophisticated image processing techniques, makes the proposed method very attractive as a diagnostic and research tool in a clinical setting.

Acknowledgements

The authors thank Ingrid Hegeman-Kleinn for technical assistance. This research was performed within the framework of CTMM, the Centre for Translational Molecular Medicine (www.ctmm.nl), project LeARN (grant 02N-101).

Reference List

Alves L, Correia AS, Miguel R, Alegria P, Bugalho P. Alzheimer's disease: a clinical practice-oriented review. *Front Neurol* 2012; 3: 63.

Bartzokis G. Alzheimer's disease as homeostatic responses to age-related myelin breakdown. *Neurobiol Aging* 2011; 32: 1341-71.

Braak H, Alafuzoff I, Arzberger T, Kretschmar H, Del TK. Staging of Alzheimer disease-associated neurofibrillary pathology using paraffin sections and immunocytochemistry. *Acta Neuropathol* 2006; 112: 389-404.

Chamberlain R, Wengenack TM, Poduslo JF, Garwood M, Jack CR, Jr. Magnetic resonance imaging of amyloid plaques in transgenic mouse models of Alzheimer's disease. *Curr Med Imaging Rev* 2011; 7: 3-7.

Chen H, Epelbaum S, Delatour B. Fiber Tracts Anomalies in APPxPS1 Transgenic Mice Modeling Alzheimer's Disease. *J Aging Res* 2011; 2011: 281274.

Cohen-Adad J, Polimeni JR, Helmer KG, Benner T, McNab JA, Wald LL et al. T(2)* mapping and B(0) orientation-dependence at 7 T reveal cyto- and myeloarchitecture organization of the human cortex. *Neuroimage* 2012; 60: 1006-14.

Collingwood J, Dobson J. Mapping and characterization of iron compounds in Alzheimer's tissue. *J Alzheimers Dis* 2006; 10: 215-22.

Duce JA, Tsatsanis A, Cater MA, James SA, Robb E, Wikke K et al. Iron-export ferroxidase activity of beta-amyloid precursor protein is inhibited by zinc in Alzheimer's disease. *Cell* 2010; 142: 857-67.

Duyckaerts C, Delatour B, Potier MC. Classification and basic pathology of Alzheimer disease. *Acta Neuropathol* 2009; 118: 5-36.

Duyn JH, van Gelderen P, Li TQ, de Zwart JA, Koretsky AP, Fukunaga M. High-field MRI of brain cortical substructure based on signal phase. *Proc Natl Acad Sci U S A* 2007; 104: 11796-801.

Fjell AM, Walhovd KB. Neuroimaging results impose new views on Alzheimer's disease--the role of amyloid revised. *Mol Neurobiol* 2012; 45: 153-72.

Fukunaga M, Li TQ, van Gelderen P, de Zwart JA, Shmueli K, Yao B et al. Layer-specific variation of iron content in cerebral cortex as a source of MRI contrast. *Proc Natl Acad Sci U S A* 2010; 107: 3834-9.

Haacke EM, Xu Y, Cheng YC, Reichenbach JR. Susceptibility weighted imaging (SWI). *Magn Reson Med* 2004; 52: 612-8.

Herrup K. Reimagining Alzheimer's disease--an age-based hypothesis. *J Neurosci* 2010; 30: 16755-62.

Jack CR, Jr., Knopman DS, Jagust WJ, Shaw LM, Aisen PS, Weiner MW et al. Hypothetical model of dynamic biomarkers of the Alzheimer's pathological cascade. *Lancet Neurol* 2010; 9: 119-28.

Jobst KA, Barnetson LP, Shepstone BJ. Accurate prediction of histologically confirmed Alzheimer's disease and the differential diagnosis of dementia: the use of NINCDS-ADRDA and DSM-III-R criteria, SPECT, X-ray CT, and Apo E4 in medial temporal lobe dementias. Oxford Project to Investigate Memory and Aging. *Int Psychogeriatr* 1998; 10: 271-302.

Karran E, Mercken M, De Strooper B. The amyloid cascade hypothesis for Alzheimer's disease: an appraisal for the development of therapeutics. *Nat Rev Drug Discov* 2011; 10: 698-712.

Langbaum JB, Chen K, Lee W, Reschke C, Bandy D, Fleisher AS et al. Categorical and correlational analyses of baseline fluorodeoxyglucose positron emission tomography images from the Alzheimer's Disease Neuroimaging Initiative (ADNI). *Neuroimage* 2009; 45: 1107-16.

Lei P, Ayton S, Finkelstein DI, Spoerri L, Ciccotosto GD, Wright DK et al. Tau deficiency induces parkinsonism with dementia by impairing APP-mediated iron export. *Nat Med* 2012; 18: 291-5.

McKhann G, Drachman D, Folstein M, Katzman R, Price D, Stadlan EM. Clinical diagnosis of Alzheimer's disease: report of the NINCDS-ADRDA Work Group under the auspices of Department of Health and Human Ser-

vices Task Force on Alzheimer's Disease. *Neurology* 1984; 34: 939-44.

Meadowcroft MD, Connor JR, Smith MB, Yang QX. MRI and histological analysis of beta-amyloid plaques in both human Alzheimer's disease and APP/PS1 transgenic mice. *J Magn Reson Imaging* 2009; 29: 997-1007.

Meguro R, Asano Y, Odagiri S, Li C, Iwatsuki H, Shoumura K. Nonheme-iron histochemistry for light and electron microscopy: a historical, theoretical and technical review. *Arch Histol Cytol* 2007; 70: 1-19.

Mitew S, Kirkcaldie MT, Halliday GM, Shepherd CE, Vickers JC, Dickson TC. Focal demyelination in Alzheimer's disease and transgenic mouse models. *Acta Neuropathol* 2010; 119: 567-77.

Montine TJ, Phelps CH, Beach TG, Bigio EH, Cairns NJ, Dickson DW et al. National Institute on Aging-Alzheimer's Association guidelines for the neuropathologic assessment of Alzheimer's disease: a practical approach. *Acta Neuropathol* 2012; 123: 1-11.

Natte R, Maat-Schieman ML, Haan J, Bornebroek M, Roos RA, van Duinen SG. Dementia in hereditary cerebral haemorrhage with amyloidosis-Dutch type is associated with cerebral amyloid angiopathy but is independent of plaques and neurofibrillary tangles. *Ann Neurol* 2001; 50: 765-72.

Roberts BR, Ryan TM, Bush AI, Masters CL, Duce JA. The role of metallobiology and amyloid-beta peptides in Alzheimer's disease. *J Neurochem* 2012; 120 Suppl 1: 149-66.

Rombouts SA, Barkhof F, Goekoop R, Stam CJ, Scheltens P. Altered resting state networks in mild cognitive impairment and mild Alzheimer's disease: an fMRI study. *Hum Brain Mapp* 2005; 26: 231-9.

Rowe CC, Villemagne VL. Brain Amyloid Imaging. *J Nucl Med* 2011.
Schar M, Kozerke S, Fischer SE, Boesiger P. Cardiac SSFP imaging at 3 Tesla. *Magn Reson Med* 2004; 51: 799-806.

Serrano-Pozo A, William CM, Ferrer I, Uro-Coste E, Delisle MB, Maurage CA et al. Beneficial effect of human anti-amyloid-beta active immunization on neurite morphology and tau pathology. *Brain* 2010; 133: 1312-27.

Shepherd TM, Thelwall PE, Stanisz GJ, Blackband SJ. Aldehyde fixative solutions alter the water relaxation and diffusion properties of nervous tissue. *Magn Reson Med* 2009; 62: 26-34.

Todorich B, Pasquini JM, Garcia CI, Paez PM, Connor JR. Oligodendrocytes and myelination: the role of iron. *Glia* 2009; 57: 467-78.

van Duijn S, Nabuurs RJ, van Duinen SG, Natta R. Comparison of histological techniques to visualize iron in paraffin-embedded brain tissue of patients with Alzheimer's disease. *J Histochem Cytochem* 2013; 61: 785-92.

van Duijn S, Nabuurs RJ, van Rooden S, Maat-Schieman ML, van Duinen SG, van Buchem MA et al. MRI artifacts in human brain tissue after prolonged formalin storage. *Magn Reson Med* 2011; 65: 1750-1758.

van Rooden S, Maat-Schieman ML, Nabuurs RJ, van der Weerd L, van DS, van Duinen SG et al. Cerebral amyloidosis: postmortem detection with human 7.0-T MR imaging system. *Radiology* 2009; 253: 788-96.

Versluis MJ, Peeters JM, van Rooden S, van der Grond J, van Buchem MA, Webb AG et al. Origin and reduction of motion and f0 artifacts in high resolution T2*-weighted magnetic resonance imaging: application in Alzheimer's disease patients. *Neuroimage* 2010; 51: 1082-8.

Wang Y, Yu Y, Li D, Bae KT, Brown JJ, Lin W et al. Artery and vein separation using susceptibility-dependent phase in contrast-enhanced MRA. *J Magn Reson Imaging* 2000; 12: 661-70.

Zhu WZ, Zhong WD, Wang W, Zhan CJ, Wang CY, Qi JP et al. Quantitative MR phase-corrected imaging to investigate increased brain iron deposition of patients with Alzheimer disease. *Radiology* 2009; 253: 497-504.

Chapter 6

Longitudinal monitoring of sex related in vivo metabolic changes in the brain of Alzheimer's disease transgenic mouse using magnetic resonance spectroscopy

S van Duijn, MSc 1*, R.J.A. Nabuurs MSc 2, S.G. van Duinen PhD, MD 1, R Natté PhD, MD 1, M.A. van Buchem PhD, MD 2, A Alia PhD 2,3

1Department of Pathology, Leiden University Medical Centre, Albinusdreef 2, Leiden, 2333 ZA Netherlands; Telnr: +31 71 5266594; Faxnr.: +31 71 5266952

2Department of Radiology, Leiden University Medical Centre, Albinusdreef 2, Leiden, 2333 ZA Netherlands

3SSNMR, Leiden Institute of Chemistry, Gorlaeus Laboratory, Einsteinweg 55, p.o.box 9502, Leiden 2300 RA, The Netherlands

J Alzheimers Dis. 2013; 34 (4): 1051-1059

Abstract

Epidemiological studies indicate that the incidence of Alzheimer's disease (AD) is higher in women than in men. There is evidence that changes in metabolites in the brain associated with the development of AD are present earlier than structural brain changes. The effect of sex on the metabolic profile during the development of AD has not yet been studied. In this study we longitudinally monitored and compared *in vivo* metabolic changes in male and female A β APP_{swe}, PSEN1^{dE9} transgenic mice brains using magnetic resonance spectroscopy. Our results show a lower level of glutamate as well as of N-acetylaspartate (NAA) in transgenic mice. The decline in NAA with age was more apparent in female mice. The level of taurine was higher in female mice and showed a faster decline over time. In conclusion, our study is the first to suggest that changes in the metabolic profile during AD development are influenced by sex.

Key words: Alzheimer's disease; magnetic resonance spectroscopy; sex differences; APP/PS1 transgenic mouse model; longitudinal studies

Introduction

Alzheimer's disease (AD) is a neurodegenerative disease that causes dementia and is an increasing health problem in the aging population; worldwide around 25 million people have AD and in 20 years this number will be doubled [1]. AD is associated with amyloid- β ($A\beta$) plaque formation, neurofibrillary tangles and cerebral cortical atrophy, mainly found in the hippocampus and the cerebral cortex [2]. There are strong indications that the clinical symptoms of AD start years after the onset of plaque formation [3]. Currently, AD can be diagnosed using a cognitive test combined with a magnetic resonance imaging (MRI) scan of the brain to detect cerebral atrophy and by determining the amount of $A\beta$ and tau in the cerebrospinal fluid, but not with complete accuracy [4]. Dementia and cerebral atrophy are very late stages of AD; therefore, drugs that are able to modify the disease process can only be expected to have little effect. If patients could be diagnosed at the onset of neurodegeneration, when symptoms are absent or subtle, the therapeutic window for disease modifying drugs would be much wider and there would be an increased expected gain. Therefore, a more accurate and earlier diagnosis of AD is of vital importance.

It is known that females are at higher risk for developing AD than men [5,6]. The effect of the mentioned sex differences on the pathophysiology of AD has not yet been carefully examined. Hormonal influences have been suggested [7], however, the underlying pathways accounting for the sex related differences remain unknown. One way to examine the metabolic pathways non-invasively during early phases of AD, and to study the influence of sex differences on these metabolic pathways, is by focusing on the metabolic changes in a transgenic(Tg) mouse model, by means of magnetic resonance spectroscopy (MRS). MRS is a non-invasive tool which can be used to measure the concentration of various brain metabolites in vivo [8]. Measuring these metabolic changes in vivo, using MRS, could help identify AD at an early stage, prior to the onset of cognitive symptoms [3]. Furthermore, changes in metabolic profiles could provide superior insight in the sex related pathophysiological mechanism of the disease.

Several Tg mouse models are available that develop pathology similar, however, not identical to human AD. These Tg mouse models allow mon-

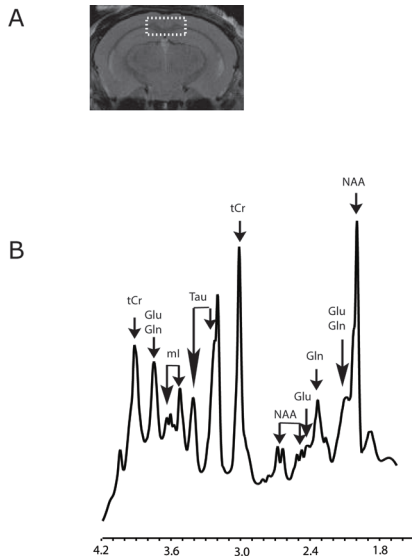


Figure 1: Representative MR image and spectrum of the mouse brain. (A) a coronal MR image of the mouse brain, obtained using a RARE sequence, showing the position of the selected 22 μ l (1.8 \times 3.5 \times 3.5 mm³) voxel covering the cortex-hippocampus region. (B) One dimension localized 1H-MR spectrum obtained from the selected 22 μ l voxel placed in the brain of an 15 month old control mouse. Spectrum was obtained using a PRESS sequence with TR=1500 ms and TE=15 ms at 9.4T.

itoring of the metabolic changes from the onset of AD, which is not detectable in patients. In the present study the A β APP^{swe},PSEN1dE9 mouse model is used. This mouse model demonstrates many of the cognitive [9] and neuropathological features of human AD, including plaque development. These mice develop plaques at 6 months of age and show decreased performance of exploratory activity and spatial learning tests at 12 months of age [9]. In reproductive phenotype no differences are found between this mouse model and control mice. Studies using this mouse model have mainly focused on histological data, including staining for A β , iron, and glial cells [10-16]. Among these histological studies, no sex-related differences were reported. However, in other AD mouse models, a sex-related difference was found, showing more A β in female mice [17,18]. For glial cells no sex difference was found yet.

Numerous MRS studies have been performed using Tg mouse models of AD. However, until now, the effect of sex on AD related metabolic changes has not been studied. The results of previous MRS studies have shown AD-related abnormalities for several metabolites [11,16,19-25]. N-acetylaspartate (NAA) in the brain is present predominantly in neuronal cell bodies. Decreased NAA levels, indicating neuronal damage, have been found in Tg mice in comparison to wild type (wt) mice [11,20-24]. Myo inositol (mIns) and taurine play a role in osmoregulation and are mainly found in astrocytes of brain tissue. These metabolites were found to be higher in Tg mice than in wt mice [11,19-22]. Glutamate (glu) is an excit-

atory neurotransmitter, involved in learning, memory forming, and cognition, which is found to be decreased in mice with AD [20-25]. Whether the changes in these metabolites during AD progression are sex specific, and whether they correlate temporally with timing of plaque deposition in male and female mice, remained to be investigated.

In this paper, we present the first systematic longitudinal MRS study to investigate the sex-related differences in metabolic changes during development of AD in the A β APP^{swe},PSEN1dE9 mouse model. The main findings of this study were the differences between male and female mice in NAA, taurine, and histological data. These results suggest that changes in the metabolic profile during AD development are clearly influenced by sex. Based on this, future MRS studies should consider specifying sex of the mice used and analyzing the data for both sexes separately.

Material and methods

Mice

In this study 20 A β APP/PS1 transgenic mice (12 male, 8 female); B6C3-Tg (A β APP^{swe},PSEN1dE9) 85Dbo/Jtg/0 from the Jackson Laboratory (Bar Harbor, ME, USA) and 20 wildtype (wt) littermates (7 male, 13 female) were used. 10 Tg mice and 10 wt mice were followed for 18 months and scanned every 3 months (timepoints: 3, 6, 9, 12, 15 and 18 months). For each timepoint, following MRI, 2 Tg and 2 wt mice of the remaining 10 Tg and 10 wt mice were sacrificed for histological analysis; at timepoint 18 months the mice used for the longitudinal study were sacrificed. The Institutional Animal Care and Animal Use Committee approved all the experiments in accordance with the NIH guide for the care and use of Laboratory animals. The mice were kept in a 12 hour light/dark circle.

Magnetic resonance spectroscopy

All measurements were conducted at 25°C on a vertical wide-bore 9.4T Bruker Avance 400WB spectrometer, with a 1000 mTm⁻¹ actively shielded imaging gradient insert (Bruker BioSpin, Ettlingen, Germany). The RF coil used was a 25 mm volume RF coil, specifically, a birdcage transmit/receive coil (Bruker BioSpin). The system was interfaced to a Linux pc running Topspin 2.0 and Paravision 5.0 imaging software (Bruker BioSpin).

Mice were anaesthetized for in vivo MRS measurements using isoflurane (Forene, Abott, UK), inhalation anaesthesia, in addition with air and oxygen (1:1) at 0.2 litre/minute. The anaesthetic gas was administered via a special facemask, which also served as a fixation device for the mouse head since it was coupled to a specially designed toothbar to hold the head in place (Bruker Biospin GmbH). The respiration rate of the mouse inside the probe was constantly monitored using a pressure transducer placed on the abdomen. The transducer was connected to a BioTrig acquisition module, which was interfaced to a BioTrig command module and laptop running BioTrig BT1 monitoring software (Bruker Biospin GmbH).

Localized T2-weighted multislice RARE images were acquired to select a volume of interest [25]. The MRS voxels were localized in the cortex-hippocampus regions in the mouse brain (1.8x3.5x3.5 mm³; 22 μ l) (fig. 1). The localized homogeneity was optimized by adjustment of first- and second-order shim coil currents using the FASTMAP sequence [26]. The field homogeneity in a 22 μ l voxel typically resulted in water line-widths of 20-25 Hz.

The PRESS (Point Resolved Spectroscopy) sequence [27] was used for 1D localized 1H MR spectroscopy. This sequence uses 3 hermite RF pulses (90°, 180°, and 180°). The sequence details are described by Mandal et al., 2007. The repetition time and echo time were 1500 ms and 15 ms, respectively. The PRESS sequence used 2048 complex points, with a spectral width of 10 ppm. The final 1D spectra were obtained with number of scans of 256 and scan times of approximately 15 minutes. The 1D PRESS sequences were preceded by a VAPOR sequence [28] for global water suppression. The sequence consists of 7 variable power RF pulses with an optimized relaxation delay. The relaxation delays τ_1 - τ_7 between the consecutive pulses were 150, 80, 160, 80, 100, 37.11 and 57.36 ms. Water suppression bandwidth was set at 350 Hz. Outer volume suppression (OVS) was combined in an interleaved mode with a water suppression scheme. This improves the localization performance and reduces the demands for spoiler gradients. The OVS scheme used a total of 18 hyperbolic secant RF pulses, each with 90° nominal flip angle and 1 ms pulse length. The OVS slice thickness was 4 mm with a 0 mm gap to the voxel.

The acquired in vivo 1D MR spectra were analyzed using LCModel [29]. This calculates the best fit of the experimental spectrum based on a linear

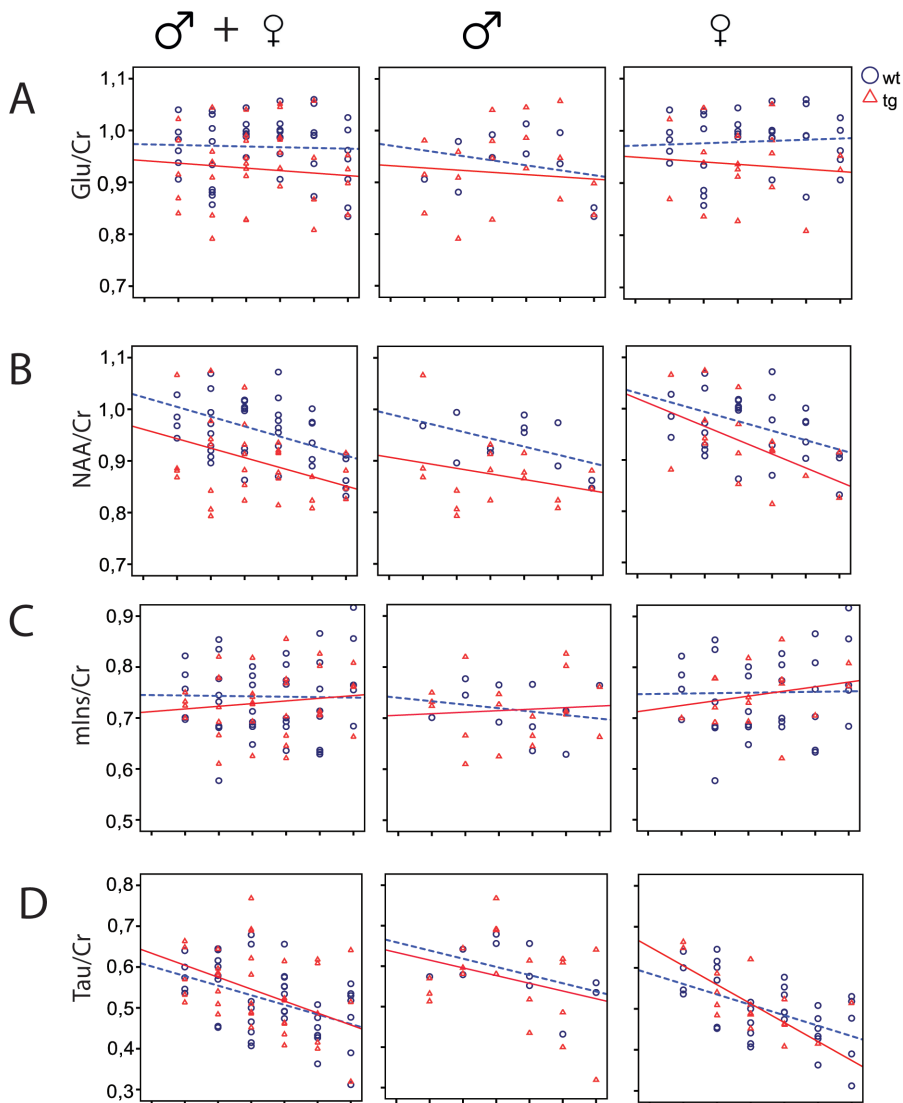


Figure 2: Longitudinal monitoring of sex related differences in (A) glutamate (glu)/Cr ratio, (B) NAA/Cr ratio (C) Tau/Cr ratio and (D) mIns/Cr ratio in the cortex-hippocampus regions of all mice, male and female mouse brain measured using in vivo MRS at 9.4 T.

combination of model spectra. The final analysis was performed in the frequency domain; however, raw data (FIDS) was used as standard data input. The following metabolites were included in the basis set for LCModel: alanine (Ala), aspartate (Asp), creatine (Cr), γ -aminobutyric acid (GABA), glucose (Glc), glutamate (Glu), glutamine (Gln), glycerophosphocholine (GPC), choline (cho), phosphocholine (PCho), myo-inositol (Ins), lactate

Table 1: R² of the linear regression line of the metabolic changes over time in wild type (wt) and transgenic (tg) mice. The differences are shown in male (M) and female (F) for glutamate, NAA, taurine and myo inositol.

| R ² | Glutamate | NAA | Taurine | Myo Inositol |
|----------------|-----------|------|---------|--------------|
| WT | 0.00 | 0.21 | 0.20 | 0.00 |
| TG | 0.01 | 0.14 | 0.19 | 0.02 |
| M WT | 0.07 | 0.26 | 0.22 | 0.04 |
| M TG | 0.01 | 0.08 | 0.08 | 0.01 |
| F WT | 0.01 | 0.18 | 0.29 | 0.00 |
| F TG | 0.01 | 0.29 | 0.54 | 0.05 |

(Lac), N-acetylacetate (NAA), N-acetylaspartylglutamate (NAAG), phosphocreatine (PCr), phosphoethanolamine (PE), scyllo-inositol (sIns), and taurine. Quantification was obtained using the tCr resonance as an internal standard, in our study no difference was found in creatine. The LCModel fitting was performed over the spectral range from 0.2 to 4.2 ppm. Signal to Noise ratio was above 5 and a %SD of 20 or lower.

Histology

Following *in vivo* MRS measurements, 2 wt and 2 Tg mice were sacrificed at each timepoint, and their brains were fixed in 4% buffered formaldehyde. Following fixation, the brain was dehydrated and embedded in paraffin, after which coronal sections (8 μ m thick) were carefully cut using a microtome. To detect the A β plaques, brain sections were pretreated for 1 hour with 70% formic acid followed by treatment with trypsin for 30 min at 37°C. Subsequently sections were washed in PBS and subjected to immunohistochemistry using the primary antibody polyclonal anti-amyloid-beta 40-42 antibody at 1:1000 (Alpha Diagnostics International, San Antonio, USA) overnight followed by a secondary antibody swine anti-rabbit (Dako) 1:600 for 1 hour. After washing 3 times with PBS immunolabelling was followed using a ABC kit (Vectastain) according to the manufacturer's instructions and visualized with DAB (3,3' diaminobenzidine, Sigma). Detection of iron was done by a DAB-enhanced Perl's staining according to Smith et al. [30]. To stain glial cells, a primary polyclonal an-

ti-GFAP (glial fibrillary acidic protein) antibody (Dako) was used following standard procedure. To detect the activated microglia and macrophages a primary polyclonal anti-IBA1 (ionized calcium binding adaptor molecule 1) antibody 1:1000 (Wako Chemicals, Neuss, Germany) was used. Prior to the IBA-1 antibody, a pretreatment with trypsin was performed for 30 min at 37°C. Since the plaque development in APP^{swe}, PSEN1^{dE9} transgenic mouse starts at approximately 6 months of age, the histological data in male and female mice are shown at the age of 3, 6 and 9 months. Histological images were acquired using a panoramic midi scanner (3D Histech, Budapest, Hungary). For quantitative histological analysis, regions of interest (ROIs) were selected in the cortex and hippocampus and the area percentage of stained tissue was calculated in these ROIs using ImageJ software (ImageJ, USA). The colours were unmixed using the plug-in colour deconvolution, the stained area was selected and the percentage of the total area was calculated using analyzing particles.

Statistical analysis

To investigate significant age-related differences between either sex or Tg and wt, a mixed model analysis was performed including scatter plots using SPSS software (version 17.0; SPSS, Inc., Chicago, IL). Mean differences were compared using one way ANOVA with statistical differences of $p < 0.05$ stated as significant.

Table 2: Mean ratio of glu, NAA, taurine and mIns with respect to Cr in 3 and 18 months old wild type (wt) and transgenic (tg) mice (mean + standard deviation). Wt and tg were separated in male (M) and female (F). *difference between male and female mice at 18 months for glutamate was significant ($p < 0.05$) for both wt and tg.

| | Glu | | NAA | | Taurine | | mIns | |
|------|-------------|--------------|-------------|-------------|-------------|-------------|-------------|-------------|
| | 3 months | 18 months | 3 months | 18 months | 3 months | 18 months | 3 months | 18 months |
| WT | 0.97 ± 0.05 | 0.93 ± 0.07 | 1.01 ± 0.08 | 0.87 ± 0.35 | 0.58 ± 0.04 | 0.47 ± 0.09 | 0.79 ± 0.11 | 0.79 ± 0.83 |
| TG | 0.93 ± 0.08 | 0.90 ± 0.05 | 0.95 ± 0.01 | 0.87 ± 0.04 | 0.59 ± 0.07 | 0.44 ± 0.17 | 0.73 ± 0.02 | 0.75 ± 0.06 |
| M WT | .91 | 0.84 ± 0.01* | .97 | 0.86 ± 0.01 | .57 | 0.55 ± 0.02 | .70 | .76 |
| M TG | 0.91 ± 0.07 | 0.87 ± 0.04* | 0.94 ± 0.11 | 0.86 ± 0.03 | 0.54 ± 0.03 | 0.48 ± 0.23 | 0.74 ± 0.01 | 0.71 ± 0.07 |
| F WT | 0.98 ± 0.04 | 0.97 ± 0.05* | 1.03 ± 0.09 | 0.88 ± 0.04 | 0.58 ± 0.05 | 0.45 ± 0.09 | 0.81 ± 0.11 | 0.80 ± 0.09 |
| F TG | 0.95 ± 0.11 | 0.94 ± 0.02* | 0.97 ± 0.13 | 0.87 ± 0.06 | 0.66 ± 0.01 | 0.39 ± 0.17 | .70 | 0.79 ± 0.03 |

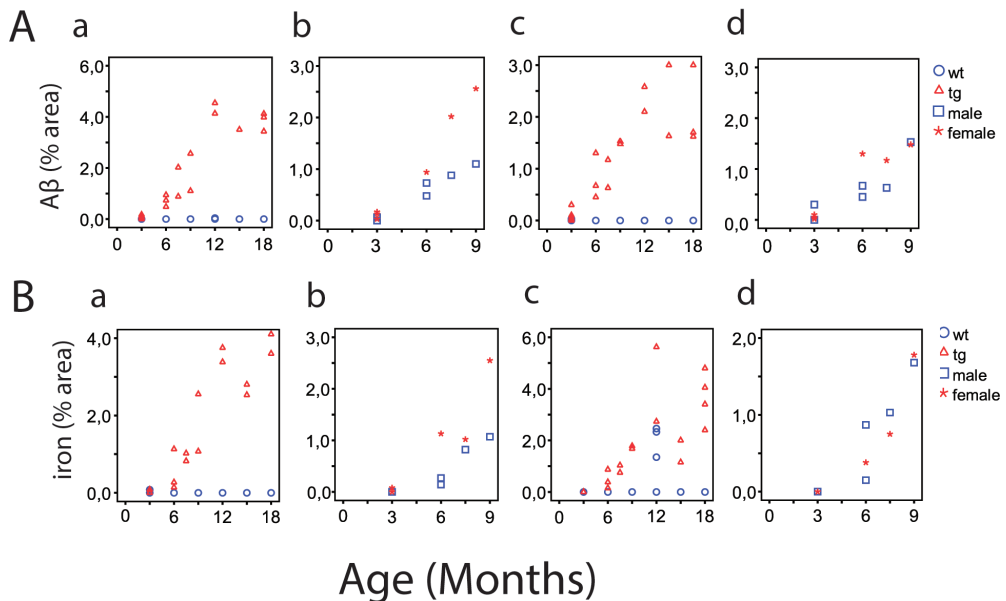


Figure 3: Quantitative analysis of sex related differences in A β (A) and iron (B) deposition in wt and tg mouse brain. (a) Surface percentage (%) of deposition in the cortex of wt and tg mice; (b) % of deposition in the cortex of male and female tg mice; (c) % of deposition in the hippocampus of wt and tg mice; (d) % of deposition in the hippocampus in male and female tg mice. Percentage of A β and iron deposition in the cortex and hippocampus elevate during the development of AD in tg mice. The elevations starts earlier in female mice as compared to male mice.

Results

Magnetic resonance spectroscopy

Of all metabolites measured only glu, NAA, tau and mIns are presented because they show either statistical significant results or a trend.

As shown in figure 2A, the glutamate (glu)/Cr ratio was lower in Tg mice compared to wt mice at all ages (Fig. 2A; table 1 and 2), and the rate of decline in glu/Cr ratio with age was more pronounced in Tg mice than in wt mice. A sex difference in the level and rate of decline in glutamate became apparent after separation of the data of male and female mice. In male wt mice, the glu/Cr ratio decreased over time, in contrast to wt female mice, in which it slightly increased. However, in Tg mice the glu/Cr ratio decreased in both male and female. At 18 months a significant difference ($p < 0.05$) is found between wt male (0.84) and wt female (0.97) mice, and between Tg male (0.87) and Tg female (0.94) mice (table 1 and 2). The NAA/Cr ratio was higher in wt mice in comparison to Tg mice (Fig. 2B; table 1 and 2) and decreased over time in both wt and in Tg mice. Overall the NAA/Cr ratio was higher in female when compared to male in

both wt and Tg mice. In female mice a faster decrease in NAA/Cr ratio was observed in Tg than in wt mice leading to a more apparent difference at 18 months of age than in males. Female Tg mice showed a faster decline than male tg mice (Fig. 2B (b,c)).

When male and female mice were taken together the ratio of taurine/Cr was similar for Tg and wt mice at all time points (Fig. 2D; table 1 and 2). Male wt and Tg mice showed a comparable taurine/Cr ratio at 3 months and a similar decrease over time. Female Tg mice showed a much stronger decline compared with male Tg and female wt mice. The taurine/Cr ratio in female Tg mice started higher at 3 months and ended lower at 18 months than in male Tg, female wt and male wt mice.

In Tg mice the mIns/Cr ratio started lower than in the wt mice and increased over time while this ratio slightly decreased in wt mice (Fig. 2C; table 1 and 2). Separating male and female mice showed comparable results.

Histology

Figure 4 shows the results of A β in the brain sections of 6 and 9 month old male Tg and female Tg mice. The A β deposition in the brain increased

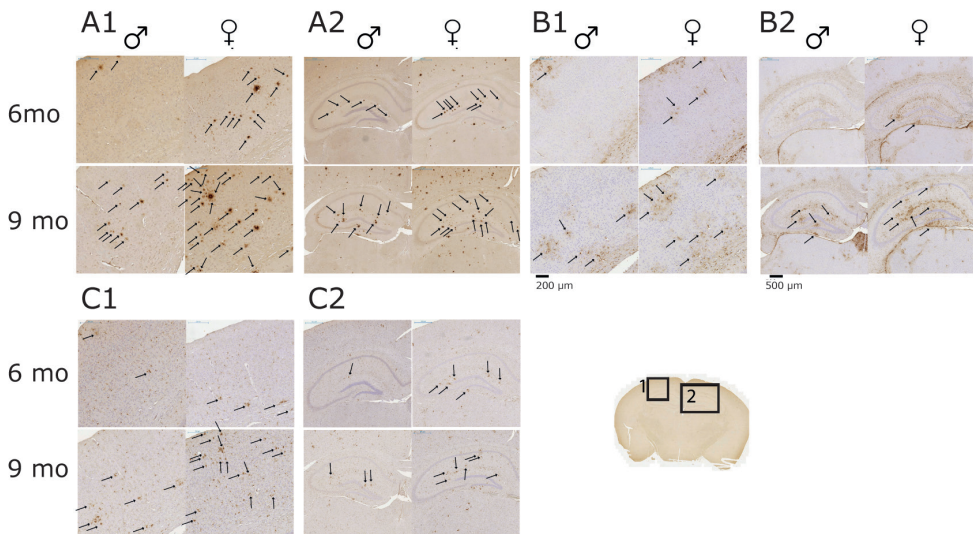


Figure 4: A β staining (A), GFAP staining (B) and IBA-1 staining (C) in brain sections of 6 months (6 mo) and 9 months (9 mo) old transgenic (tg) male and tg female mouse. Magnified area of (1) cortex (scale bar 200 μ m) and (2) hippocampus (scale bar 500 μ m) is shown. Arrows indicated immune stained A β plaques, GFAP depositions and IBA-1 depositions.

more rapidly in Tg female mice than in Tg male mice (Fig 4A). Iron deposition showed the same pattern as A β deposition. No A β or iron deposition was found in wt mice, even at 9 months.

This difference between male and female was more prominent in the cortex than in the hippocampus (fig 3 and 4).

Quantification of the amount of GFAP and IBA-1 showed no difference between wt and Tg mice. However, in the Tg mouse brain the distribution of both GFAP and IBA-1 became irregular over time, because GFAP and IBA-1 positive cells aggregate around plaques (Fig. 4B, C). In wt mice the deposition of GFAP and IBA-1 was more evenly distributed than in Tg mice (Fig. 4B,C). The presence of these plaque associated GFAP depositions was visible earlier in female brain than in male brain (Fig. 4B).

Discussion

This is the first longitudinal study showing that changes in metabolic profile during AD development are influenced by sex in a mouse model of AD. The main findings of this study are: (1) female mice have increased plaque development as well as increased activation of microglia surrounding the plaques compared with male mice, and (2) the decline in NAA and taurine during AD development is more apparent in female Tg mice than in male Tg mice in both the cortex and hippocampus. Most of these differences are statistically not significant, probably due to the low number of mice and lower inter individual variability at the different time points, but a trend is apparent. We tried to limit inter individual variability by scanning the wt and Tg mice for each time point at the same day with the same protocol. Instrumental limitations were excluded as far as possible by doing phantom studies, being preparations with known amounts of metabolites.

One lesson we learned from our study is that sex-specific differences between animals can influence study results. Comparison of wt and Tg mice show different results than comparison of the individual male and female subpopulation. For instance, the difference in NAA/Cr ratio between female wt and Tg mice increases over time, while for male Tg and wt mice the difference in NAA/Cr ratio decreases. This may explain why the results, as presented in our study, differ at some parameters from earlier studies [11,22,23,25].

We observed an increase of the glu/Cr ratio in female wt mice and a de-

crease in male wt mice over time, which indicates that the glu/Cr ratio between wt and Tg is sex dependent. In several earlier studies glu/Cr ratio changes were observed, but the sex of the studied mice was not mentioned or sex was not taken into account in the analysis of the data [11,21,22,24].

In a previous study [22], mIns was increased in Tg mice compared with wt mice, however male and female mice in the Tg group were presented together, while only female wt mice were used, which means the 2 groups could in fact not be compared due to the sex differences. Chen et al. [11] found no significant differences between male and female and this study confirmed the differences between Tg and wt mice found by Marjanska et al. [22]

The ratio of taurine/Cr was higher in female Tg mice than in wt mice at an early age (3 and 6 month), but at 9 months the taurine/Cr ratio was lower in female Tg mice. However, the mIns/Cr ratio started slightly lower in the Tg mice than in the wt mice (3 and 6 months), but, at 12 month the ratio of mIns/Cr was higher in the Tg mice than in the wt mice. Myo inositol and taurine are known to be involved in osmotic regulation across the cellular membrane and are mostly present in glial cells [22]. Despite these functional similarities our results indicate that in tg mice the two metabolites show an opposite trend; mIns slightly increases with age (as opposed to a stable amount in wt) and taurine decreases with age (more than the decrease in wt).

Our histological data show an increase in plaque deposition in Tg mice which was correlated with an increase in iron as well as an increase of GFAP positive glial cells around plaques with age. This increase was more apparent in the female mice. Previous histological studies in A β APP/PS1 mice have shown an increase in plaque deposition after 3 to 5 months. In addition, an increase in GFAP positive glial cells is reported in these mice at 5-8 months [11,14,15,31]. However, these studies did not show sex differences in deposition of plaque, iron or GFAP.

Although the pattern of GFAP positive cells changes while plaques develop in the brain, the overall density of these cells is not clearly different between wt and Tg brain tissue. This is reflected by the minimal increase of myo inositol and even a decrease of taurine, both osmoregulatory proteins, which are particularly present in glial cells.

The increased level of the NAA/Cr ratio in the female brain, for both wt and Tg mice, can be explained by the fact that females seem to have a higher cerebral axonal density than males [32]. The mechanisms responsible for the sex differences in A β and iron deposition are not yet known.

Our study is the first study to systematically investigate the influence of sex on metabolic and histological changes in AD over time using an AD mouse model. The use of a mouse model allows examining early changes in AD, which is not possible in humans. Our findings show for the first time that changes in metabolic profile during AD development is influenced by sex. These results are in line with the known higher risk of AD in women [5,6]. The area of sex differences in AD is still largely unexplored but knowledge of metabolic differences would offer great promise for diagnosis and for the future development of better strategies for intervention in patients.

Acknowledgement

We thank Ingrid Hegeman for her excellent assistance and H.E. Kan, A.G. Webb and I. Ronen for useful suggestions and discussions. This work was supported by grants from Department of pathology (LUMC). Alia thanks grant support from Internationale Stichting Alzheimer Onderzoek (ISAO) and Centre for Medical Systems Biology (CMSB).

Reference List

- [1] Ferri CP, Prince M, Brayne C, Brodaty H, Fratiglioni L, Ganguli M, Hall K, Hasegawa K, Hendrie H, Huang Y, Jorm A, Mathers C, Menezes PR, Rimmer E, Scazufca M (2005) Global prevalence of dementia: a Delphi consensus study. *Lancet* 366, 2112-2117.
- [2] Price JL, Davis PB, Morris JC, White DL (1991) The distribution of tangles, plaques and related immunohistochemical markers in healthy aging and Alzheimer's disease. *Neurobiol Aging* 12, 295-312.
- [3] Jack CR, Jr., Knopman DS, Jagust WJ, Shaw LM, Aisen PS, Weiner MW, Petersen RC, Trojanowski JQ (2010) Hypothetical model of dynamic biomarkers of the Alzheimer's pathological cascade. *Lancet Neurol* 9, 119-128.
- [4] Fox NC, Freeborough PA, Rossor MN (1996) Visualisation and quantification of rates of atrophy in Alzheimer's disease. *Lancet* 348, 94-97.
- [5] Musicco M (2009) Gender differences in the occurrence of Alzheimer's disease. *Funct Neurol* 24, 89-92.
- [6] Andersen K, Launer LJ, Dewey ME, Letenneur L, Ott A, Copeland JR, Dartigues JF, Kragh-Sorensen P, Baldereschi M, Brayne C, Lobo A, Martinez-Lage JM, Stijnen T, Hofman A (1999) Gender differences in the incidence of AD and vascular dementia: The EURODEM Studies. EURODEM Incidence Research Group. *Neurology* 53, 1992-1997.
- [7] Janicki SC, Schupf N (2010) Hormonal influences on cognition and risk for Alzheimer's disease. *Curr Neurol Neurosci Rep* 10, 359-366.
- [8] Rupsingh R, Borrie M, Smith M, Wells JL, Bartha R (2011) Reduced hippocampal glutamate in Alzheimer disease. *Neurobiol Aging* 32, 802-810.
- [9] Lalonde R, Kim HD, Maxwell JA, Fukuchi K (2005) Exploratory activity and spatial learning in 12-month-old APP(695)SWE/co+PS1/Del-

taE9 mice with amyloid plaques. *Neurosci Lett* 390, 87-92.

[10] Bereczki E, Bernat G, Csont T, Ferdinandy P, Scheich H, Santha M (2008) Overexpression of human apolipoprotein B-100 induces severe neurodegeneration in transgenic mice. *J Proteome Res* 7, 2246-2252.

[11] Chen SQ, Wang PJ, Ten GJ, Zhan W, Li MH, Zang FC (2009) Role of myo-inositol by magnetic resonance spectroscopy in early diagnosis of Alzheimer's disease in APP/PS1 transgenic mice. *Dement Geriatr Cogn Disord* 28, 558-566.

[12] Connor DM, Benveniste H, Dilmanian FA, Kritzer MF, Miller LM, Zhong Z (2009) Computed tomography of amyloid plaques in a mouse model of Alzheimer's disease using diffraction enhanced imaging. *Neuroimage* 46, 908-914.

[13] Hooijmans CR, Rutters F, Dederen PJ, Gambarota G, Veltien A, van GT, Broersen LM, Lutjohann D, Heerschap A, Tanila H, Kiliaan AJ (2007) Changes in cerebral blood volume and amyloid pathology in aged Alzheimer APP/PS1 mice on a docosahexaenoic acid (DHA) diet or cholesterol enriched Typical Western Diet (TWD). *Neurobiol Dis* 28, 16-29.

[14] Manaye KF, Wang PC, O'Neil JN, Huang SY, Xu T, Lei DL, Tizabi Y, Ottinger MA, Ingram DK, Mouton PR (2007) Neuropathological quantification of dtg APP/PS1: neuroimaging, stereology, and biochemistry. *Age* 29, 87-96.

[15] Ruan L, Kang Z, Pei G, Le Y (2009) Amyloid deposition and inflammation in APP^{swe}/PS1^{dE9} mouse model of Alzheimer's disease. *Curr Alzheimer Res* 6, 531-540.

[16] Xu W, Zhan YQ, Huang W, Wang XX, Zhang SM, Lei H (2010) Reduction of Hippocampal N-Acetyl Aspartate Level in Aged APP(Swe)/PS1(dE9) Transgenic Mice Is Associated With Degeneration of CA3 Pyramidal Neurons. *Journal of Neuroscience Research* 88, 3155-3160.

[17] Wang J, Tanila H, Puolivali J, Kadish I, van GT (2003) Gender differences in the amount and deposition of amyloidbeta in APP^{swe} and PS1 double transgenic mice. *Neurobiol Dis* 14, 318-327.

- [18] Callahan MJ, Lipinski WJ, Bian F, Durham RA, Pack A, Walker LC (2001) Augmented senile plaque load in aged female beta-amyloid precursor protein-transgenic mice. *Am J Pathol* 158, 1173-1177.
- [19] Westman E, Spenger C, Oberg J, Reyer H, Pahnke J, Wahlund LO (2009) In vivo ¹H-magnetic resonance spectroscopy can detect metabolic changes in APP/PS1 mice after donepezil treatment. *BMC Neurosci* 10, 33-
- [20] Choi JK, Jenkins BG, Carreras I, Kaymakcalan S, Cormier K, Kowall NW, Dedeoglu A (2010) Anti-inflammatory treatment in AD mice protects against neuronal pathology. *Exp Neurol* 223, 377-384.
- [21] Dedeoglu A, Choi JK, Cormier K, Kowall NW, Jenkins BG (2004) Magnetic resonance spectroscopic analysis of Alzheimer's disease mouse brain that express mutant human APP shows altered neurochemical profile. *Brain Res* 1012, 60-65.
- [22] Marjanska M, Curran GL, Wengenack TM, Henry PG, Bliss RL, Poduslo JF, Jack CR, Jr., Ugurbil K, Garwood M (2005) Monitoring disease progression in transgenic mouse models of Alzheimer's disease with proton magnetic resonance spectroscopy. *Proc Natl Acad Sci U S A* 102, 11906-11910.
- [23] Oberg J, Spenger C, Wang FH, Andersson A, Westman E, Skoglund P, Sunnemark D, Norinder U, Klason T, Wahlund LO, Lindberg M (2008) Age related changes in brain metabolites observed by ¹H MRS in APP/PS1 mice. *Neurobiol Aging* 29, 1423-1433.
- [24] von Kienlin M., Kunnecke B, Metzger F, Steiner G, Richards JG, Ozmen L, Jacobsen H, Loetscher H (2005) Altered metabolic profile in the frontal cortex of PS2APP transgenic mice, monitored throughout their life span. *Neurobiol Dis* 18, 32-39.
- [25] Braakman N, Oerther T, de Groot HJ, Alia A (2008) High resolution localized two-dimensional MR spectroscopy in mouse brain in vivo. *Magn Reson Med* 60, 449-456.

- [26] Gruetter R (1993) Automatic, localized in vivo adjustment of all first- and second-order shim coils. *Magn Reson Med* 29, 804-811.
- [27] Bottomley PA (1987) Spatial localization in NMR spectroscopy in vivo. *Ann N Y Acad Sci* 508, 333-348.
- [28] Tkac I, Starcuk Z, Choi IY, Gruetter R (1999) In vivo ¹H NMR spectroscopy of rat brain at 1 ms echo time. *Magn Reson Med* 41, 649-656.
- [29] Provencher SW (1993) Estimation of metabolite concentrations from localized in vivo proton NMR spectra. *Magn Reson Med* 30, 672-679.
- [30] Smith MA, Harris PL, Sayre LM, Perry G (1997) Iron accumulation in Alzheimer disease is a source of redox-generated free radicals. *Proc Natl Acad Sci U S A* 94, 9866-9868.
- [31] Taniuchi N, Niidome T, Goto Y, Akaike A, Kihara T, Sugimoto H (2007) Decreased proliferation of hippocampal progenitor cells in APP^{swe}/PS1^{dE9} transgenic mice. *Neuroreport* 18, 1801-1805.
- [32] Wilkinson ID, Paley MN, Miszkiel KA, Hall-Craggs MA, Kendall BE, Chinn RJ, Harrison MJ (1997) Cerebral volumes and spectroscopic proton metabolites on MR: is sex important? *Magn Reson Imaging* 15, 243-248.

Chapter 7

Summary and general discussion

Summary

The central theme of this thesis is to study the possibilities of an early diagnosis of Alzheimer's disease (AD) using different MR techniques with pathological confirmation.

The current view on AD is that neuropathological changes start two decades before the occurrence of clinical symptoms (Jack, Jr. et al., 2010). The cognitive decline associated with AD represents a late stage of the disease when neurodegeneration is extensive and therapeutic interventions may be too late. In the coming years, the radiological changes associated with AD need to be validated and expanded to allow diagnosis *in vivo*, perhaps even at an early stage of the disease. The search for new imaging methods is driven by the promise that earlier diagnosis, preferably before obvious dementia is present, may help in the search for treatment and to identify patients early enough to benefit from future treatment.

In the study discussed in chapter 2 the findings of coarse hypointensities on postmortem brain MRI were examined, correlated with pathology and discussed. During experiments with *ex vivo* human brain material, large hypointensities were visible on MRI scans. These turned out to be tissue artifacts induced by prolonged formalin storage without refreshing the formalin. This chapter describes the usability and limitations of postmortem brain tissue for MRI. Postmortem brain tissue is often used for MRI and pathological research (Benveniste et al., 1999; Bobinski et al., 2000; Bronge et al., 2002; Englund et al., 2004; Fernando et al., 2004; Geurts et al., 2005; Gouw et al., 2008; House et al., 2007; Kangarlu et al., 2007; Larsson et al., 2004; Schmierer et al., 2010; van Rooden et al., 2009) but there are limitations. Fixed brain tissue stored in unrefreshed formalin for prolonged periods (longer than a year), shows structural tissue changes associated with hypointensities on MR images. The fixation protocol for prolonged storage of tissue without refreshment of the formalin may be common practice in brain banks. Researchers should be aware of this fixation artifact.

Iron

For many years, research has been focusing on A β accumulation in plaques and the intraneuronal accumulation of hyperphosphorylated tau, as these are the pathological hallmarks of AD (Nelson et al., 2009). The last decade, increasing evidence suggests the importance of iron in the

pathogenesis of AD (Bartzokis, 2011; Crichton et al., 2002; Haacke et al., 2005; Meadowcroft et al., 2009; Meadowcroft et al., 2015a; Nabuurs et al., 2011). Iron is present in plaques and microglia, which may serve as an early marker for AD. To demonstrate iron, various histological staining methods have been developed (LeVine, 1991; Meguro et al., 2007; Smith et al., 1997). In chapter 3 we describe the comparison of three histological iron staining methods and ferritin immunohistochemistry to visualize iron in paraffin-embedded human AD brain tissue. The specificity of the histochemical techniques was tested by staining sections after iron extraction. Iron was demonstrated in the white matter, in cortical layers IV and V of the frontal neocortex, in iron positive plaques and in microglia. In our hands, these structures were best visualized using the Meguro iron staining method (Meguro et al., 2007), a method that has not yet been described for iron staining in human brain or AD.

Chapter 4 discusses the iron changes in the frontal cortex of AD brains compared to control brains. The aim of this study was to assess the histological distribution of iron in aging and in AD. The frontal cortex with AD pathology showed iron accumulation in plaques and activated microglia. This is in line with earlier studies showing iron in human A β plaques (LeVine, 1997; Nabuurs et al., 2011; Nabuurs et al., 2013; Smith et al., 1997) and in activated microglia (Connor et al., 1992; LeVine, 1997; Nabuurs et al., 2011; Nabuurs et al., 2013). In addition to iron in plaques and microglia in AD cortex, we confirmed our preliminary observation (van Duijn et al., 2013) of an increased labelling of iron and myelin protein along myelinated fibres in and around cortical layers IV/V in a subset of AD patients with the most severe tau pathology. This is in line with the close relationship between iron and myelin synthesis extensively described in the literature. For example, activated microglia have been described to drive the recruitment and proliferation of oligodendrocyte proliferating cells (OPC) and their differentiation to oligodendrocytes, as well as the formation of myelin sheath around available axons (Crawford et al., 2013; Gudi et al., 2014; Miron and Franklin, 2014). Moreover, it is thought that microglia provide the high iron concentrations needed for myelination and oligodendrocyte differentiation (Schonberg et al., 2012; Schonberg and McTigue, 2009; Todorich et al., 2009).

We observed that aging in the absence of A β plaques does not lead to changes in iron distribution. Finally, we showed a semi-quantitative association between iron accumulation and the stage of AD pathology. This

opens the possibility to grade the severity of AD pathology by MR in vivo. Figure 1 shows iron aggregations correlated with other histological changes during the development of AD. Plaque load does not increase much from Braak IV to VI stages but iron accumulation and tau pathology both progress, although we still do not understand how they are related.

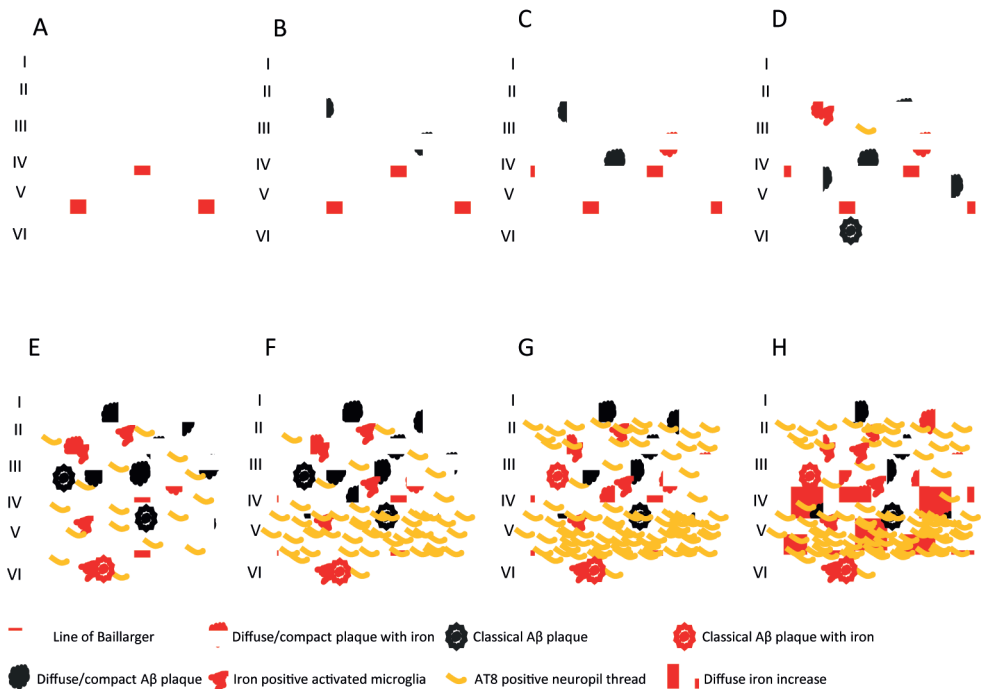


Figure 1: Schematic representation of the relation between AD pathology and pathological Fe accumulation in frontal cortex. a: normal aging showing diffuse myelin associated iron in the lines of Baillarger; b: controls with few diffuse plaques without pathological Fe accumulation; c: controls with little diffuse plaques and minimal pathological iron accumulation; d: controls with increasing plaques, including classical plaques and minimal AT8+ neuropil threads (AT8+NT) with increasing Fe accumulation in plaques and activated microglia; e: AD with maximum Aβ plaques and diffuse increase of AT8+NT with increased iron in plaques and activated microglia; f: AD with similar Aβ plaques and increased AT8+NT, macroscopically visible on the slide in cortical layer V and increased iron in plaques and activated microglia; g: AD with similar Aβ plaques and increased AT8+NT, macroscopically visible in cortical layer V and other layers; h: Same severe AD pathology as in g but with diffuse myelin associated increase of Fe in and around cortical layer IV/V

Magnetic Resonance Imaging

The clinical diagnosis of AD is based on neuropsychological testing combined with hippocampal atrophy assessed by magnetic resonance imaging (MRI) and A β and tau levels in CSF (Fox et al., 1996; Hyman et al., 2012; Jack, Jr. et al., 2010; Li and Wahlund, 2011; Nasrallah and Wolk, 2014). Over the past few years, the feasibility to detect the histological hallmarks of AD using MRI has been explored; in general these efforts have focused on detecting individual amyloid plaques (Chamberlain et al., 2011; Wadghiri et al., 2013). Increased iron accumulation in amyloid plaques induces a magnetic susceptibility effect, visible as hypointense foci on T2*-weighted or susceptibility-weighted (SW) MRI in the cerebral cortex of transgenic AD mouse models and in human post-mortem brain slices (Chamberlain et al., 2011; Meadowcroft et al., 2009; van Rooden et al., 2009). These findings have not yet been convincingly replicated in vivo in patients. It is doubtful whether detecting individual amyloid plaques with MRI will be possible in a clinical setting given the required high resolution, limited scanning time and physiological movement of the patient. However, recent advances in human MRI systems operating at an ultra-high magnetic field strength (7 Tesla and higher) show that the increased sensitivity to susceptibility effects generates iron based contrasts in the human brain that have not been observed before (Fukunaga et al., 2010; Meadowcroft et al., 2015b).

Previous studies showed band like changes (van Rooden et al., 2009) and single plaques (Chamberlain et al., 2011; Meadowcroft et al., 2009) in the frontal cortex of AD patients and not in non-demented controls. These studies suggested effects of the amyloid plaques on the MR images. In chapter 5 we examined changes in cortical appearance of AD patients using susceptibility weighted 7T MRI and correlated these findings with ex vivo scans and pathology. The aim of this study was to establish whether 7T MRI allows in vivo detection of differences in the cerebral cortex between probable AD patients and healthy controls. Having observed a difference, we then determined the histological substrate of the changes by comparing MRI, light- and electron microscopic analyses on human post-mortem material of AD patients and controls. On MRI, diffuse hypointense bands were frequently found in the cortex of the frontal lobe of AD patients (57%), which were not observed in healthy age matched control subjects. Further histologic correlation revealed that the pattern of the susceptibility-weighted contrast in the cortex of AD patients did not primarily co-localize with amyloid plaques or neurofibrillary tangles, but

with myelin-associated iron accumulation and with an altered myelin cytoarchitecture. This band like pattern of iron/myelin in the neuropil fibres of cortical layers III-V appears to be accentuated by the iron accumulation in A β plaques found more frequently in layer III of the cortex, confirming the findings in chapter 4. Iron is, due to its magnetic characteristics, easy to see on an MRI (Fjell and Walhovd, 2012; Karran et al., 2011). The current findings show great promise for the in vivo detection of the underlying pathological changes in AD.

To verify our results in the frontal cortex, described in chapter 5, a larger set of ex vivo brain material of different brain locations should be studied. Another study should include comparison of AD patients to other neurodegenerative diseases and control subjects. The study described in chapter 5, suggests that MRI changes can be observed only in a late stage in AD. This has potential use to follow treatment and to improve the clinical diagnosis at a late stage, however is not useful for early diagnosis

Magnetic Resonance Spectroscopy

One way to examine the metabolic pathways non-invasively during the early phases of AD is by focusing on the metabolic changes in a transgenic (tg) mouse model, by means of magnetic resonance spectroscopy (MRS). MRS is a non-invasive tool which can be used to measure the concentration of various brain metabolites in vivo (Rupsingh et al., 2011), making it possible to follow family members of AD patients with the possibility to identify AD at an early stage, prior to the onset of cognitive symptoms (Jack 2010).

Numerous MRS studies have been performed using tg AD mice. Until now N-acetylaspartate (NAA) and glutamate (glu) have been found to decrease in tg mice compared to control mice (Braakman et al., 2008; Choi et al., 2010; Dedeoglu et al., 2004; Marjanska et al., 2005; Oberg et al., 2008; von Kienlin M. et al., 2005). NAA is found in neuronal cell bodies and is a source of myelin synthesis in oligodendrocytes, the glial cells that myelinated neuronal axons. A decrease in NAA indicates neuronal damage. Glu is a neurotransmitter involved in memory formation and learning; decrease of glu indicates less neuronal activity. Myo-inositol (mIns) and taurine (tau) are involved in osmoregulation and are found in astrocytes, indicating an immune response; both increase during the development of AD in tg mouse compared to wt mice (Chen et al., 2009; Choi et al., 2010; Dedeoglu et al., 2004; Marjanska et al., 2005; Westman et al., 2009).

Chapter 6 describes the findings in the first longitudinal MRS study on a

transgenic mouse model. This study showed decreased glu and NAA in tg mice compared to wt mice at all time points. There was a decrease in mIns found in tg mice compared to wt mice at 3 months. Over time this decrease became less and at 18 months there was no difference between tg and wt mice in the level of mIns. At 3 months the level of tau was increased in tg mice compared to wt mice, this difference disappeared over time and at 18 months there was no difference in tau levels between tg and wt mice. Our findings confirm earlier findings in studies on transgenic mice (Braakman et al., 2008; Chen et al., 2009; Dedeoglu et al., 2004; Li and Wahlund, 2011; Marjanska et al., 2005; Oberg et al., 2008; Rupsingh et al., 2011; von Kienlin M. et al., 2005; Westman et al., 2009; Xu et al., 2010). These differences were not significant, probably due to the small size of the study group.

Currently, the long acquisition times limit the use of MRS in AD patients. If technical improvements are successful, the obvious next step would be to study large test groups of AD patients over time and compare those to non-demented subjects and, in a later stage, to patients with other neurodegenerative diseases.

Another finding, described in chapter 6 is a sex difference in AD mice and wt mice using MRS. It is known that females are at higher risk for developing AD than men (Andersen et al., 1999; Kim et al., 2015; Musicco, 2009). In this study female mice started with increased levels of NAA, compared to male mice, in both tg and wt mice. Female mice have a larger axonal density compared to male, which might explain the higher levels of NAA in both female control and tg mice at 3 months of age. The decline of NAA in tg female mice was more precipitous compared to control mice. The difference in glu levels between male and female wt mice at 18 months was a significant one. Female wt mice showed higher levels of glu compared to male wt mice. The level of taurine was higher in tg female mice compared to tg male mice at 3 months and showed a faster decline over time.

The effect of sex on the pathophysiology of AD has not yet been carefully examined. Hormonal influences have been suggested, however more research is necessary (Janicki and Schupf, 2010). It will be of great interest to study sex differences between AD and control groups in animals or in a non-invasive way in human subjects.

Our study is the first to show that metabolic changes during AD development are influenced by sex differences. This study is done in a small test group and should be considered a pilot, giving information for further

research.

Conclusions

This thesis aimed to improve the clinical diagnosis of AD by using native contrast MRI and MRS. MRI was correlated to histology with a special focus on iron because iron has high magnetic susceptibility effects on MRI and some reports show iron accumulation in A β plaques (LeVine, 1997; Nabuurs et al., 2011; Nabuurs et al., 2013; Smith et al., 1997) as well as in activated microglia (Connor et al., 1992; LeVine, 1997; Nabuurs et al., 2011; Nabuurs et al., 2013) and myelin (van Duijn et al., 2013).

We found changes in neocortical layers III-V, seen as band like hypointensities, on MRI scans which were correlated to a histological band-like pattern of iron/myelin in the neuropil fibres of cortical layers III-V. This band reflects a more crowded network of neuropil fibres with thicker and darker staining for iron. Iron was found in plaques, microglia and myelin in the neuropil. We also found a correlation between iron and neurofibrillar degeneration and plaques.

These MRI changes were observed only in a later stage of AD but may improve clinical diagnosis and enable monitoring effect of future experimental treatments.

The MRS studies showed early changes in metabolic levels between control mice and AD mice and between male and female mice.

Our results on MRI and MRS have potential to improve the clinical diagnosis of AD, however, more research is necessary. Follow up studies should be done in human test groups using MRI and MRS to confirm our findings that a hypointense band on MRI and metabolic changes predict AD. These studies should focus on a large group of direct family members of early AD patients, who are at risk for AD and compare these to a control group. These groups should be followed over time, doing MRI scans to check for the myelin/iron band and MRS scans to check for metabolic changes with caution for sex differences. Another study should focus on the specificity of the band like changes found on MRI scans. These band like hypointensities might not be specific for AD, which makes it necessary to compare AD patients also to other neurodegenerative diseases.

Reference List

Andersen, K., Launer, L.J., Dewey, M.E., Letenneur, L., Ott, A., Copeland, J.R., Dartigues, J.F., Kragh-Sorensen, P., Baldereschi, M., Brayne, C., Lobo, A., Martinez-Lage, J.M., Stijnen, T., Hofman, A., 1999. Gender differences in the incidence of AD and vascular dementia: The EURODEM Studies. EURODEM Incidence Research Group. *Neurology* 53, 1992-1997.

Bartzokis, G., 2011. Alzheimer's disease as homeostatic responses to age-related myelin breakdown. *Neurobiol.Aging* 32, 1341-1371.

Benveniste, H., Einstein, G., Kim, K.R., Hulette, C., Johnson, G.A., 1999. Detection of neuritic plaques in Alzheimer's disease by magnetic resonance microscopy. *Proc. Natl. Acad. Sci. U.S.A* 96, 14079-14084.

Bobinski, M., de Leon, M.J., Wegiel, J., DeSanti, S., Convit, A., Saint Louis, L.A., Rusinek, H., Wisniewski, H.M., 2000. The histological validation of post mortem magnetic resonance imaging-determined hippocampal volume in Alzheimer's disease. *Neuroscience* 95, 721-725.

Braakman, N., Oerther, T., de Groot, H.J., Alia, A., 2008. High resolution localized two-dimensional MR spectroscopy in mouse brain in vivo. *Magn Reson. Med.* 60, 449-456.

Bronge, L., Bogdanovic, N., Wahlund, L.O., 2002. Postmortem MRI and histopathology of white matter changes in Alzheimer brains. A quantitative, comparative study. *Dement. Geriatr. Cogn Disord.* 13, 205-212.

Chamberlain, R., Wengenack, T.M., Poduslo, J.F., Garwood, M., Jack, C.R., Jr., 2011. Magnetic resonance imaging of amyloid plaques in transgenic mouse models of Alzheimer's disease. *Curr. Med. Imaging Rev.* 7, 3-7.

Chen, S.Q., Wang, P.J., Ten, G.J., Zhan, W., Li, M.H., Zang, F.C., 2009. Role of myo-inositol by magnetic resonance spectroscopy in early diagnosis of Alzheimer's disease in APP/PS1 transgenic mice. *Dement. Geriatr. Cogn Disord.* 28, 558-566.

Choi, J.K., Jenkins, B.G., Carreras, I., Kaymakcalan, S., Cormier, K., Kowall, N.W., Dedeoglu, A., 2010. Anti-inflammatory treatment in AD mice

protects against neuronal pathology. *Exp. Neurol.* 223, 377-384.

Connor, J.R., Menzies, S.L., St Martin, S.M., Mufson, E.J., 1992. A histochemical study of iron, transferrin, and ferritin in Alzheimer's diseased brains. *J. Neurosci. Res.* 31, 75-83.

Crawford, A.H., Chambers, C., Franklin, R.J., 2013. Remyelination: the true regeneration of the central nervous system. *J. Comp Pathol.* 149, 242-254.

Crichton, R.R., Wilmet, S., Legssyer, R., Ward, R.J., 2002. Molecular and cellular mechanisms of iron homeostasis and toxicity in mammalian cells. *J. Inorg. Biochem.* 91, 9-18.

Dedeoglu, A., Choi, J.K., Cormier, K., Kowall, N.W., Jenkins, B.G., 2004. Magnetic resonance spectroscopic analysis of Alzheimer's disease mouse brain that express mutant human APP shows altered neurochemical profile. *Brain Res.* 1012, 60-65.

Englund, E., Sjobeck, M., Brockstedt, S., Latt, J., Larsson, E.M., 2004. Diffusion tensor MRI post mortem demonstrated cerebral white matter pathology. *J. Neurol.* 251, 350-352.

Fernando, M.S., O'Brien, J.T., Perry, R.H., English, P., Forster, G., McMeekin, W., Slade, J.Y., Golkhar, A., Matthews, F.E., Barber, R., Kalaria, R.N., Ince, P.G., 2004. Comparison of the pathology of cerebral white matter with post-mortem magnetic resonance imaging (MRI) in the elderly brain. *Neuropathol. Appl. Neurobiol.* 30, 385-395.

Fjell, A.M., Walhovd, K.B., 2012. Neuroimaging results impose new views on Alzheimer's disease--the role of amyloid revised. *Mol. Neurobiol.* 45, 153-172.

Fox, N.C., Freeborough, P.A., Rossor, M.N., 1996. Visualisation and quantification of rates of atrophy in Alzheimer's disease. *Lancet* 348, 94-97.

Fukunaga, M., Li, T.Q., van, G.P., de Zwart, J.A., Shmueli, K., Yao, B., Lee, J., Maric, D., Aronova, M.A., Zhang, G., Leapman, R.D., Schenck, J.F., Merkle, H., Duyn, J.H., 2010. Layer-specific variation of iron content in

cerebral cortex as a source of MRI contrast. *Proc. Natl. Acad. Sci. U.S.A* 107, 3834-3839.

Geurts, J.J., Bo, L., Pouwels, P.J., Castelijns, J.A., Polman, C.H., Barkhof, F., 2005. Cortical lesions in multiple sclerosis: combined postmortem MR imaging and histopathology. *AJNR Am. J. Neuroradiol.* 26, 572-577.

Gouw, A.A., Seewann, A., Vrenken, H., van der Flier, W.M., Rozemuller, J.M., Barkhof, F., Scheltens, P., Geurts, J.J., 2008. Heterogeneity of white matter hypointensities in Alzheimer's disease: post-mortem quantitative MRI and neuropathology. *Brain* 131, 3286-3298.

Gudi, V., Gingele, S., Skripuletz, T., Stangel, M., 2014. Glial response during cuprizone-induced de- and remyelination in the CNS: lessons learned. *Front Cell Neurosci.* 8, 73.

Haacke, E.M., Cheng, N.Y., House, M.J., Liu, Q., Neelavalli, J., Ogg, R.J., Khan, A., Ayaz, M., Kirsch, W., Obenaus, A., 2005. Imaging iron stores in the brain using magnetic resonance imaging. *Magn Reson. Imaging* 23, 1-25.

House, M.J., St Pierre, T.G., Kowdley, K.V., Montine, T., Connor, J., Beard, J., Berger, J., Siddaiah, N., Shankland, E., Jin, L.W., 2007. Correlation of proton transverse relaxation rates (R2) with iron concentrations in post-mortem brain tissue from Alzheimer's disease patients. *Magn Reson. Med.* 57, 172-180.

Hyman, B.T., Phelps, C.H., Beach, T.G., Bigio, E.H., Cairns, N.J., Carrillo, M.C., Dickson, D.W., Duyckaerts, C., Frosch, M.P., Masliah, E., Mirra, S.S., Nelson, P.T., Schneider, J.A., Thal, D.R., Thies, B., Trojanowski, J.Q., Vinters, H.V., Montine, T.J., 2012. National Institute on Aging-Alzheimer's Association guidelines for the neuropathologic assessment of Alzheimer's disease. *Alzheimers Dement.* 8, 1-13.

Jack, C.R., Jr., Knopman, D.S., Jagust, W.J., Shaw, L.M., Aisen, P.S., Weiner, M.W., Petersen, R.C., Trojanowski, J.Q., 2010. Hypothetical model of dynamic biomarkers of the Alzheimer's pathological cascade. *Lancet Neurol.* 9, 119-128.

Janicki, S.C., Schupf, N., 2010. Hormonal influences on cognition and risk for Alzheimer's disease. *Curr.Neurol.Neurosci.Rep.* 10, 359-366.

Kangarlu, A., Bourekas, E.C., Ray-Chaudhury, A., Rammohan, K.W., 2007. Cerebral cortical lesions in multiple sclerosis detected by MR imaging at 8 Tesla. *AJNR Am. J. Neuroradiol.* 28, 262-266.

Karran, E., Mercken, M., De, S.B., 2011. The amyloid cascade hypothesis for Alzheimer's disease: an appraisal for the development of therapeutics. *Nat. Rev. Drug Discov.* 10, 698-712.

Kim, S., Kim, M.J., Kim, S., Kang, H.S., Lim, S.W., Myung, W., Lee, Y., Hong, C.H., Choi, S.H., Na, D.L., Seo, S.W., Ku, B.D., Kim, S.Y., Kim, S.Y., Jeong, J.H., Park, S.A., Carroll, B.J., Kim, D.K., 2015. Gender differences in risk factors for transition from mild cognitive impairment to Alzheimer's disease: A CREDOS study. *Compr. Psychiatry* 62, 114-122.

Larsson, E.M., Englund, E., Sjobeck, M., Latt, J., Brockstedt, S., 2004. MRI with diffusion tensor imaging post-mortem at 3.0 T in a patient with frontotemporal dementia. *Dement. Geriatr. Cogn Disord.* 17, 316-319.

LeVine, S.M., 1991. Oligodendrocytes and myelin sheaths in normal, quaking and shiverer brains are enriched in iron. *J. Neurosci. Res.* 29, 413-419.

LeVine, S.M., 1997. Iron deposits in multiple sclerosis and Alzheimer's disease brains. *Brain Research* 760, 298-303.

Li, T.Q., Wahlund, L.O., 2011. The search for neuroimaging biomarkers of Alzheimer's disease with advanced MRI techniques. *Acta Radiol.* 52, 211-222.

Marjanska, M., Curran, G.L., Wengenack, T.M., Henry, P.G., Bliss, R.L., Poduslo, J.F., Jack, C.R., Jr, Ugurbil, K., Garwood, M., 2005. Monitoring disease progression in transgenic mouse models of Alzheimer's disease with proton magnetic resonance spectroscopy. *Proc. Natl. Acad. Sci. U.S.A* 102, 11906-11910.

Meadowcroft, M.D., Connor, J.R., Smith, M.B., Yang, Q.X., 2009. MRI and

Histological Analysis of Beta-Amyloid Plaques in Both Human Alzheimer's Disease and APP/PS1 Transgenic Mice. *Journal of Magnetic Resonance Imaging* 29, 997-1007.

Meadowcroft, M.D., Connor, J.R., Yang, Q.X., 2015a. Cortical iron regulation and inflammatory response in Alzheimer's disease and APPSWE/PS1DeltaE9 mice: a histological perspective. *Front Neurosci.* 9, 255.

Meadowcroft, M.D., Peters, D.G., Dewal, R.P., Connor, J.R., Yang, Q.X., 2015b. The effect of iron in MRI and transverse relaxation of amyloid-beta plaques in Alzheimer's disease. *NMR Biomed.* 28, 297-305.

Meguro, R., Asano, Y., Odagiri, S., Li, C., Iwatsuki, H., Shoumura, K., 2007. Nonheme-iron histochemistry for light and electron microscopy: a historical, theoretical and technical review. *Arch. Histol. Cytol.* 70, 1-19.

Miron, V.E., Franklin, R.J., 2014. Macrophages and CNS remyelination. *J. Neurochem.* 130, 165-171.

Musicco, M., 2009. Gender differences in the occurrence of Alzheimer's disease. *Funct. Neurol.* 24, 89-92.

Nabuurs, R.J., Hegeman, I., Natte, R., van Duinen, S.G., van Buchem, M.A., van der Weerd, L., Webb, A.G., 2011. High-field MRI of single histological slices using an inductively coupled, self-resonant microcoil: application to ex vivo samples of patients with Alzheimer's disease. *NMR Biomed.* 24, 351-357.

Nabuurs, R.J.A., van Rooden, S., van Rooden, S., van Duijn, S., Versluis, M.J., Emmer, B.J., Liem, M.K., Milles, J.R., R, Webb, A., Frosch, M., , van Duinen, S., Natte, R., van der Grond, J., van der Weerd, L., van Buchem, M.A., 2013. Cortical changes in Alzheimer's disease at ultra-high field MRI.

Nasrallah, I.M., Wolk, D.A., 2014. Multimodality imaging of Alzheimer disease and other neurodegenerative dementias. *J. Nucl. Med.* 55, 2003-2011.

Nelson, P.T., Braak, H., Markesbery, W.R., 2009. Neuropathology and cog-

nitive impairment in Alzheimer disease: a complex but coherent relationship. *J. Neuropathol. Exp. Neurol.* 68, 1-14.

Oberg, J., Spenger, C., Wang, F.H., Andersson, A., Westman, E., Skoglund, P., Sunnemark, D., Norinder, U., Klason, T., Wahlund, L.O., Lindberg, M., 2008. Age related changes in brain metabolites observed by ¹H MRS in APP/PS1 mice. *Neurobiol.Aging* 29, 1423-1433.

Rupsingh, R., Borrie, M., Smith, M., Wells, J.L., Bartha, R., 2011. Reduced hippocampal glutamate in Alzheimer disease. *Neurobiol.Aging* 32, 802-810.

Schmierer, K., Parkes, H.G., So, P.W., An, S.F., Brandner, S., Ordidge, R.J., Yousry, T.A., Miller, D.H., 2010. High field (9.4 Tesla) magnetic resonance imaging of cortical grey matter lesions in multiple sclerosis. *Brain* 133, 858-867.

Schonberg, D.L., Goldstein, E.Z., Sahinkaya, F.R., Wei, P., Popovich, P.G., McTigue, D.M., 2012. Ferritin Stimulates Oligodendrocyte Genesis in the Adult Spinal Cord and Can Be Transferred from Macrophages to NG2 Cells In Vivo. *Journal of Neuroscience* 32, 5374-5384.

Schonberg, D.L., McTigue, D.M., 2009. Iron is essential for oligodendrocyte genesis following intraspinal macrophage activation. *Exp. Neurol.* 218, 64-74.

Smith, M.A., Harris, P.L., Sayre, L.M., Perry, G., 1997. Iron accumulation in Alzheimer disease is a source of redox-generated free radicals. *Proc. Natl. Acad. Sci. U.S.A* 94, 9866-9868.

Todorich, B., Pasquini, J.M., Garcia, C.I., Paez, P.M., Connor, J.R., 2009. Oligodendrocytes and Myelination: The Role of Iron. *Glia* 57, 467-478.

van Duijn, S., Nabuurs, R.J., van Duinen, S.G., Natta, R., 2013. Comparison of histological techniques to visualize iron in paraffin-embedded brain tissue of patients with Alzheimer's disease. *J. Histochem. Cytochem.* 61, 785-792.

van Rooden, S., Maat-Schieman, M.L., Nabuurs, R.J., van der Weerd, L.,

van Duijn, S., van Duinen, S.G., Nettekoven, R., van Buchem, M.A., van der Grond, J., 2009. Cerebral amyloidosis: postmortem detection with human 7.0-T MR imaging system. *Radiology* 253, 788-796.

von Kienlin M., Kunnecke, B., Metzger, F., Steiner, G., Richards, J.G., Ozmen, L., Jacobsen, H., Loetscher, H., 2005. Altered metabolic profile in the frontal cortex of PS2APP transgenic mice, monitored throughout their life span. *Neurobiol. Dis.* 18, 32-39.

Wadghiri, Y.Z., Li, J., Wang, J., Hoang, D.M., Sun, Y., Xu, H., Tsui, W., Li, Y., Boutajangout, A., Wang, A., de, L.M., Wisniewski, T., 2013. Detection of amyloid plaques targeted by bifunctional USPIO in Alzheimer's disease transgenic mice using magnetic resonance microimaging. *PLoS. One.* 8, e57097.

Westman, E., Spenger, C., Oberg, J., Reyer, H., Pahnke, J., Wahlund, L.O., 2009. In vivo ¹H-magnetic resonance spectroscopy can detect metabolic changes in APP/PS1 mice after donepezil treatment. *BMC. Neurosci.* 10, 33.

Xu, W., Zhan, Y.Q., Huang, W., Wang, X.X., Zhang, S.M., Lei, H., 2010. Reduction of Hippocampal N-Acetyl Aspartate Level in Aged APP(Swe)/PS1(dE9) Transgenic Mice Is Associated With Degeneration of CA3 Pyramidal Neurons. *Journal of Neuroscience Research* 88, 3155-3160.

Nederlandse samenvatting

De ziekte van Alzheimer (AD) is de meest voorkomende vorm van dementie met veroudering als belangrijkste risicofactor. De toenemende vergrijzing gaat dan ook gepaard met een stijgende incidentie van AD en drukt hierbij een zwaar stempel op de maatschappij, zowel op sociaal-economisch als op medisch vlak. De precieze oorzaak van deze ziekte is echter onbekend en helaas ontbreekt tot nu toe een behandeling. AD wordt veroorzaakt door de ophoping van twee verschillende eiwitten in de cortex van de hersenen. Het meest bekende eiwit is het amyloid- β ($A\beta$) peptide hetgeen amyloid plaques vormt. Het tweede eiwit is gehyperfosforyleerd tau in de vorm van neurofibrillaire tangles. De ophoping van beide eiwitten lijkt vroeg te beginnen, tientallen jaren voor de eerste klinische symptomen zichtbaar worden. Detectie van deze accumulatie in vivo in een vroeg stadium is voornamelijk niet mogelijk. Op dit moment is een definitieve diagnose van AD alleen postmortem te stellen.

Een vroege diagnose zou het mogelijk maken de ontwikkeling van de ziekte te volgen en het begrip van het verloop van AD te vergroten. Hierdoor zou behandeling weer een stap dichterbij zijn. In dit proefschrift heb ik mij gericht op verschillende technieken die een vroege diagnose mogelijk zouden kunnen maken, namelijk magnetische resonantie imaging (MRI) en magnetische resonantie spectroscopie (MRS) technieken. Hierbij heb ik mij gericht op ex vivo humaan hersenweefsel (MRI) en op muizen met een AD mutatie (MRI en MRS).

Het humane hersenweefsel dat gebruikt is in deze studie is gefixeerd in formaline. Bij langdurige fixatietijden bleken in het hersenweefsel artefacten op te treden. Deze artefacten waren als hypointense gebieden zichtbaar op verschillende MRI-sequenties (hoofdstuk 2). Aangezien formaline gefixeerd postmortem hersenmateriaal vaak voor AD onderzoek wordt gebruikt, raden wij aan alleen met hersenweefsel te werken dat minder dan een jaar gefixeerd is in formaline waarbij deze formaline regelmatig verversd is ter voorkoming van deze artefacten.

De rol van ijzer is in de afgelopen jaren steeds belangrijker gebleken bij de ontwikkeling van AD. Aangezien ijzer, door zijn magnetische karakter, goed zichtbaar kan worden gemaakt met behulp van MRI, lag hier onze focus. De histologische kleuringen die gebruikt worden om ijzer aan te tonen, zijn echter niet altijd specifiek en consistent. In hoofdstuk 3 wordt de vergelijking van verschillende histochemische kleuringen op hersenweefsel van AD patiënten beschreven. Uit dit onderzoek bleek dat de kleuring ontwikkeld door Meguro de beste techniek was voor onze doeleinden. Deze werd dan ook gedurende de rest van het proefschrift gebruikt.

Vervolgens werd hersenweefsel van 10 AD-patiënten vergeleken met het brein materiaal van 10 jonge, 10 middeloude en 10 oude controles (hoofdstuk 4). Dit materiaal werd getest op de aanwezigheid van ijzer

(met de Meguro kleuring), A β , myeline en tau. Uit dit onderzoek bleek dat ijzer bij AD-patiënten in vergevorderd stadium zich ophoopt in de lagen 3 tot en met 5 van de cortex. Hierbij vormt het ijzer een band die goed zichtbaar zou kunnen zijn op een MRI-scan. Deze ijzerophoping bleek te zijn gecorreleerd aan de accumulatie van tau en de verandering van het myelinepatroon in het AD-brein. De hoeveelheid A β in het brein leek hier los van te staan. De hoeveelheid ijzer in het brein nam pas toe nadat de ophoping van A β in de cortex al zijn maximale hoeveelheid heeft bereikt. In hoofdstuk 5 hebben we de veranderingen in corticale patronen van gezonde ouderen en AD-patiënten in vivo onderzocht met behulp van 7T MRI. Tegelijkertijd werden soortgelijke corticale patronen waargenomen bij MRI verricht op postmortem AD-hersenenmateriaal. Dit materiaal bood tevens de mogelijkheid tot correlatie met de onderliggende pathologie verantwoordelijk voor deze signaalverandering, zoals zichtbaar op de MRI. In de frontale cortex van AD-patiënten was in vivo een diffuse hypointense corticale band zichtbaar die niet werd gezien bij gezonde controles van dezelfde leeftijd. Uit de histologische studie bleek dat de corticale patronen op de MRI niet primair overeen kwamen met de distributie van amyloid plaques of neurofibrillaire tangles. Deze patronen lieten een duidelijke correlatie zien met microglia en myeline-geassocieerde ijzerophoppingen evenals een veranderde corticale myeline cytoarchitectuur.

Deze resultaten zijn veelbelovend voor de in vivo detectie van de onderliggende pathologische veranderingen in AD door middel van MRI. Toekomstige onderzoek dient uit te wijzen of dit patroon specifiek is voor AD. Het laatste hoofdstuk (hoofdstuk 6) beschrijft een studie, waarbij de metaboliëtenhuishouding van muizen met AD-mutatie op verschillende momenten gedurende het leven van deze muizen werd gemeten met behulp van de MRS. Deze bevindingen werden vergeleken met controle muizen. Hieruit bleek dat op vroege leeftijd, als er nog geen symptomatische verschillen zijn tussen de AD-muizen en de controle muizen, al een verandering in de metaboliëtenhuishouding zichtbaar was. Hierbij werd specifiek gekeken naar metaboliëten die te maken hebben met schade aan neuronen, die betrokken zijn bij het geheugen en metaboliëten die betrokken zijn bij immunoreacties. Een opvallende bevinding in dit onderzoek was het verschil tussen mannelijke en vrouwelijke muizen. De metaboliëten huishouding bleek bij zowel controle als AD-muizen anders te zijn in mannen dan in vrouwen.

Dankwoord

Prof. Dr. M.A. van Buchem: dank voor het geloven in mij.

Dr. S. G. van Duinen en dr. R. Natte: dank voor het eindeloze geduld bij het schrijven en herschrijven van dit hele boekje.

Dr. A. Alia: thanks for your support with the MRS study.

Rob: fijn dat je er was. Altijd. Voor de broodnodige ontspanning, inspanning, het lachen en het huilen.

Karin, Marian, Wietske, Renate, Vincent, Sofie en Jappe: bedankt dat jullie mij geadopteerd hebben. Dit maakte mijn tijd op de pathologie absoluut grappiger.

Sanneke: fijn om af en toe met je te sparren, mopperen en lachen.

Collega's van het Gorleaus: dank voor de ondersteuning op MRI, MRS en muizen gebied.

Frans P: bijzonder om samen te werken met een oud collega van mijn opa. En wat voor een samenwerking, altijd kon ik bij je terecht. Dank daarvoor.

Ingrid en Corry: mijn eeuwige steun en toeverlaat. Niets was te gek. Altijd bereid mee te denken, te helpen en even een praatje te maken. Heel erg fijn dat jullie er waren.

Minqukuls, Ragazze, het 26e bestuur, mukkels: dank voor alle afleiding, uitjes, grappen.

Fransje, Marieke, Merel, Inger: Dank voor het eeuwigdurende vertrouwen in mij op welk vlak dan ook. Voor het er altijd zijn, in goede en in slechte tijden.

Paps, mams, Joris, Marije en Trifie: jullie zijn mijn verleden en mijn heden, zonder jullie was ik niet wie ik nu ben. Het was niet altijd makkelijk maar jullie hebben nooit getwijfeld.

Sam, Jonathan, Ebbe, Casper en Louise: hoe klein ook, jullie maken mijn leven absoluut mooier.

Lieve Jeanine: ondanks je late instroom bij dit project ben jij in alles belangrijk. Je maakt mij een beter en mooier mens. Op naar de toekomst.

Curriculum vitae

Sara van Duijn was born on the 26th of September, 1979 in Amsterdam, the Netherlands. In 1997 she graduated at the Rijnlands Lyceum in Oegstgeest. After a few years of traveling, studying and searching, she started Biology at Leiden University. After her bachelor, she did the master Experimental Neuroscience at the University of Utrecht.

During this master study she was fascinated by the Hereditary Cerebral Hemorrhage with Amyloid Disease (HCHWA-D). After an internship at the LUMC at the department of pathology, studying this disease, she started as a full time Ph.D. student working on this thesis at the LUMC.

After five years full time studying Alzheimer's disease, she changed direction and became a teacher at primary school.

Publication list

Pijpe J, Pul N, van Duijn S, Brakefield PM, Zwaan BJ; Changed gene expression for candidate ageing genes in long-lived *Bicyclus anynana* butterflies *Exp Gerontol* (2011) 46 (6): 426-434

Van Duijn S, Nabuurs RJA, van Duinen SG, Natté R, van Buchem MA, Alia A; Longitudinal monitoring of sex-related in vivo metabolic changes in the brain of Alzheimer's disease transgenic mouse using magnetic resonance spectroscopy *J Alzheimers Dis* (2013) 34 (4): 1051-1059

Nabuurs RJA, van Duijn S, van Rooden S, Maat-Schieman MLC, van Duinen SG, van Buchem MA, van der Weerd L, Natté R; MRI artefacts in human brain tissue after prolonged formalin storage *Magn Reson Med* (2011) 65 (6): 1750-1758

Van Rooden S, Maat-Schieman ML, Nabuurs RJA, van der Weerd L, van Duijn S, van Duinen SG, Natté R, van Buchem MA, van der Grond J; Cerebral amyloidosis: post-mortem detection with human 7.0-T MR imaging system *Radiology* (2009) 31(9): 1577-1583

Van Duijn S, Nabuurs RJA, van Duinen SG, Natté R; Comparison of histological techniques to visualize iron in paraffin embedded brain tissue of patients with Alzheimer's disease *J Histochem Cytochem* (2013) 61 (11): 785-792

Van Duijn S, van Duinen SG, Nabuurs RJA, van Buche MA, van der Weerd L, Natté R; Cortical iron reflects severity of Alzheimer's disease. Accepted *J. Alzh Dis* 2017; 60 (4): 1533-1545

In Progress:

Nabuurs RJA, van Rooden S, van Duijn S, Versluis MR, Emmer BJ, Liem MK, Milles JR, Webb AG, Frosch MP, van Duinen SG, Natté R, van der Grond J, van der Weerd L, van Buchem MA; Detection of cortical changes in Alzheimer's disease patients at ultra-high field MRI